

# Mass Balance Modeling of Calcite in the Epilimnion of an Ultraoligotrophic Lake

A dissertation  
submitted by

Elizabeth S. Homa

In partial fulfillment of the requirements  
for the degree of

Doctor of Philosophy

in

*Civil and Environmental Engineering*

TUFTS UNIVERSITY

February 2010

© 2010, ELIZABETH S. HOMA

## Abstract

Seasonal calcite precipitation was observed and analyzed in a calcareous, ultra-oligotrophic lake, Torch Lake, Michigan (USA). A mass-balance model of the lake's epilimnion was developed to synthesize the observations and investigate the interactions of the various processes that generates calcite and greatly reduces clarity during summer stratification.

Phytoplankton growth is the most often cited driver of calcite precipitation in lakes. Given the ultra-oligotrophic conditions of Torch Lake, it was hypothesized that the seasonal temperature change of the lake water may have more of an effect on calcite precipitation than primary production.

Using the model to quantify the roles of the various chemical, biological and physical processes interacting in the lake, the discovery was made that air exchange effects the calcite precipitation rate more than the temperature change or primary production.

## Acknowledgements

XXX:

## Table of Contents

<b>CHAPTER 1 : INTRODUCTION .....</b>	<b>1</b>
<b>CHAPTER 2 TORCH LAKE BACKGROUND.....</b>	<b>5</b>
<b>CHAPTER 3 TORCH LAKE DATA .....</b>	<b>9</b>
2002 SEDIMENT CORE .....	9
2005 WATER QUALITY STUDY .....	10
2006 DATA COLLECTION FOR CALCITE STUDY .....	12
2006 PARTICLE DISTRIBUTION DATA .....	14
<b>CHAPTER 4 INTRODUCTION TO THE TORCH LAKE MODEL.....</b>	<b>24</b>
MODEL STRUCTURE .....	24
MODEL STATE VARIABLES AND BIOCHEMICAL PROCESSES .....	25
COMPUTED VARIABLES.....	28
<b>CHAPTER 5 THE CALCITE PRECIPITATION RATE .....</b>	<b>32</b>
LITERATURE REVIEW .....	33
MODEL STRUCTURE .....	38
ANALYSIS OF PRIMARY FACTORS.....	45
CALIBRATION METHODS .....	55
<b>CHAPTER 6 THE CO<sub>2</sub> AIR-WATER EXCHANGE RATE .....</b>	<b>59</b>
LITERATURE REVIEW .....	59
MODEL STRUCTURE .....	64
<b>CHAPTER 7 THE CALCITE SETTLING VELOCITY.....</b>	<b>80</b>
CALIBRATION METHODS .....	80
<b>CHAPTER 8 THE PRIMARY PRODUCTION RATE.....</b>	<b>83</b>
MODEL STRUCTURE .....	83
PUBLISHED PRIMARY PRODUCTION RATES .....	85
CALIBRATION METHODS .....	87
<b>CHAPTER 9 THE RATE OF COPRECIPITATION OF PHOSPHORUS.....</b>	<b>92</b>
LITERATURE REVIEW .....	92
MODEL STRUCTURE .....	94
CALIBRATION METHODS .....	98
SUMMARY .....	100
<b>CHAPTER 10 RESULTS AND ANALYSIS.....</b>	<b>101</b>
RESULTS.....	101
ANALYSIS.....	106
CONCLUSIONS .....	114
<b>REFERENCES .....</b>	<b>116</b>

## LIST OF TABLES

TABLE 2-1 CHEMICAL, BIOLOGICAL AND OPTICAL CHARACTERISTICS OF TORCH LAKE, MI. ....	6
TABLE 3-1 SUMMARY OF THE TORCH LAKE DATA USED IN THIS STUDY. ....	9
TABLE 3-2 SUMMARY OF THE 2006 DATA COLLECTION BY TLA.....	14
TABLE 3-3 SUMMARY IPA/SAX DATA FOR TORCH LAKE PARTICLES FOR EACH 2M DEPTH SAMPLE. ....	19
TABLE 3-4 PERCENT OF EACH PARTICLE CATEGORY FOR ALL THE TORCH LAKE PARTICLES. ....	19
TABLE 4-1 MODEL STATE VARIABLES .....	26
TABLE 4-2 KINETIC INTERACTIONS AND STOICHIOMETRY. TERMS DEFINED IN CHAPTER SHOWN.....	28
TABLE 4-3 COMPUTED VARIABLES.....	28
TABLE 5-1 REPORTED EXPERIMENTAL RATE COEFFICIENTS FOR CALCITE PRECIPITATION AND DISSOLUTION. ....	40
TABLE 5-2 SUMMARY OF TEMPERATURE CHANGE SCENARIOS ON SI AND (IAP- $K_{sp}$ ).....	52
TABLE 5-3 SUMMARY OF TORCH LAKE PRECIPITATION RATE CALIBRATION METHODS. ....	56
TABLE 8-1 KINETIC INTERACTIONS AND STOICHIOMETRY FOR BIOLOGICAL PROCESSES. ....	84
TABLE 8-2 ESTIMATES OF PRIMARY PRODUCTION FOR TORCH LAKE .....	89
TABLE 10-1 SUMMARY OF THE MAIN AND INTERACTION EFFECTS OF PREDICTED FACTORS ON CUMULATIVE CALCITE PRECIPITATION IN TORCH LAKE (IN MG/L $\text{CaCO}_{3(s)}$ ).....	107

## List of Figures

FIGURE 2-1 TORCH LAKE, MICHIGAN. THE INSET PROVIDES A SUMMARY OF THE LAKE'S CHARACTERISTICS.	5
FIGURE 2-2 PHOTOGRAPH OF SAILBOATS ON TORCH LAKE, JUNE 2006.	6
FIGURE 2-3 TORCH LAKE AREA AND VOLUME VS. DEPTH	7
FIGURE 2-4 SECCHI DISC DEPTH (M) VERSUS DATE FOR TORCH LAKE, MICHIGAN COLLECTED BY THE TIP OF THE MITT WATERSHED COUNCIL FROM 1996 – 2006.	8
FIGURE 3-1 SEDIMENT CORE COLLECTED FROM TORCH LAKE IN 2002. (YOHAN ET AL. 2003)	10
FIGURE 3-2 MONITORING AND SAMPLING LOCATIONS FOR TORCH LAKE (ENDICOTT ET AL. 2006)	10
FIGURE 3-3 PHOSPHORUS MASS BALANCE FOR TORCH LAKE FOR NOVEMBER 2004 - OCTOBER 2005	11
FIGURE 3-4 HYDROLOGIC BUDGET FOR TORCH LAKE FOR NOVEMBER 2004 - OCTOBER 2005	12
FIGURE 3-5 SAMPLE TAKEN 7/6/06 AT 2M DEPTH IN TORCH LAKE, MI	15
FIGURE 3-6 SAMPLE TAKEN 8/3/06 AT 2M DEPTH IN TORCH LAKE, MI.	16
FIGURE 3-7 CLOSER VIEW OF SAMPLE TAKEN 8/3/06 AT 2M DEPTH IN TORCH LAKE, MI.	16
FIGURE 3-8 PLOT OF BOTH DISTRIBUTION TYPES FOR THE CALCIUM PARTICLES, SAMPLED ON AUGUST 3, 2006.	17
FIGURE 3-9 PLOT OF THE TORCH LAKE PARTICLE COUNTS PER LITER OVER TIME.	20
FIGURE 3-10 PLOT OF TORCH LAKE TURBIDITY OVER TIME.	20
FIGURE 3-11 PLOT OF THE PARTICULATE SURFACE AREA OVER TIME, SEPARATED BY ALL PARTICLES, CALCIUM PARTICLES AND NON-CALCIUM PARTICLES.	21
FIGURE 3-12 PLOT OF CALCITE MASS OVER TIME CALCULATED FROM PARTICLE ANALYSIS OF 2M DEPTH SAMPLES (UFI) AND FROM ON BOARD FILTERING OF EPILIMNION COMPOSITE SAMPLES (TLA).	22
FIGURE 4-1 PROCESS DIAGRAM FOR THE TORCH LAKE PH2K MODEL	25
FIGURE 4-2 STATE DIAGRAM FOR THE TORCH LAKE PH2K MODEL	26
FIGURE 5-1 PLOT OF THE MODEL ESTIMATES OF SURFACE AREA (LINES) COMPARED TO SURFACE AREAS CALCULATED FROM UFI DATA (CIRCLES) AND TLA DATA (TRIANGLES), OVER TIME.	45
FIGURE 5-2 TEMPERATURE DEPENDENCE OF PROCESSES IMPACTING THE CALCITE PRECIPITATION RATE	46
FIGURE 5-3 DIRECT EFFECTS OF TEMPERATURE ON THE CALCITE PRECIPITATION RATE.	47
FIGURE 5-4 VARIOUS EQUATIONS FOR THE TEMPERATURE DEPENDENCE OF CALCITE PKSP.	49
FIGURE 5-5 A PLOT OF pH AS A FUNCTION OF TEMPERATURE.	53
FIGURE 5-6 PLOT OF THE MODEL ESTIMATE OF THE TORCH LAKE PRECIPITATION RATE OVER	58
FIGURE 6-1 PRIMARY FACTORS IMPACTING THE AIR-WATER EXCHANGE RATE.	65
FIGURE 6-2 COMPARISON OF MODELS FOR AIR EXCHANGE VELOCITIES OF CO <sub>2</sub> AT 20C AS A FUNCTION OF WIND SPEED.	68
FIGURE 6-3 SCHMIDT NUMBER FOR CO <sub>2</sub> IN FRESHWATER AS A FUNCTION OF TEMPERATURE. THE RED	70
FIGURE 6-4 MODEL ESTIMATE OF AIR EXCHANGE VELOCITY OVER TIME USING SEASONAL AVERAGE WIND SPEED OF 2 M/S FOR COLE AND CARACO 1998 AND WANNINKHOF 1991 MODELS.	71
FIGURE 6-5 SATURATION CO <sub>2</sub> AS A FUNCTION OF TEMPERATURE.	72
FIGURE 6-6 SATURATION CO <sub>2</sub> ([CO <sub>2</sub> ] <sub>s</sub> ) AND [CO <sub>2</sub> ] IN MOLES/L MODELED AS A FUNCTION OF TIME IN TORCH LAKE.	73
FIGURE 6-7 SATURATION C <sub>T</sub> AS A FUNCTION OF pH WITH TEMPERATURE = 20C AND CONDUCTIVITY = 300 UM/S	73
FIGURE 6-8 RANGE OF TORCH LAKE TOTAL INORGANIC CARBON (C <sub>T</sub> ) AND SATURATION C <sub>T</sub> AS A FUNCTION OF pH FOR TEMPERATURE = 10C AND TEMPERATURE = 20C. (CONDUCTIVITY = 300 μS/CM).	74
FIGURE 6-9 HOOVER AND BERKSHIRE (1969) ENHANCEMENT AS A FUNCTION OF pH	76
FIGURE 6-10 EQUILIBRIUM ENHANCEMENT FOR LOW (1 MG C/L), TORCH LAKE C <sub>T</sub> LEVEL (30-32 MG C/L)	77
FIGURE 6-11 H&B ENHANCEMENT VERSUS TEMPERATURE, WITH V <sub>x</sub> HELD AT, V <sub>x-20</sub> = 0.56.	78
FIGURE 6-12 H&B ENHANCEMENT VERSUS TEMPERATURE, WITH INPUT V <sub>x</sub> ALSO	78
FIGURE 6-13 THE HOOVER AND BERKSHIRE (1969) ENHANCEMENT FACTOR AS A FUNCTION OF AIR EXCHANGE VELOCITY, WITH ALL OTHER INPUTS HELD CONSTANT AS NOTED.	79
FIGURE 8-1 CARBON CYCLE IN BIOLOGICAL PROCESSES IN TORCH LAKE MODEL.	85
FIGURE 9-1 THE FRACTION OF PHOSPHORUS THAT IS ADSORBED TO PARTICULATE CaCO <sub>3</sub> (F <sub>p</sub> )	97
FIGURE 10-1 MODEL OUTPUT (LINE) AND DATA (CIRCLE) FOR THE STATE VARIABLE,	102
FIGURE 10-2 MODEL OUTPUT (LINE) AND DATA (CIRCLE) FOR THE STATE VARIABLE,	102
FIGURE 10-3 MODEL OUTPUT FOR THE STATE VARIABLE, TOTAL INORGANIC CARBON (C <sub>T</sub> ), OVER TIME.	103

FIGURE 10-4 MODEL OUTPUT (LINE) AND DATA (CIRCLE) FOR THE CALCULATED VARIABLE, pH, OVER TIME. .....	103
FIGURE 10-5 MODEL OUTPUT (LINE) AND DATA (CIRCLE) FOR THE CALCULATED VARIABLE, .....	104
FIGURE 10-6 MODEL OUTPUT (LINE) AND DATA (CIRCLE) FOR THE CALCULATED .....	105
FIGURE 10-7 MODEL OUTPUT (LINE) AND DATA (CIRCLE) FOR THE CALCULATED VARIABLE, TURBIDITY, OVER TIME.....	105
FIGURE 10-8 MODEL OUTPUT (LINE) AND DATA (CIRCLE) FOR THE CALCULATED VARIABLE, .....	106
FIGURE 10-9 MODEL OUTPUT (LINE) AND DATA (CIRCLE) FOR THE CALCULATED VARIABLE, .....	106
FIGURE 10-10 CHANGE IN THE SATURATION INDEX AT EACH MODEL TIME STEP DUE TO AIR EXCHANGE, PRIMARY PRODUCTION OR THE TEMPERATURE CHANGE. NPP = 4 MGC/M <sup>2</sup> /DAY .....	111
FIGURE 10-11 CHANGE IN THE SATURATION INDEX AT EACH MODEL TIME STEP DUE TO AIR EXCHANGE, PRIMARY PRODUCTION OR THE TEMPERATURE CHANGE. NPP = 26 MGC/M <sup>2</sup> /DAY .....	111
FIGURE 10-12 CHANGE IN THE CALCITE PRECIPITATION RATE AT EACH MODEL TIME STEP DUE TO AIR EXCHANGE, PRIMARY PRODUCTION, OR THE TEMPERATURE CHANGE. NPP = 4 MGC/M <sup>2</sup> /DAY .....	112
FIGURE 10-13 CHANGE IN THE CALCITE PRECIPITATION RATE AT EACH MODEL TIME STEP DUE TO AIR EXCHANGE, PRIMARY PRODUCTION, OR THE TEMPERATURE CHANGE. NPP = 26 MGC/M <sup>2</sup> /DAY .....	113

## Chapter 1 : Introduction

Autochthonous precipitation of calcite occurs commonly during summer stratification in calcareous lakes (Kalf, Koschel, Kelts and Hsü 1978, Weidemann et al. 1985). The extent of precipitation depends on both the degree of supersaturation and the presence of nucleation sites.

Supersaturation, which occurs when the product of the calcium and carbonate ion activities exceeds calcite's solubility product, depends on multiple factors. First, from a strictly physicochemical perspective, rising epilimnetic temperatures contribute to supersaturation by decreasing calcite's solubility product while shifting the inorganic carbon equilibrium towards more carbonate (Stumm and Morgan 1996). Second, in productive systems, photosynthetic uptake of carbon dioxide raises the pH with an attendant shift of inorganic carbon speciation towards carbonate (Muller et al 2006, Ramisch et al. 1999, Hodell et al 1998).

Although supersaturation is a prerequisite for precipitation, a large supersaturation of calcite is often observed in natural waters before precipitation actually occurs (Hodell et al 1998, Morel and Hering 1993). The level of oversaturation required is greatly reduced by the presence of seed particles. For example, picoplankton have been identified as providing surfaces for calcite nucleation in oligotrophic lakes (Obst, Dittrich and Kuehn 2006, Dittrich, Kurz and Wehrli 2004, Dittrich and Obst 2004, Yates and Robbins 1998, Thompson et al. 1997, Thompson and Ferris 1990). In addition, beyond providing

nucleation sites, picoplankton may also enhance precipitation by creating a favorable microenvironment which may provide increased local saturation levels and other surface characteristics supporting nucleation (Dittrich and Obst 2004, Dittrich, Kurz and Wehrli 2004, Thompson et al. 1997, Hartley et al. 1995, Thompson and Ferris 1990)

Once formed, calcite has a number of environmental impacts. Because of their size and optical properties, calcite crystals settle slowly and scatter light very efficiently. As a consequence, they remain in suspension with a significant reduction in water clarity. The phenomenon is commonly called a “whiting” due to the characteristic milky-white color imparted to the water by the calcite crystals (Kalff 2002). In addition to aesthetic impacts, the reduction in light penetration has both biological (photosynthesis) and physical (heating) impacts.

Beyond water clarity and light transmission, calcite precipitation serves as a safety valve that moderates pH rises by removing carbonate. It is also known that both inorganic nutrients such as phosphorus as well as dissolved organic compounds can attach to calcite particles (Danenlouwerse et al 1995, House 1990, Kleiner 1988). In the short-term, this reduces the availability of these compounds for biological utilization. If the settling particles do not dissolve and are permanently buried in the lake’s bottom sediments, the process can enhance the long-term removal of calcium and inorganic carbon, as well as nutrients and organics (Dittrich and Koschel 2002).

The current study investigates the evolution of calcite precipitation for the epilimnion of an ultraoligotrophic, calcareous lake: Torch Lake (Michigan). The lake, which is noteworthy for its exceptional clarity, was chosen because it routinely experiences dramatic reductions in Secchi disk depth during the summer stratified period. Because it is so nutrient poor, the lake is particularly well-suited for assessing the impact of calcite precipitation on the water quality of a pristine, low-productivity lake.

An extensive data set consisting of physical, chemical and biological was collected during the summers of 2004-2006. A mass-balance model of the lake's epilimnion is employed to synthesize these observations and investigate the interactions of the various processes that generate and remove calcite and other chemical constituents during summer stratification. Along with the chemical budgets, a model of water transparency is also developed to link calcite precipitation to light extinction, turbidity, and Secchi disc depth. Multiple cross checks and triangulation methods were used to estimate bounds for the model parameters.

The proposed driver for calcite precipitation in many lake studies of calcite precipitation has been the increase in pH due to CO<sub>2</sub> removal during primary production (Muller et al 2006, Ramisch et al. 1999, Hodell et al. 1998,). Given the ultraoligotrophic conditions and related low productivity of Torch Lake, the questions we proposed to evaluate with this model was whether the seasonal temperature change could instead be the driver of the calcite precipitation in this lake. Using the model to analyze the interactions of the basic biological, physical and chemical processes affecting the lake's

carbon cycle, we assert that CO<sub>2</sub> loss to the air shifts the carbonate cycle towards precipitation more than phytoplankton growth. Temperature also acts as driver by both directly affecting the rate of calcite precipitation as well as affecting the rates of air exchange and phytoplankton growth.

Chapters 2 and 3 provide background on Torch Lake and a description of the data used in this study. A description of the structure of the Torch Lake model is covered in Chapter 4, followed by analysis of the key processes affecting calcite precipitation in Chapters 5 through 9. The results and discussion of the model analysis is found in Chapter 9.

## Chapter 2 Torch Lake Background

Torch Lake is located in Antrim County, Michigan, in the lower peninsula of Michigan to the east of Grand Traverse Bay (Figure 2-1). The glacial lake is deep and elongated with a residence time of about a decade. It is noted for its exceptional beauty because of its unusually clear and turquoise-hued waters. This quality has made the lake a popular spot for the development of resorts and second homes. The lake is part of a chain of three lakes where the active Three Lakes Association (TLA) was formed in 1967 and has been coordinating water quality management efforts since then.

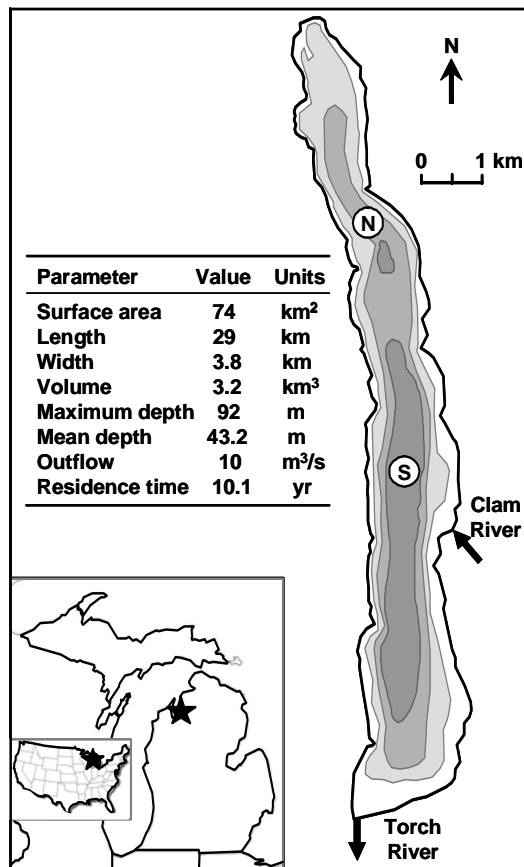


Figure 2-1 Torch Lake, Michigan. The inset provides a summary of the lake's characteristics



**Figure 2-2 Photograph of sailboats on Torch Lake, June 2006.**

As summarized in Table 2-1, Torch Lake is ultraoligotrophic with very low levels of total phosphorus (average 2.5  $\mu\text{g/L}$ ) and phytoplankton biomass (average 0.5  $\mu\text{g/L}$  chlorophyll a). In addition, the lake is high in calcium (1 mM, 40 mg/L) and alkalinity (2.7 meq/L, 135 mg/L as  $\text{CaCO}_3$ ), both typical for lakes in the area and similar to neighboring Lake Michigan.

**Table 2-1 Chemical, biological and optical characteristics of Torch Lake, MI.**

Parameter	Value	Units
Alkalinity	2.7	meq/L
	135	mgCaCO <sub>3</sub> /L
Calcium	1	mM
	40	mg/L
Total phosphorus	0.08	mM
	2.5	ugP/L
Summer chlorophyll a	0.5	ugChla/L
Secchi depth		
Spring	12	m
Late summer	5	m

The Torch Lake watershed, which includes the other two lakes upstream in the chain of lakes, Lake Bellair and Clam Lake, covers over 76,000 acres. The area is 60% forest and less than 0.5% developed, with the remaining area split between grassland, wetland and cropland.

The lake has a shallow littoral zone which drops off into a deep central trench. The lake bathymetry data has been plotted as area and volume over depth and is shown in Figure 2-3. As is typical for lakes in the north temperature climate, the lake is stratified between June and October with the thermocline at a depth of 10-15 meters.

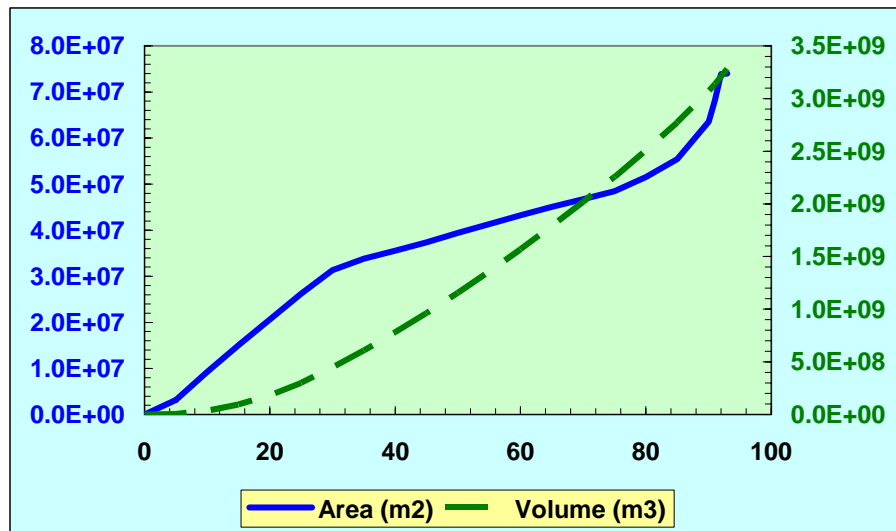


Figure 2-3 Torch Lake Area and Volume vs. Depth

Although it is certainly ultraoligotrophic from the standpoint of nutrients and phytoplankton biomass, the lake experiences a consistent decrease in clarity every summer. As depicted in Figure 2-4, the Secchi disk decreases from 12 meters to 5 meters over the period from late May through late August. This reduction is due overwhelmingly to calcite precipitation.

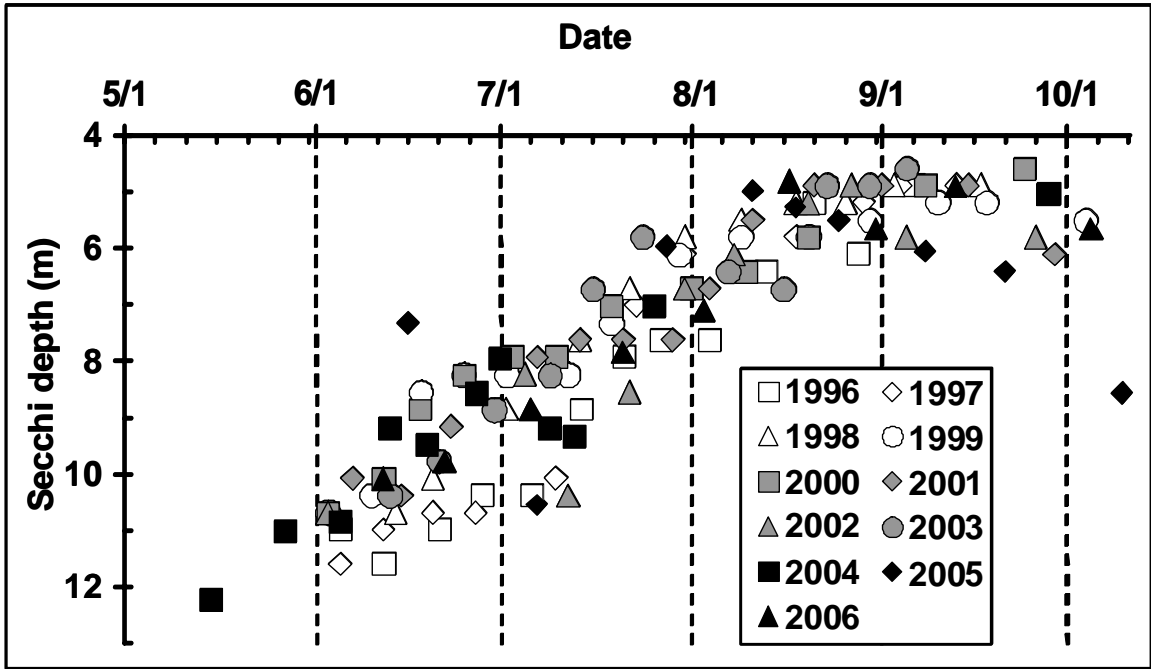


Figure 2-4 Secchi disc depth (m) versus date for Torch Lake, Michigan collected by the Tip of the Mitt Watershed Council from 1996 – 2006.

## Chapter 3 Torch Lake Data

Historically a number of studies of Torch Lake have been done over the years. The data used in this study comes from three different field collection efforts. The three studies are summarized in Table 3-1. They include sediment cores taken in 2002, a comprehensive water quality study done in 2004-05 and data collected in 2006 specifically for this study of calcite precipitation in the lake. These are described in more detail below.

**Table 3-1 Summary of the Torch Lake Data used in this study.**

Type	Year	Source
Sediment Core	2002-03	Michigan State University
Comprehensive Sampling	2004-05	TLA and GLEC
Calcite Study	2006	TLA, MWRC, Tufts University
Particle Analysis	2006	UFI

TLA	Three Lakes Association
GLEC	Great Lakes Environmental Center
UFI	Upstate Freshwater Institute
MWRC	Michigan Water Research Center

### **2002 Sediment Core**

Sediment cores of Torch Lake, shown in Figure 3-1, were collected in 2002 as part of a Michigan State University study of trends in the sediment quality of Michigan lakes. (Yohn et al 2003) The sedimentation rate for Torch Lake of 447 g/m<sup>2</sup>/yr, along with the calcium (31.2%) and phosphorus (0.035%) content of the cores, was used to calibrate the

calcite settling velocity parameter (Chapter 7) and the coprecipitation rate (Chapter 9) in the model.



Figure 3-1 Sediment core collected from Torch Lake in 2002. (Yohn et al. 2003)

## 2005 Water Quality Study

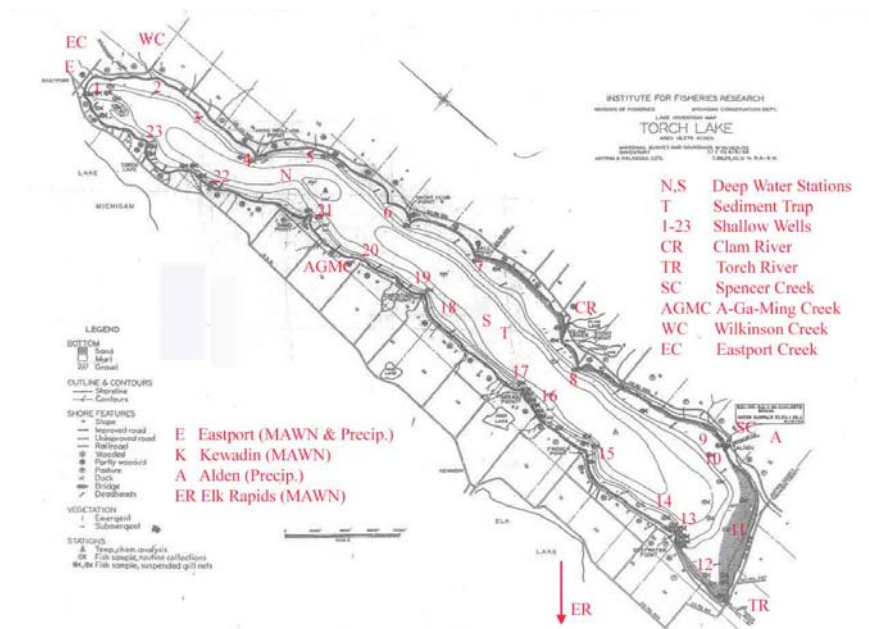


Figure 3-2 Monitoring and Sampling Locations for Torch Lake (Endicott et al. 2006)

In 2004 and 2005 the Three Lakes Association (TLA) and Great Lakes Environmental Center (GLEC) undertook a study that included comprehensive field data collection. The monitoring and sampling locations are shown in Figure 3-2. From July of 2004 through October of 2005, pH, DO, temperature, and conductivity were measured at various depth in the water column. Lake samples were collected and analyzed for total phosphorus (TP), nitrogen, chlorophyll a. TP was also measured in tributaries, groundwater and lake sediments. (Hannert et al 2004) Flow measurements were taken at all tributaries as well as in groundwater in order to calculate a water budget (Figure 3-4), phosphorus budget and provide data required to develop a predictive water quality model for the lake. A forcing function was used to add inorganic suspended solids (ISS) to the water column over time since the model did not include the creation of calcite by precipitation.

Component	Annual loading or loss, kilograms	% of P loading	% of P loss
Tributary loading	1590	33	
Groundwater loading	1480	31	
Atmospheric deposition	1770	37	
Settling loss	4120		83
Torch River outflow	830		17

**Figure 3-3 Phosphorus mass balance for Torch Lake for November 2004 - October 2005 ( Endicott et al. 2006)**

Flow Component (inflows and outflows)	Annual flow (cubic foot <sup>1</sup> per second, cfs)	% of water source	% of water loss
Clam River	289	72	
Spencer Creek	11	3	
Other minor tributaries	3	1	
Precipitation	47	12	
Groundwater seepage	52	13	
Torch River outflow	354		88
Evaporation	48		12

(1) Note: 1 cubic foot = 7.5 gallons

**Figure 3-4 Hydrologic Budget for Torch Lake for November 2004 - October 2005.  
( Endicott et al. 2006)**

### ***2006 Data Collection for Calcite Study***

Missing from the 2004-05 data set was any measure or characterization of particulates in the water column or determination of calcite in the sediment traps. “Fine white powder” had been found in the sediment traps set in 2005, but the lab analysis did not include a measure of calcium or inorganic carbon. In order to study the calcite precipitation event each summer both of these measures were conducted as well as the necessary water quality measurements to quantify the carbon and calcium cycles in the lake. A detailed description of the field collection methods follows.

From June 8<sup>th</sup> to September 13<sup>th</sup>, 2006, samples were collected by a field team from the Three Lakes Association at the same location in the South Basin of Torch Lake every two weeks. The various data collected are summarized in Table 3-2. Temperature, pH, conductivity, and DO data were collected with a Hydrolab Quanta® every 3 meters to a

depth of 30m, then every 10m to bottom. A volume weighted average was calculated from these measurements for the epilimnion and hypolimnion.

Lake samples were collected with a Vandorn Sampler at three different depths (2m, 6m and 10m) and then composited as an epilimnion sample. The same was done at depths of 40m, 50m, and 60m for the hypolimnion. Subsamples of each composite were used to measure turbidity, particulate calcium, dissolved calcium and alkalinity for both the epilimnion and hypolimnion. The turbidity was measured on board with a Hach 2100P Portable Turbidimeter.

Approximately 500 mL of each composite was filtered on board through Gelman Nylaflo 0.45um, 47mm filters. The filters were then sent to A & L Great Lakes Laboratories, where they were digested in nitric acid, diluted to approximately 25mL and analyzed for mg/L Calcium by ICP-MS. The amount of particulate calcium found on the filter in relation to the exact amount of lake water filtered was used as the measurement of the particulate calcite concentration.

Subsamples of each composite were also sent to the Michigan Water Research Center for determination of dissolved calcium by EDTA titration and alkalinity by titration.

Light extinction was measured every 3 meters to a depth of 36m or until 1% of the top measurement was reached with a Licor LI193SA Spherical Quantum Sensor and

LI250A Light Meter. Secchi disk was measured by two different individuals and the average taken of these measurements.

**Table 3-2 Summary of the 2006 Data Collection by TLA**

Dates	Data	Equipment	Location Processed
6/8	Ion Balance	Vandorn Sampler	Great Lakes Environmental Center
6/8 - 9/13	Alkalinity, Calcium	Vandorn Sampler	Michigan Water Research Center
6/8 - 9/13	pH, cond, DO, Temp	Hydrolab	On Board.
6/8 - 9/13	Light Extinction	Licor	On Board.
6/8 - 9/13	Secchi Disk Depth	Secchi Disk	On Board.
6/22 - 9/13	Turbidity	Vandorn Sampler -> Turbidity Meter	On Board.
6/22 - 9/13	Particulate Calcium	Vandorn Sampler -> Filters	A & L GREAT LAKES LABORATORIES
7/21 - 9/13	Particle Distriubtions	IPA / SAX	Upstate Freshwater Institute

A four-inch diameter cylindrical sediment trap was set at a depth of 40 meters on 6/26/06 and was retrieved on 10/5/06. The contents were analyzed at GLEC for total dry mass (1.28 g), magnesium (0.01 %) and calcium (42%).

These data measurements are shown in the results section of Chapter 9 in comparison to model predicted values.

### ***2006 Particle Distribution Data***

In order to quantify the number and volume of calcite particles in Torch Lake as well as provide a view of the shape of the calcite particles, a collaboration with the Upstate Freshwater Institute (UFI) provided an opportunity to conduct further particle analysis.

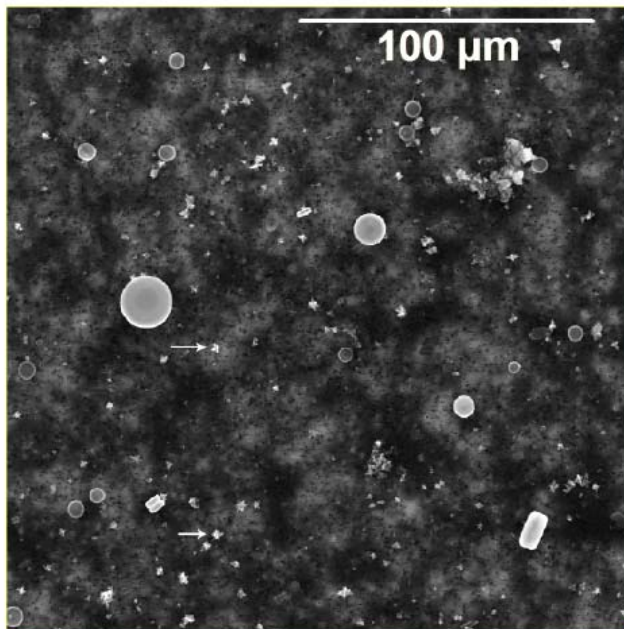
The biweekly samples collected from June to September, 2006 at a 2m depth were sent overnight in a foam un-iced cooler to the Upstate Freshwater Institute for analysis.

There the samples were analyzed using individual particle analysis conducted with scanning electron microscopy interfaced with automated image and X-ray analyses (IPA/SAX). The analysis provided valuable data on the morphometry (size and shape) and elemental composition of the particles. The particles were assigned to eight categories based on mineral composition, including a 'Ca-rich' type corresponding to  $\text{CaCO}_3$  precipitates, and a 'Ca-agg' type defined as " $\text{CaCO}_3$  coating on other particles". Particle distributions were generated both by number and by volume. For additional detailed information on the methods used see Peng and Effler 2005.

## Data

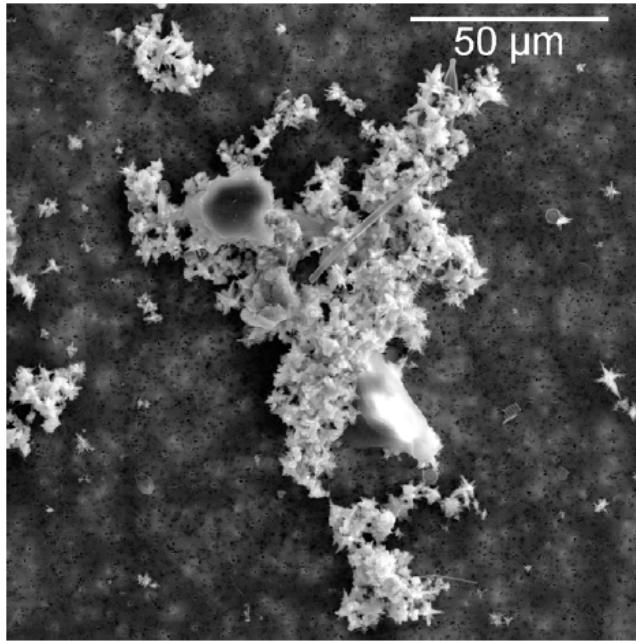
### Torch Images

Microscopic images of the Torch Lake particles are shown below in Figure 3-5 to Figure 3-7.



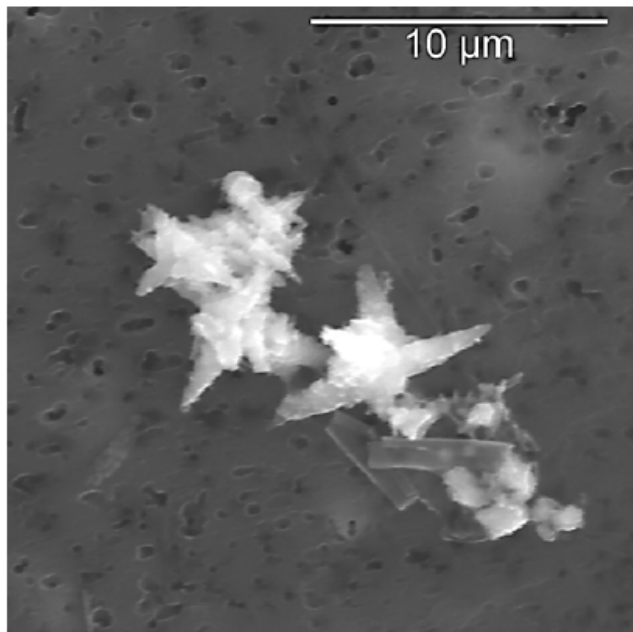
In this sample (7/6/06, E-2m), centric diatoms are abundant, and calcite particles (e.g., as indicated by arrows) are present.

**Figure 3-5 Sample taken 7/6/06 at 2m depth in Torch Lake, MI**



Calcite particles, and other particles, form aggregates in this sample (8/3/06, E-2m), with.

**Figure 3-6 Sample taken 8/3/06 at 2m depth in Torch Lake, MI.**



A closer look at the calcite particles detected by SAX in Torch Lake.

**Figure 3-7 Closer view of sample taken 8/3/06 at 2m depth in Torch Lake, MI.**

## Particle Distribution Data

Two types of data for the particle distributions were produced by UFI:

Particle Size Distribution,  $F(d)$  (particles / L / mm)

Particle Volume in each bin ( $\text{mm}^3/\text{L}$ )

The two distribution types were generated for both ‘all particles’ and ‘calcium particles’. The label ‘calcium particles’ represents the sum of the two calcium containing particle types: ‘Ca-rich’ and ‘Ca-agg’. The Particle Size Distribution (PSD) is expressed as the numbers of particles per unit volume divided by the (size) bin width ( $\Delta d$ ), so that  $F(d) (\Delta d)$  gives the numbers of particles per unit volume in each size bin.

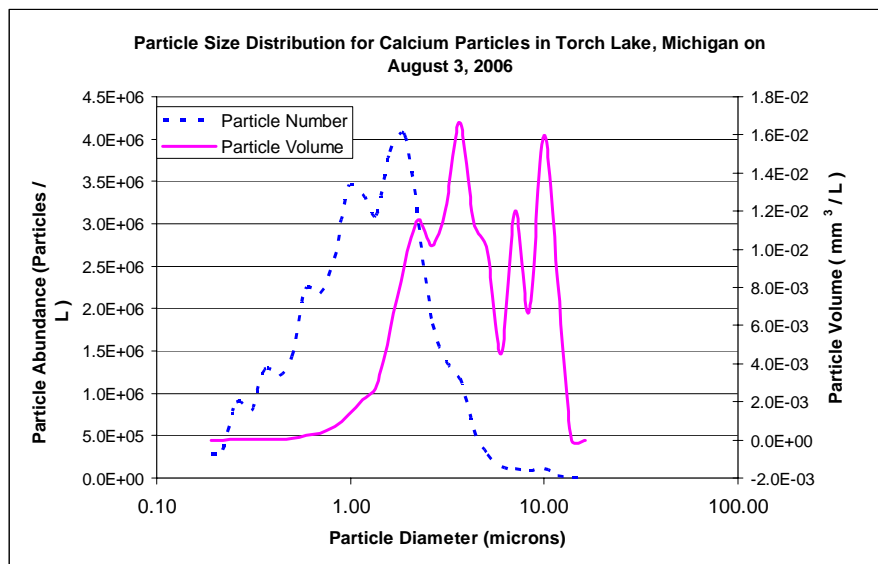


Figure 3-8 Plot of both distribution types for the calcium particles, sampled on August 3, 2006.

Figure 3-8 shown above is a plot of both the particle size distribution and particle volume in each bin for the calcium particles sampled on one representative date: August 3, 2006. The “Particle Number” series is a plot of the number of particles per liter in a bin vs. the median diameter for that bin, calculated from the product  $F(d) \cdot \Delta d$  as described above. The “Particle Volume” series is a plot of the particle volume ( $\text{mm}^3/\text{L}$ ) in a bin vs. the median diameter for that bin.

The plots show a peak number of particles around 2 microns and two peaks in volume in the range of 8 to 10 microns. Data published by Vanderploeg and Eadie for Lake Michigan particle distributions calculated from samples taken in September 1978-82 and 1985 show peak number between 2 and 4 microns and one peak volume around 8 microns, which is consistent with the particle sizes shown here in Torch Lake. (Vanderploeg and Eadie 1986).

### **Summary Data - Raw**

Key data for each 2m depth sample is shown below in Table 3-3 and is plotted in Figure 3-9 and Figure 3-10. The median particle diameter ranges from 0.7 to 1.2 microns and does not demonstrate a discernable trend over time. The particle volume per liter of lake water ranges from 0.03 to 0.4  $\text{mm}^3/\text{L}$ . However, the low value of 0.03  $\text{mm}^3/\text{L}$  occurred on 8/31 when other data described below indicate an unusual diatom count, or possible data entry error, which needs to be considered in interpreting all data for that sample date. The particle count and turbidity values over time are plotted in Figure 3-9 and Figure 3-10 respectively.

**Table 3-3 Summary IPA/SAX data for Torch Lake particles for each 2m depth sample.**

Date/Time	Turbidity (NTU)	Num/L	Vol. mm <sup>3</sup> /liter	Median Size (µm)
7/6/2006	0.42	5.32E+07	0.23	0.81
7/21/2006	0.84	4.75E+07	0.39	1.20
8/3/2006	1.05	5.00E+07	0.21	1.08
8/17/2006	0.4	6.47E+07	0.31	0.71
8/31/2006	0.23	6.47E+06	0.03	0.92
9/13/2006	0.86	8.56E+07	0.15	0.74

**Table 3-4 Percent of each particle category for all the Torch Lake particles.**

Date/Time	PAV Type Distribution (%)							
	Organics	Clay	Ca-rich	Quartz	Si-rich	Diatom	Ca-agg	Misc
7/6/2006	10.58	1.04	31.59		2.4	27.46	21.48	5.44
7/21/2006	0.82	0.91	72.56		0.09	10.51	13.05	2.06
8/3/2006	0.59	1.36	78.75		0.73	7.52	8.43	2.61
8/17/2006	7.64	0.95	64.66		1.32	2.82	16.65	5.96
8/31/2006	2.22	7.75	0.49	12.61	0.79	67.89	2.3	5.95
9/13/2006	0.09	1.25	86.43	0.47	0.04	3.9	6.62	1.19

Table 3-4 above shows the particle types found on each sampling date. (The PAV is the “total particle projected area per unit volume of water”. ) The Ca-rich and Ca-agg types are clearly the most abundant except for the presence of organics and diatoms at the beginning of July and the sample on 8/31/06 which is completely dominated by diatoms. The 8/31 sample is suspect given that the other data collected on the same date does not indicate any diatom bloom. Two possible explanations are either a data entry error (the numbers may have been entered in the wrong fields and should be swapped) or a non-representative cluster of diatoms was collected in the 2m depth UFI sample. Therefore the 8/31 data point has been removed from consideration. Figure 3-9 below shows the number of particles per liter of lake water over the sampling period.

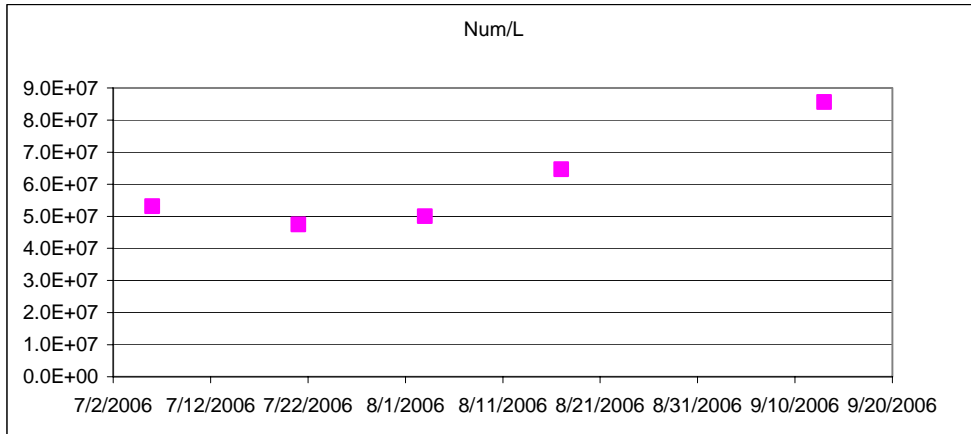


**Figure 3-9 Plot of the Torch Lake particle counts per liter over time.**

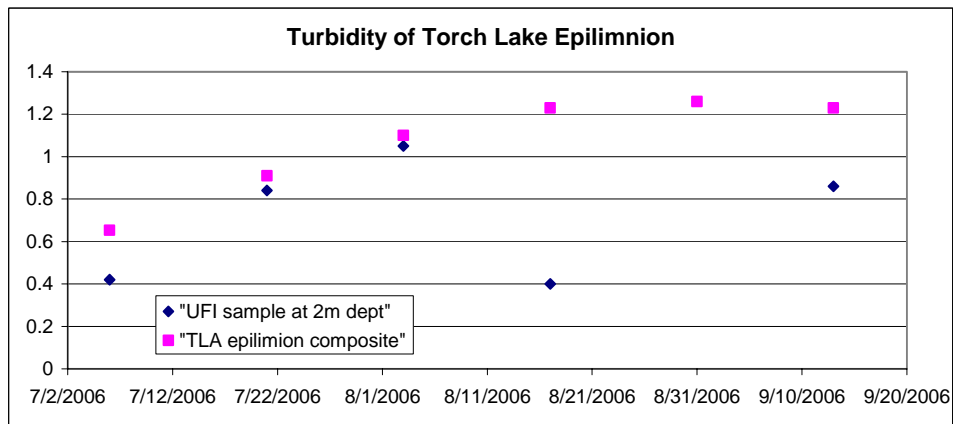


**Figure 3-10 Plot of Torch Lake turbidity over time.**

The UFI samples are individual samples at 2m and the measurement was done at the UFI lab. The TLA turbidity measurements were done on board within an hour of the sample collection which was a composite of three epilimnion depths: 2m, 6m and 10m. The turbidity measurements of the samples done by UFI show a dip on 8/17, but this is not seen in the turbidity measurements done by the TLA team.

## Summary Data – Calculated

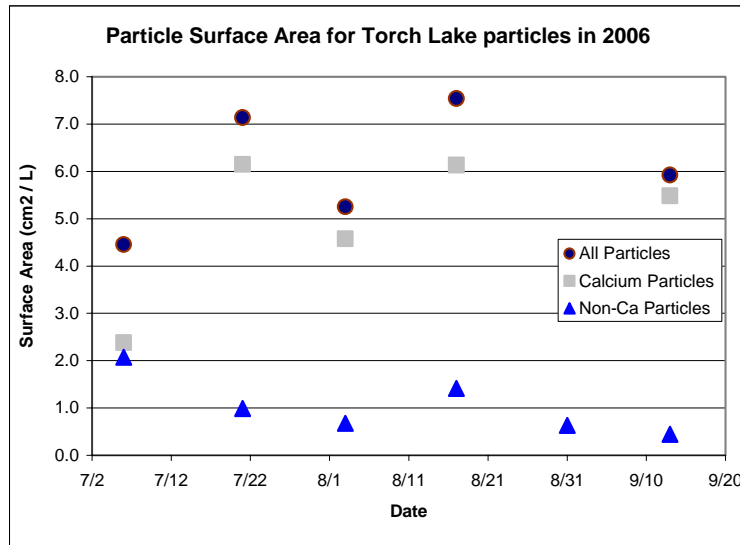


**Figure 3-11 Plot of the Particulate Surface Area over time, separated by all particles, calcium particles and non-calcium particles.**

The surface area per particle was calculated for each bin size, assuming that each particle is a sphere. The total surface area for a bin is the product of the number of particles per liter and the surface area per particle calculated from the mean diameter for each bin. The surface area (SA) for each date was summed across all the bin sizes of the surface area calculated in this way and the results are shown in Figure 3-11.

Note that the use of spheres to estimate the surface area should be a significant underestimate since the actual irregular shape of these particles would provide much more surface area than a sphere. There is additional uncertainty in the surface area estimates since particle types may be different shapes and therefore some types may be closer to a sphere than others. However the ratio between the possible sources of particulate surface area is valuable information.

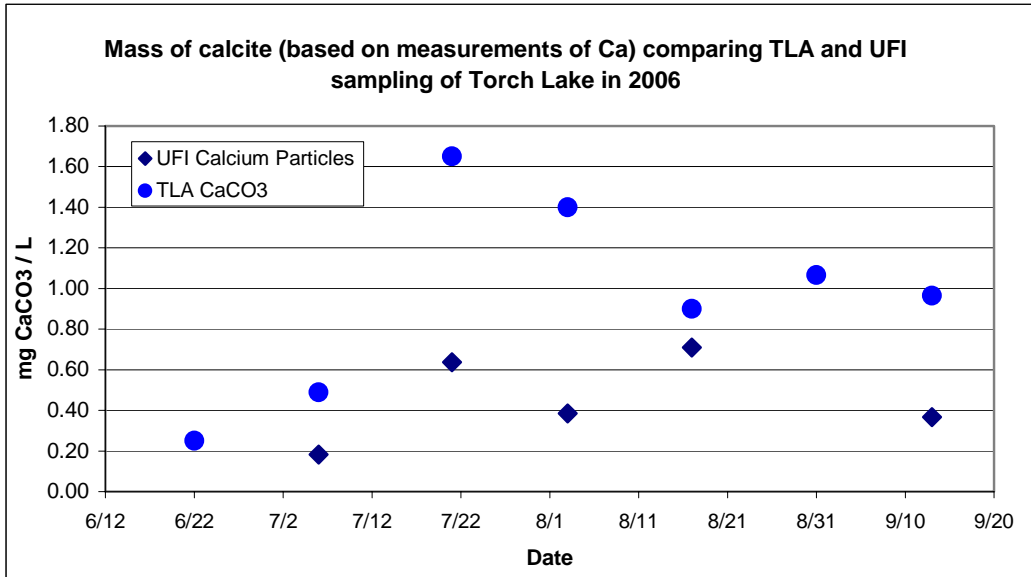


**Figure 3-12 Plot of calcite mass over time calculated from particle analysis of 2m depth samples (UFI) and from on board filtering of epilimnion composite samples (TLA).**

Figure 3-12 provides a comparison of two different estimates of the calcite in the lake over the sampling period. For the ‘TLA CaCO<sub>3</sub>’ data series the calcium mass was measured on the filters after immediate on-board filtering of epilimnion composite water samples. This measure of calcium was then extrapolated to CaCO<sub>3</sub> assuming that 100% of the calcium found was in the form of calcite. For the ‘UFI Calcium Particles’ data series the total volume per liter of the sum of “ca-rich” and “ca-agg” particles was converted to mass/L assuming that 100% of these calcium rich particles was calcite. This assumption is an upper bound, especially for the “ca-agg” type, representing calcite coated particles. The 7/22 and 8/1 samples are significantly higher for the TLA measurements than for the UFI data collected on those dates.

In summary, the particulate analysis conducted by UFI provides a view of the shape, size, abundance and constituents of particles in Torch Lake. The particles have long angular protrusions and tend to be grouped into loosely connected clusters. (Figure 3-7.) The median diameter of the particles is 2 microns and the volume weighted average diameters ranges 8-10 microns.

The data supports the choice of model structure and can be used to calibrate the surface area parameters, ratio of particles types (eg. plankton vs. calcite), and the amount of calcite suspended in the water column. When the calcium particle types are summed and converted from volume to mass using the density of calcite, this calculated mass (except for 7/22 and 8/1) is within 50% of the calcite mass estimates from the TLA particulate calcium measurements. (Figure 3-12).

## **Chapter 4 Introduction to the Torch Lake Model**

### ***Model Structure***

The Torch Lake model is a time variable mass balance model of the epilimnion of the lake from June to October, 2006. The use of mass balance modeling allows for an additional check on the structure and logic of the model since all mass must be accounted for by element.

The model was implemented using the pH2K structure which is described in detail in Appendix D. As shown in Figure 4-1, the epilimnion is represented as a completely-mixed volume. Only the epilimnion is included in this model in order to focus on the location of the change in water clarity and the calcite precipitation. The time is limited to June to October in order to focus on the timing of these events and not add complexity with a longer time horizon that may not increase our understanding of these summer events.

Particulates settle across the thermocline and gaseous species are transferred across the air-water interface. Flows in and out of the lake are not included here due to the long residence time of the water in the lake.

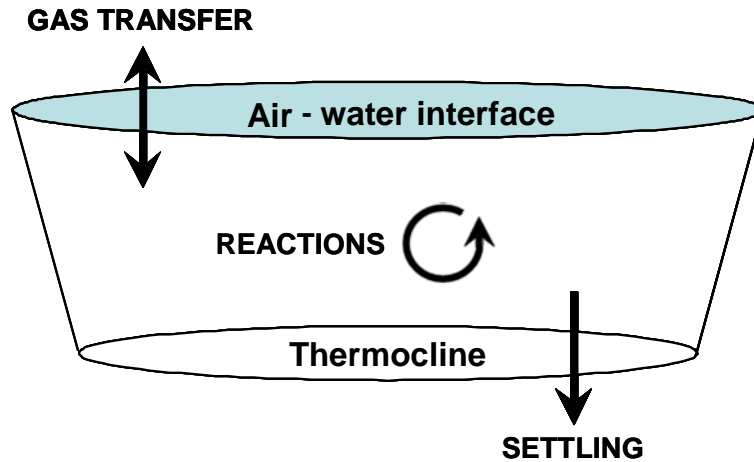


Figure 4-1 Process Diagram for the Torch Lake pH2K Model

### ***Model State Variables and Biochemical Processes***

The state variables selected for the model are the minimal set required for a basic eutrophication model and a representation of the inorganic process of calcite precipitation.

The eutrophication state variables include one aggregate variable representing all phytoplankton, measured as chlorophyll  $a$  ( $a_p$ ), inorganic phosphorus ( $p_i$ ) which is the limiting nutrient controlling growth in Torch Lake, and organic or detrital phosphorus ( $p_o$ ) which is the link in the recycle of phosphorus between the plankton and the inorganic, available form.

The calcite state variables include total dissolved inorganic carbon ( $c_T$ ) and total dissolved calcium ( $[Ca^{2+}]$ ) which determine the saturation level of calcite through the

calculation of pH and alkalinity. The last state variable in this set is that which tracks the amount of particulate calcite in the water column of the epilimnion ( $[CaCO_{3(s)}]$ ).

These model state variables are listed in Table 4-1. Note that concentrations are expressed in a variety of units.

**Table 4-1 Model state variables**

Variable	Symbol	Units*
Phytoplankton	$a_p$	$\mu\text{gChla/L}$
Detrital phosphorus	$p_o$	$\mu\text{gP/L}$
Inorganic phosphorus	$p_i$	$\mu\text{gP/L}$
Total inorganic carbon	$c_T$	M
Total dissolved calcium	$[Ca^{2+}]$	M
Calcite	$[CaCO_{3(s)}]$	M

\*  $\text{mg/L} \equiv \text{g/m}^3$ ,  $\mu\text{g/L} \equiv \text{mg/m}^3$ ; and  $\text{M} \equiv \text{mol/L}$ . In addition, the terms Chla and P refer to chlorophyll a and phosphorus, respectively.

The kinetic interrelationships between state variables are depicted in Figure 4-2 and the stoichiometry and kinetic interactions summarized in Table 4-2. The blue boxes in Figure 4-2 represent the state variables and the lines represent processes that result in a state change.

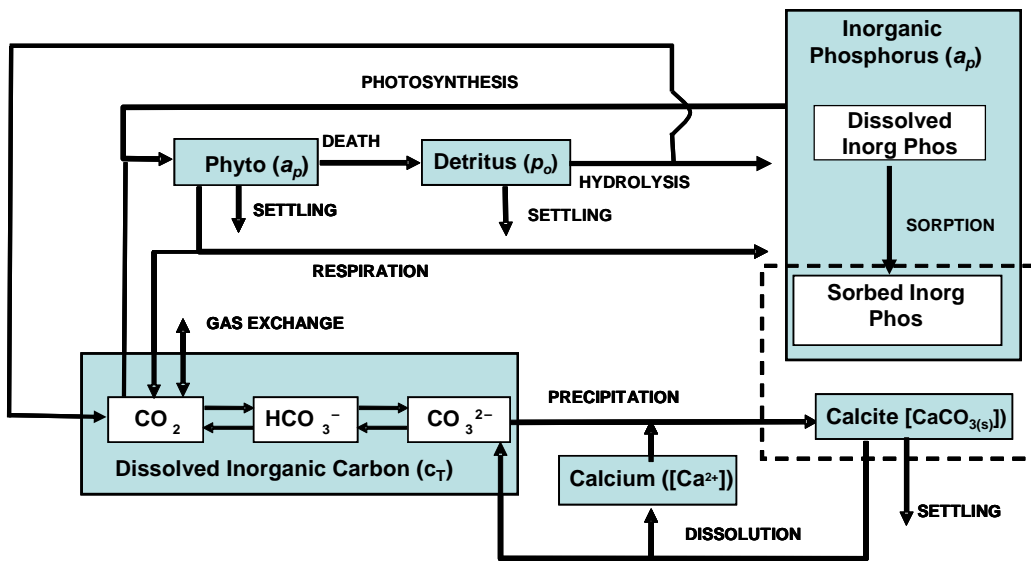


**Figure 4-2 State Diagram for the Torch Lake pH2K Model**

The state variable for phytoplankton ( $a_p$ ) increases through growth (photosynthesis) which decreases inorganic phosphorus and total inorganic carbon. The value of  $a_p$  decreases through phytoplankton settling out of the epilimnion, respiring, or dying. The death of phytoplankton increases  $p_o$ .

The state variable for detrital phosphorus ( $p_o$ ) increases, as mentioned above, through the death of phytoplankton. The value of  $p_o$  decreases when it settles out of the epilimnion or hydrolyzes to  $p_i$  and  $c_T$ .

The state variable for inorganic phosphorus ( $p_i$ ) increases, as mentioned above, through the hydrolysis of  $p_o$  or the respiration of phytoplankton. The value of  $p_i$  decreases through photosynthesis or coprecipitating (adsorption followed by settling) with calcite.

The state variable for total inorganic carbon ( $c_T$ ) increases through respiration by phytoplankton, hydrolysis of  $p_o$ , or dissolution of calcite. The value of  $c_T$  decreases through photosynthesis and the precipitation of calcite. The process of air-water exchange of  $\text{CO}_2$  could either increase or decrease  $c_T$  depending on the level of saturation of the water relative to the air.

The state variable for total dissolved calcium ( $[\text{Ca}^{2+}]$ ) increases with calcite dissolution and decreases with calcite precipitation.

The state variable for calcite ( $[\text{CaCO}_{3(s)}]$ ) increases with calcite precipitation and decreases with calcite dissolution or by settling out of the epilimnion.

**Table 4-2 Kinetic interactions and stoichiometry. Terms defined in chapter shown.**

Component→ Process↓	$a_p$	$p_o$	$p_i$	$c_T$	$[\text{Ca}^{2+}]$	$[\text{CaCO}_{3(s)}]$	Process rates, M/(L <sup>3</sup> T)	
Calcite precipitation				-1	-1	1	$k_f S([\text{Ca}][\text{CO}_3] - K_{sp})$	0
CO <sub>2</sub> gas transfer				1			$f v_x([\text{CO}_2]_s - [\text{CO}_2])$	Chapter 6
Calcite settling			$-K_{dp} F_d p_i$			-1	$v_s A([\text{Ca}][\text{CO}_3])$	Chapter 7 & 9
Photosynthesis	1		$-r_{pa}$	$-r_{ca}$			$k_g a_p$	Chapter 8
Respiration/excretion	-1		$r_{pa}$	$r_{ca}$			$k_{re} a_p$	"
Hydrolysis		-1	1	$r_{cp}$			$k_{hy} p_o$	"
Death	-1	$r_{pa}$					$k_{de} a_p$	"
Phytoplankton settling	-1						$v_a A a_p$	"
Detrital P settling		-1					$v_o A p_o$	"

## Computed Variables

As listed in Table 4-3, the state variables can be used to compute a number of secondary variables.

**Table 4-3 Computed variables.**

Variable	Symbol	Units*
Alkalinity	$Alk$	eq/L
Specific conductance	Cond	$\mu\text{S}\cdot\text{cm}^{-1}$
Carbon dioxide	$[\text{CO}_2]$	M
Bicarbonate	$[\text{HCO}_3^-]$	M
Carbonate	$[\text{CO}_3^{2-}]$	M
pH	pH	s.u.
Secchi depth	$SD$	m
Extinction coefficient	$k_e$	/m
Turbidity	$Turb$	NTU

**Alkalinity.** Alkalinity is calculated as the equivalent sum of the base cations minus the conjugate bases of the strong acids (Stumm and Morgan 1996),

$$Alk = Alk_{nc} + 2[\text{Ca}^{2+}] \quad (4-1)$$

where  $Alk_{nc}$  = the non-calcium alkalinity,

$$Alk_{nc} = 2[Mg^{2+}] + [Na^+] + [K^+] - [Cl^-] - 2[SO_4^{2-}] - [NO_3^-] \quad (4-2)$$

The non-calcium alkalinity is assumed to be constant.

**Specific Conductance.** Conductivity can be computed from the concentrations of the major ions (APHA 2005). First, the infinite dilution conductivity,  $Cond^0$  ( $\mu S/cm$ ), is calculated as

$$Cond^0 = \sum_{i=1}^n |z_i| \lambda_i mM_i \quad (4-3)$$

where  $\lambda_i$  = the equivalent conductance of the  $i^{th}$  ion ( $\mu S \cdot cm^2/eq$ )

$z_i$  = charge of the  $i^{th}$  ion

$mM_i$  = millimolar concentration of the  $i^{th}$  ion

The specific conductance can then be computed as

$$Cond = \gamma(1)^2 Cond^0 \quad (4-4)$$

where  $\gamma(I)$  = the monovalent activity coefficient. (See Appendix D)

**Extinction Coefficient.** The light extinction coefficient is related to model variables by (Di Toro 1978)

$$k_e = a + (1 - \gamma)b \quad (4-5)$$

where

a absorption coefficient [ $m^{-1}$ ]

b scattering coefficient [ $m^{-1}$ ]

$\gamma$  the fraction of particle scattering that is directly forward scattered [dimensionless]

Calcite contributes to scattering but not to absorption. See Appendix D for details on the calculations of the absorption and scattering coefficients.

**Secchi Depth.** The Secchi depth,  $SD$  (m), is calculated with,

$$SD = \frac{8.69}{k_e + c} \quad (4-6)$$

where  $c$  = the beam attenuation coefficient ( $m^{-1}$ ), which is equal to the sum of the absorption and scattering coefficients,  $c = a + b$ . See Appendix D for references.

**Turbidity.** Turbidity is calculated as,

$$T = Nb \quad (4-7)$$

where  $N$  ranges from 0.8 to 1.2 NTU m. See Appendix D for references.

This analysis will focus on the rates of five processes that impact the carbon cycle in the lake and therefore are potentially directly involved in the calcite precipitation process. In addition to calcite precipitation (0), the  $CO_2$  gas transfer sub model will be analyzed (Chapter 6), as well as calcite settling (Chapter 7), and its role as a removal mechanism for inorganic phosphorus (Chapter 9). The biological processes are summarized together (Chapter 8) in order to quantify their impact on the carbon cycle and thus on calcite precipitation.

For the calculation method used for pH and the carbon species, and for further details on the pH2K model see Appendix D

# Chapter 5 The Calcite Precipitation Rate

<b>CHAPTER 5 THE CALCITE PRECIPITATION RATE .....</b>	<b>32</b>
LITERATURE REVIEW .....	33
MODEL STRUCTURE .....	38
<i>Calcite Precipitation Rate Coefficient: <math>k_f</math></i> .....	39
<i>Calcite Saturation Level, <math>\gamma_2[Ca^{2+}][CO_3^{2-}] - K_{sp}</math></i> .....	40
<i>Particulate Surface Area, S</i> .....	41
Calcite Surface Area .....	41
Biomass Surface Area .....	43
ANALYSIS OF PRIMARY FACTORS.....	45
<i>Temperature</i> .....	48
Calcite Solubility Product: $K_{sp}$ .....	48
Carbonate Concentration: $[CO_3^{2-}]$ .....	51
A Note on pH.....	52
Calcite Precipitation Rate Coefficient: $k_f$ .....	53
<i>Primary Production</i> .....	54
<i>Air/Water Exchange of <math>CO_2</math></i> .....	54
CALIBRATION METHODS .....	55

This chapter will start with a literature review of calcite precipitation rate models. This will be followed by a detailed description of the structure of the rate equation selected for this study including how each subcomponent of the rate equation is modeled. External factors that drive the precipitation are introduced, including temperature and other physical and biological processes. The rest of the chapter is devoted to an analysis of the temperature dependence of the subcomponents of the rate model, including comparisons of how temperature drives the precipitation rate through each subcomponent.

## ***Literature Review***

Plummer (1978) developed a model of calcite dissolution and precipitation that has been widely used for many different applications – natural systems as well as controlled industrial applications. Plummer’s formulation is one of the most cited models of calcite precipitation kinetics, with over 400 citations as of May 2009. In contrast to other rate models, Plummer’s covers a broad range of conditions, from low to high pH and low to high total inorganic carbon ( $c_T$ ). Note, however, that his experiments were limited to low pH ( $\text{pH} < 7$ ) and most experiments were conducted with  $\text{pH} < 5$ .

The dissolution rate is represented as

$$r_d = k_1 \gamma_1 [H^+] + k_2 [H_2CO_3] + k_3 \quad (5-1)$$

where:

$r_d$	Dissolution rate
$k_1$	Plummer’s first dissolution rate coefficient

$\gamma_1$	Activity coefficient for hydrogen ion
$[H^+]$	Hydrogen ion concentration
$k_2$	Plummer's second dissolution rate coefficient
$[H_2CO_3]$	Concentration of carbonic acid
$k_3$	Plummer's third dissolution rate coefficient

In most cases only one of the three terms applies to a system. The  $k_1$  term applies to systems with very low pH (< 5) and also very low total inorganic carbon ( $c_T$ ), so that the rate is thus a first order function of the hydrogen ion concentration. The  $k_2$  term applies to systems with high carbonic acid (low pH and high  $c_T$ ) and the rate is a first order function of the carbonic acid concentration. The  $k_3$  term applies to conditions when pH > 7.5 where the simple hydration of calcite prevails and thus  $r_d = k_3$ .

In Plummer's model the reverse rate of dissolution (precipitation) near equilibrium is represented as

$$r_p = k_{-3}\gamma_2^2[Ca^{2+}][CO_3^{2-}] \quad (5-2)$$

where:

$r_p$	Precipitation rate
$k_{-3}$	Plummer's precipitation rate coefficient
$[Ca^{2+}]$	Concentration of dissolved calcium ( $mol/L$ )
$[CO_3^{2-}]$	Concentration of carbonate ( $mol/L$ )
$\gamma_2$	Activity coefficient for calcium and carbonate

The dissolution rate coefficient  $k_3$  is related to the precipitation rate coefficient  $k_{-3}$  through the solubility product for calcite ( $K_{sp}$ ).

$$k_3 = K_{sp} \cdot k_{-3} \quad (5-3)$$

where

$K_{sp}$  Solubility product for calcite

The net rate of precipitation that dominates in high alkalinity waters is shown to be consistent with the empirical rate equation used by many authors, given an order of  $n = 1$ .

$$r = r_p - r_d = k_{-3}(SI - 1)^n \quad (5-4)$$

where:

$SI$  Saturation Index

$n$  Reaction order

and

$$SI = \gamma_2^2 ([Ca^{2+}][CO_3^{2-}] / K_{sp}) \quad (5-5)$$

Inskeep and Bloom (1985) conducted an in-depth evaluation of calcite precipitation rate models. A set of 35 different experiments were run over a range of pH from 8.25 to 8.7 and this experimental data was used to analyze the applicability of various rate models. They concluded that the best results came from the Nancollas and Reddy (1971) rate model after the addition of the activity coefficient to account for ionic strength dependence. According to Inskeep and Bloom (1985) the model is only applicable for  $pH > 7.5$  when dissolution is solely a function of  $H_2O$  attack. (Dissolution by carbonic acid and  $H^+$  do not need to be considered.)

$$R = \gamma_2^2 k_f S ([Ca^{2+}][CO_3^{2-}] - K_{sp} \gamma_2^{-2}) \quad (5-6)$$

Inskeep and Bloom (1985) note that Plummer's (1978) model becomes identical to the Nancollas and Reddy (1971) model when applied to systems with  $pH > 7.5$  if the bulk pH equals the pH at the surface of the particles where precipitation and dissolution are

taking place. Thus  $k_f S$  in equation (5-6) is equivalent to Plummer's precipitation rate coefficient  $k_{-3}$  shown in equation (5-2).

Chou, L., Garrels, R. M., and Wollast, R. (1988) replicated the experiments of Inskeep and Bloom (1985) with a fluidized bed reactor and found Plummer's model to be the best fit to their data. They proposed that surface concentrations should be used and these could be estimated since the surface concentrations were proportional to bulk solution concentrations. Chou et al. confirmed that only the  $k_3$  term in the Plummer rate model was needed to represent a system with  $\text{pH} > 7.5$ .

De Pinto et al 1989 used the full Plummer dissolution model for developing models to predict the reacidification of calcite treated lakes. The pH of these acid lakes is often very low so, unlike most natural waters, the  $k_1$  and  $k_2$  terms in the Plummer model also applied to these conditions.

Compton and Pritchard (1990) applied Plummer's model to their experimental results but, like Chou et al (1988), replaced all the bulk concentrations with concentrations at the surface of the particles. The surface concentrations were measurable under the very specific hydrodynamic conditions they maintained in their experiment. However it is unclear how this surface concentration approach could be applied generally. Either extensive lab research for each system would be required or many simplifying assumptions to the model would result in reverting to the use of the bulk concentrations.

Plummer's model has become a standard reference for modeling the rate of precipitation and dissolution in the carbonate system. For example, Plummer's model is presented in Wollast's (1990) chapter on the carbonate system and the model is used in software packages such as "phreeqc" and "Visual MINTEQ".

Much literature suggests possible inhibitors to calcite precipitation such as dissolved organic carbon (DOC) (Mueller et al 2003, Lebron and Suarez 1996, Inskeep and Bloom 1986) and inorganic phosphorus (Lin and Singer 2005, Plant and House 2002, House 1987). These limiting factors are not considered in this study since the levels required to inhibit precipitation are not reached in highly oligotrophic Torch Lake. This is potentially a model limitation and an area that should be addressed if the model is applied to systems with higher DOC or inorganic phosphorus levels.

Recent research on calcite rate models by Lin and Singer has included use of surface complexation models to predict calcite precipitation rates. (Lin and Singer 2005) The use of different partial reaction orders for the activity of carbonate versus the activity of calcium has also been proposed in order to account for the effect of the changes in  $c_T/Ca$  ratio on the precipitation rate (Lin and Singer 2005, Nilsson 1999). Teng (2000) conducted analyses of calcite crystal growth mechanisms using Atomic Force Microscopy and determined that different mechanisms of crystal growth take place at different levels of supersaturation (eg. spiral growth vs. two dimensional surface nucleation).

In summary, more detailed mechanistic models are being developed as new approaches and new technology are applied to gain understanding of the chemical, physical and biological processes involved in calcite dissolution and precipitation. However, with only basic data available from a lake water quality study, forms of Plummer's basic precipitation rate model are still useful for representing calcite dissolution and precipitation kinetics.

### **Model Structure**

The rate equation used in this study is that proposed by Inskeep and Bloom (1985) as the best fit for natural waters with high alkalinity and pH > 8. The precipitation rate is driven by the dissolved concentrations of calcium and carbonate in relation to the solubility product, as well as the particulate surface area available for crystal growth. This model is consistent with the rate equations proposed by both Plummer (1978) and Nancollas and Reddy (1971) for the pH and  $c_T$  levels found in Torch Lake.

$$\text{Precipitation} = \gamma_2^2 k_f S [Ca^{2+}] [CO_3^{2-}] \quad (5-7)$$

The dissolution rate for this pH level (> 8) is a fixed rate.

where $k_f$	Precipitation rate coefficient (L <sup>2</sup> /mol/m <sup>2</sup> /min)
$S$	Available particulate surface area (m <sup>2</sup> /L)
$[Ca^{2+}]$	Concentration of dissolved calcium (mol/L)
$[CO_3^{2-}]$	Concentration of carbonate (mol/L)
$\gamma_2$	Activity coefficient for divalent ions

$$Dissolution = k_f S \cdot K_{sp} \quad (5-8)$$

where  $K_{sp}$  Solubility product for calcite,  $10^{-8.33}$  at  $T = 25^\circ\text{C}$  ( $\text{mol}^2/\text{L}^2$ )

The net rate is the sum of the two equations.

$$Net\ Precipitation = k_f S (\gamma_2^2 [Ca^{2+}] [CO_3^{2-}] - K_{sp}) \quad (5-9)$$

### **Calcite Precipitation Rate Coefficient: $k_f$**

The precipitation rate coefficient for the Torch Lake model was estimated by calibration. Both chemical data (alkalinity, calcium, carbon, pH, particulate calcium) and optical data (turbidity, Secchi depth, light extinction) were compared with model predictions in order to determine a value for  $k_f$  of  $80,000 \text{ L}^2/\text{mol}/\text{m}^2/\text{day}$ .

The value of  $k_f$  used in the Torch Lake model an order of magnitude or two smaller than rate coefficients published for experimental work (see Table 5-1), but was determined to be reasonable given time lags in mixing and other processes in lakes that may result in conditions different from a laboratory experiment. The temperature dependence of this parameter will be described later in this chapter.

**Table 5-1 Reported experimental rate coefficients for calcite precipitation and dissolution.**

Name	pH	Temp	k-precip	log(k-precip)	k-diss	log(k-diss)	k-precip
		C	L2/mol/cm2/s		mol/cm2/s		L2/mol/m2/day
Stumm & Morgan	8	20	2.49E-03	-2.60	8.78E-12	-11.1	2.2E+06
Plummer 1978	< 7	20	3.41E-02	-1.47	1.20E-10	-9.9	2.9E+07
Compton 1990	> 7	20	2.70E-02	-1.57	9.50E-11	-10.0	2.3E+07
L. Chou 1989	> 7	20	1.85E-02	-1.73	6.50E-11	-10.2	1.6E+07
Inskeep & Bloom (1985)	8.4	20	1.18E-02	-1.93	4.16E-11	-10.4	1.02E+07

### Calcite Saturation Level, $\gamma_2[Ca^{2+}][CO_3^{2-}] - K_{sp}$

As we can see from the structure of the rate equation shown in equation (5-9), the level of oversaturation in this model is the driving force of calcite precipitation. When the system is at equilibrium, the  $(\gamma_2[Ca^{2+}][CO_3^{2-}] - K_{sp})$  term is equal to zero and no net precipitation occurs. (We should note that chemists will point out that reactions in both directions are still occurring, but they balance each other at this equilibrium point.)

An alternate variable that is often used to indicate the degree of oversaturation is the Saturation Index (*SI*). This is defined as the ratio of the product of the  $Ca^{2+}$  and  $CO_3^{2-}$  activities, or Ion Activity Product (*IAP*), and the Solubility Product for calcite,  $K_{sp}$ . An *SI* value of 1 indicates that the system is at equilibrium since the *IAP* and  $K_{sp}$  are equal.

$$IAP = \{Ca^{2+}\} \{CO_3^{2-}\} = \gamma_2[Ca^{2+}][CO_3^{2-}] \quad \text{Ion Activity Product}$$

$$SI = IAP / K_{sp} \quad \text{Saturation Index}$$

Thus, the oversaturation level is a function of the calcium concentration, the pH, the total inorganic carbon ( $c_T$ ) and temperature.

## **Particulate Surface Area, S**

The particulate surface area available for calcite precipitation is modeled as the sum of the surface area provided by existing calcite particles and the surface area provided by non-calcite particles such as picoplankton.

$$S = S_c + S_p \quad (5-10)$$

where  $S_c$  and  $S_p$  = the volume-specific surface areas ( $\text{m}^2/\text{L}$ ) of calcite particles and non-calcite particles, respectively. As described by Kalff (2002), picoplankton (i.e., plankton between 0.2 and 2  $\mu\text{m}$ ) are the dominant form of plankton in ultraoligotrophic lakes such as Torch Lake.

### **Calcite Surface Area**

The value of calcite surface area is estimated in the model from the state variable for the mass of calcite, which is converted to surface area by using density, assuming a spherical shape and an average particle diameter.

The particle-specific surface area and volume for spherical particles can be computed as

$$S_p = \pi d_p^2 \left[ = \frac{\mu\text{m}^2}{\text{particle}} \right] \quad (5-11)$$

$$V_p = \frac{\pi d_p^3}{6} = \frac{\mu\text{m}^3}{\text{particle}} \quad (5-12)$$

where  $d_p$  is in  $\mu\text{m}$ . The particle-specific mass can then be computed as

$$m_p = \rho_p V_p \left[ = \frac{\text{g}}{\text{cm}^3} \times \frac{\mu\text{m}^3}{\text{particle}} \times \frac{10^6 \text{cm}^3}{\text{m}^3} \times \frac{\text{m}^3}{10^{18} \mu\text{m}^3} = 10^{-12} \frac{\text{g}}{\text{particle}} = \frac{\text{pg}}{\text{particle}} \right] \quad (5-13)$$

where  $\rho_p$  is in  $\text{g}/\text{cm}^3$ . The number of particles per liter is calculated as

$$n_p = \frac{c}{m_p} = \frac{c}{\rho_p V_p} = \frac{6c}{\rho_p \pi d_p^3} = \frac{6}{\pi d_p^3 \rho_p} c \left[ = \frac{\text{mg particle}}{\text{L}} \times \frac{\text{pg}}{10^{-12} \text{g}} \times \frac{\text{g}}{10^3 \text{mg}} = 10^9 \frac{\text{particle}}{\text{L}} \right] \quad (5-14)$$

where  $n_p$  = number of particles per unit volume ( $10^9$  particles/L). The surface area per liter can then be computed as

$$S = n_p S_p = \frac{6}{\pi d_p^3 \rho_p} c \times \pi d_p^2 = \frac{6}{\rho_p d_p} c \quad (5-15)$$

$$\left[ = 10^9 \frac{\text{particle}}{\text{L}} \times \frac{\mu\text{m}^2}{\text{particle}} = 10^9 \frac{\mu\text{m}^2}{\text{L}} \times \frac{\text{m}^2}{10^6 \mu\text{m}^2} = 1000 \frac{\text{m}^2}{\text{L}} \right]$$

Therefore, the general formula in units of  $\text{m}^2/\text{L}$  is

$$S = \frac{6}{1000 \rho_p d_p} c \quad (5-16)$$

To apply this value to specific particle types, a conversion is required to convert from the particles units to  $\text{mg}/\text{L}$ . For calcite expressed as mole/L,

$$c = r_{dc}[\text{CaCO}_3(\text{s})] \quad (5-17)$$

where

$$r_{dc} = \frac{100 \text{ gCaCO}_3}{\text{mole}} \times \frac{1000 \text{ mgCaCO}_3}{\text{gCaCO}_3} = 100,000 \frac{\text{mgCaCO}_3}{\text{mole}} \quad (5-18)$$

Therefore, the formula for calcite is

$$S_c = \frac{6}{1000\rho_c d_c} r_{dc}[\text{CaCO}_3(\text{s})] \quad (5-19)$$

Substituting  $r_{dc} = 100,000 \text{ mgCaCO}_3/\text{mole}$ ,  $\rho_p = 2.711 \text{ g/cm}^3$ ,  $d_p = 1.8 \text{ }\mu\text{m}$ ,

$$S_c = \frac{6}{1000(2.711)1.8} 100,000[\text{CaCO}_3(\text{s})] = 122.956 \times [\text{CaCO}_3(\text{s})] \quad (5-20)$$

## Biomass Surface Area

Picoplankton have been identified as providing the primary surfaces for calcite nucleation in oligotrophic lakes. (Dittrich and Obst 2004, Dittrich, Kurz and Wehrli 2004, Thompson et al. 1997, Hartley et al. 1995, Thompson and Ferris 1990). Dittrich et al. (2004) suggest that different picoplankton drive different mechanisms of precipitation. Some picoplankton become completely covered in calcite and produce particles with small holes where the picoplankton had been. [Note: I'm not sure that I understand what you mean by the previous sentence. Please reword to clarify.] Other picoplankton have

calcite form on their cell walls but then peel away once the particle reaches a certain size, allowing the cells to remain viable.

Since the microscopy images for Torch Lake showed no evidence of holes in the particle surfaces, the latter model (i.e., particle growth followed by separation) is assumed to hold. The surface area on which calcite precipitation occurs is either existing calcite crystals or picoplankton cell walls.

For the Torch Lake model the amount of fixed background surface area provided by non-calcite particles (i.e., picoplankton or other suspended particulate) is set at  $1 \text{ cm}^2/\text{L}$  throughout the model time horizon. This amount is based on the surface area of non-Ca particles in the Torch Lake 2006 UFI particle distribution data plotted in Figure 3-11. The calcite surface area is computed dynamically with Eq. (5-20).

Figure 5-1 shows the model estimate of the surface areas compared to the surface area values from the UFI particle distribution data, and the values calculated from the TLA particulate calcium measurements converted to surface area using equation (5-20). Note that the UFI surface area data is lower than the TLA calculated surface area. This outcome was not unexpected given that the UFI calcite mass calculations were also lower than TLA particulate calcium mass data as shown in Figure 3-12. This may be explained by the 24+ hour time period that elapsed while the water samples were shipped to UFI for processing. Hence, dissolution of some of the calcite particles may have occurred. The

TLA particulate calcium measurements were taken from filters through which water samples were filtered on board within two hours of collection.

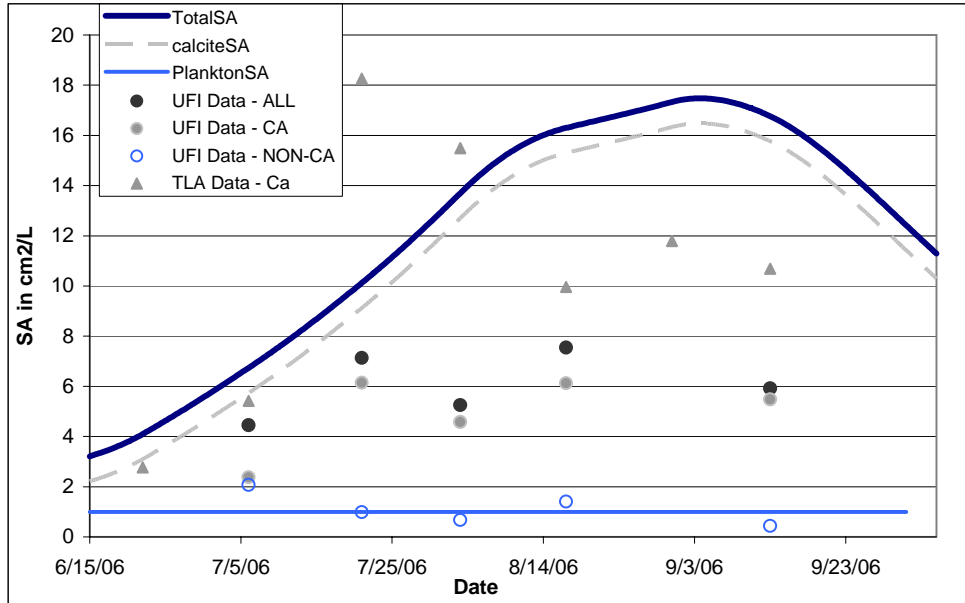


**Figure 5-1 Plot of the model estimates of surface area (lines) compared to surface areas calculated from UFI data (circles) and TLA data (triangles), over time.**

In addition, beyond providing nucleation sites, picoplankton may also enhance precipitation by creating a favorable microenvironment which provides increased local saturation levels and other surface characteristics supporting nucleation. (Dittrich and Obst 2004, Dittrich, Kurz and Wehrli 2004) This is an area of current research and beyond the scope of this study which uses only bulk concentrations.

### ***Analysis of Primary Factors***

Further analysis of the precipitation rate model can provide insight into the potential impact of different factors on the calcite precipitation rate for a given system. These factors include temperature, primary production and air exchange.

Figure 5-2 shows the factors affecting the rate of calcite precipitation. The circles correspond to external factors, with solid lines representing an instant/direct effect and a dotted line representing an indirect effect. Temperature interacts with the precipitation rate through many different mechanisms. The mechanisms can be separated logically into two categories – the mechanisms through which temperature directly affects the precipitation rate, and the mechanisms through which temperature indirectly affects the precipitation rate by affecting biological and atmospheric exchange processes.

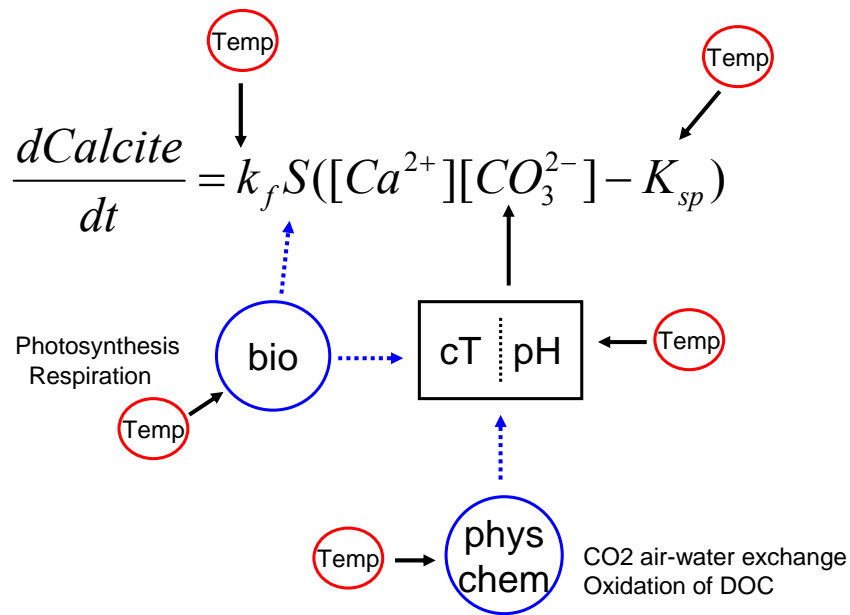


**Figure 5-2 Temperature dependence of processes impacting the calcite precipitation rate.**

The direct effects of temperature on the precipitation rate take place through chemical equilibrium reactions that occur instantly. These direct effects, shown in Figure 5-3, occur through the temperature dependence of the solubility product of calcite ( $K_{sp}$ ), the temperature dependence of the equilibrium constants for the carbonate system ( $K_1$  and  $K_2$ ) and the increase of the precipitation reaction rate itself which is represented here as a temperature dependence of the rate coefficient  $k_f$ .

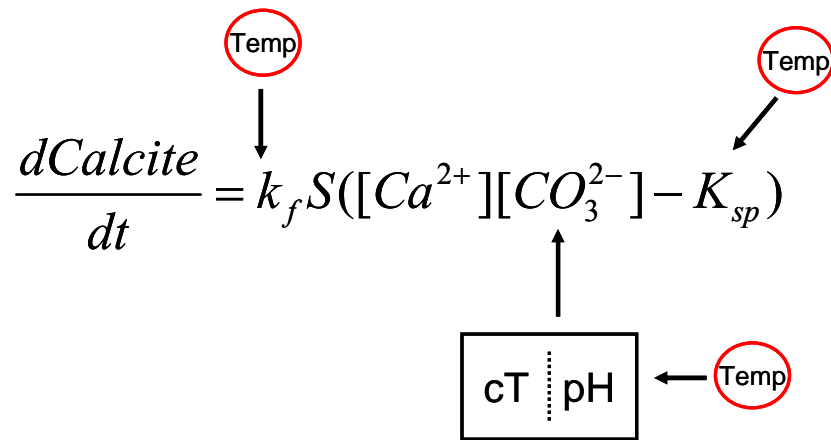


Figure 5-3 Direct effects of temperature on the calcite precipitation rate.

The indirect effects of temperature on the precipitation rate occur through the biological processes of photosynthesis and respiration and the physiochemical process of air-water exchange of carbon dioxide. These processes affect the precipitation rate through the removal or additional of carbon dioxide which shifts the carbonate equilibrium (adding/removing  $c_T$  and decreasing/increasing  $\text{pH}$ ), potentially changing the  $\text{CO}_3^{2-}$  concentration in the water and thus the degree of calcium carbonate saturation. In

addition, the dotted line from the biological processes to the surface area term represents the phytoplankton providing particulate surface area for the growth of calcite.

## **Temperature**

Temperature directly affects the precipitation rate through various mechanisms as shown in Figure 5-3. Through all three mechanisms, described in detail below, an increase in temperature increases the rate of calcite precipitation.

## **Calcite Solubility Product: $K_{sp}$**

The most commonly referenced effect of temperature on calcite precipitation is the decrease in the calcite solubility product ( $K_{sp}$ ) with increased temperature. The sensitivity of the  $K_{sp}$  for calcite to temperature is shown in Figure 5-4. Note that there is also variation between reported values of  $K_{sp}$  at the standard temperature of 20°C.

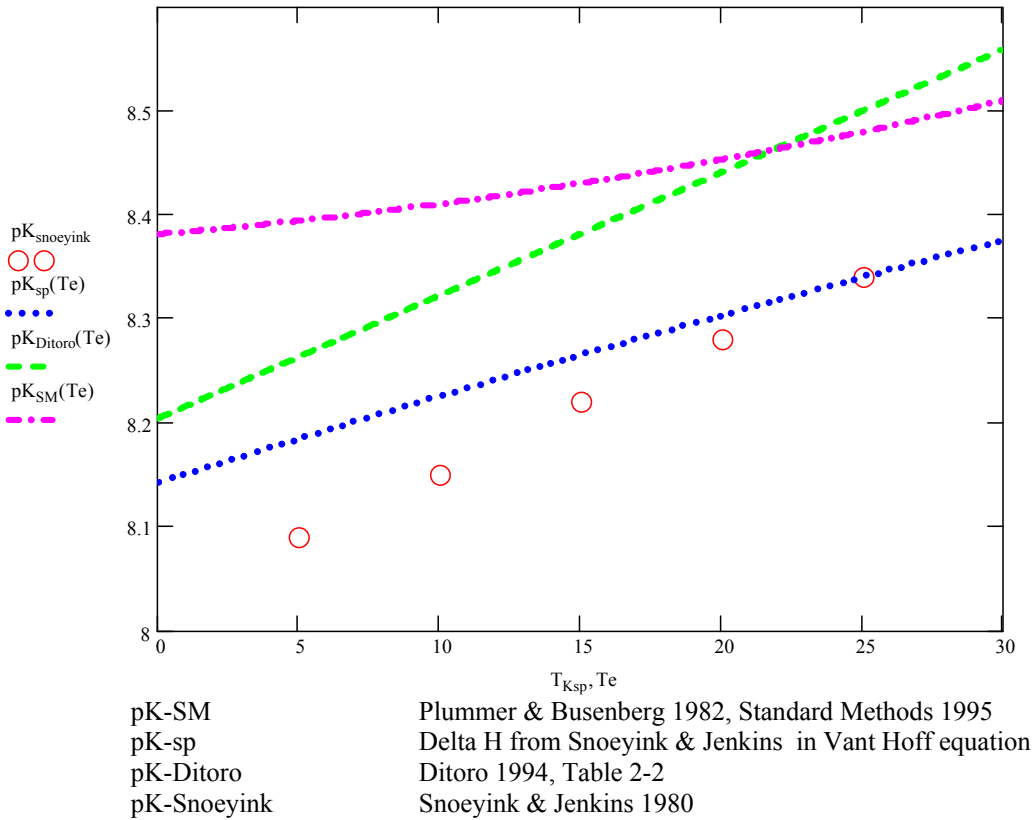


**Figure 5-4 Various equations for the temperature dependence of calcite pKsp.**

Various experiments have been conducted documenting the solubility product of calcite as a function of temperature. (Snoeyink and Jenkins 1980, Plummer and Busenberg 1982, Di Toro 1995, Stumm and Morgan 1996) The most extensive and most often cited study was conducted by Plummer and Busenberg (1982) and their resulting temperature dependent equation for the solubility of calcite is used in Standard Methods. (Standard Methods 1995). Note that the  $pK_{sp}$  values increasing with temperature reflect a decreasing  $K_{sp}$  which means that the solubility of calcite decreases with increasing temperature. This is atypical of a salt as the solubility of most salts increases with temperature.

The equation from Plummer & Busenberg 1982, shown in Equation (5-21), was selected for use in the model since it is used by Standard Methods and is the most in-depth and most often cited study available to date.

$$pK = 171.9065 + 0.077993T_a - \frac{2839.319}{T_a} - 71.595 \log(T_a) \quad (5-21)$$

where:  $T_a$  = absolute temperature (K)

Note that a change in the  $K_{sp}$  affects the saturation level,  $(\{Ca^{2+}\}\{CO_3^{2-}\} - K_{sp})$ , which then drives the precipitation rate. Thus, for fixed amounts of calcium and carbonate, a decrease in the solubility product will increase the degree of saturation and increase the precipitation rate.

An example based on conditions in Torch Lake was calculated with fixed levels of total inorganic carbon at 33 mgC/L, alkalinity at 138 mg/L as  $CaCO_{3(s)}$ , calcium at 43 mg/L, and the carbonate equilibrium based on a temperature of 10°C. Using the equations describe above, a temperature increase from 5 to 20°C increases the Saturation Index ( $SI = IAP/K_{sp}$ ) from 3.7 to 4.3 ( $\Delta SI = 0.6$ ). Note that this change in the SI is solely through the change in the solubility product due to temperature dependence and not through the carbonate equilibrium since the  $K_1$  and  $K_2$  values for the carbonate system have been held constant at a temperature of 10°C. This represents a 5.5 % change in the precipitation rate which can be compared to the mechanisms that follow.

### **Carbonate Concentration: [ $CO_3^{2-}$ ]**

A change in temperature also causes a shift in the carbonate species equilibrium as shown by the temperature dependence of the carbonate equilibrium constants,  $K_1$  and  $K_2$ . With a fixed amount of total inorganic carbon and a fixed amount of alkalinity, an increase in temperature will increase the proportion of inorganic carbon in the form of carbonate,  $CO_3^{2-}$ . Equations for these carbonate equilibrium constants can be found in Plummer and Busenberg (1982).

Like the solubility product, a change in the carbonate concentration affects the calcite precipitation rate through a change in the degree of saturation, ( $\{Ca^{2+}\} \{CO_3^{2-}\} - K_{sp}$ ). A temperature increase causes an increase in the carbonate concentration which increases the saturation level. Thus temperature affects the saturation level through both the  $K_{sp}$  and the  $CO_3^{2-}$  concentration. These effects are in the same direction and additive.

With fixed levels of total inorganic carbon (33 mgC/L), alkalinity (138 mgCaCO<sub>3</sub>/L), and calcium (43 mg/L), and this time with the  $K_{sp}$  held fixed at a temperature of 10°C (approximating the temperature of Torch Lake in June), the temperature increase from 5°C to 20°C increases the  $SI$  from 3.9 to 4.1. Thus, due only to the higher  $[CO_3^{2-}]$ , a delta of 0.2 occurs. This result corresponds to a 5.8 % change in the precipitation rate.

The change in the Saturation Index when both  $K_{sp}$  and  $CO_3^{2-}$  concentration change with temperature is  $\Delta SI = 0.8$ . Combined, this is an 11.3 % change in the precipitation rate as the temperature increases from 5 to 20°C.

Note that it is important to be careful when interpreting an index such as *SI* since it is not an exact substitute for the saturation level ( $IAP - K_{sp}$ ) which has a linear relationship with the precipitation rate. The values summarized in Table 5-2 show the difference between the % change in the *SI* and the % change in the precipitation rate (represented in the table as the % change in the saturation level). It is interesting to note that although the *SI* increase was 4 times smaller due to the change in  $[CO_3^{2-}]$  compared to  $K_{sp}$ , the saturation level increase was close to the same as that of the temperature effect on  $K_{sp}$ . The calculation of percent change ends up being different due to the different denominator.

**Table 5-2 Summary of temperature change scenarios on SI and (IAP- $K_{sp}$ )**

	$\Delta SI$	SI % Change	$\Delta Sat$ Level	Sat Level % Change
$K_{sp}(T)$	0.6	17%	0.1	5.5%
$CO_3(T)$	0.2	4%	0.1	5.8%
Both	0.8	22%	0.2	11.3%

### **A Note on pH**

With a fixed amount of total inorganic carbon and a fixed amount of alkalinity, the shift in the carbonate equilibrium caused by an increase in temperature will also increase the concentration of  $H^+$ , which represents a decrease in the pH as shown in Figure 5-5. Note that, as described above, this shift in carbonate equilibrium results in an increase in  $[CO_3^{2-}]$ . This is counterintuitive since an increase in  $[CO_3^{2-}]$  is typically associated with

an increase in pH, not a decrease. Increases in pH due to changes in either  $c_T$  or alkalinity, at a fixed temperature, do cause an increase in  $[\text{CO}_3^{2-}]$ . For example, removal of  $\text{CO}_2$  causes a pH increase and an increase in the  $\text{CO}_3^{2-}$  concentration.

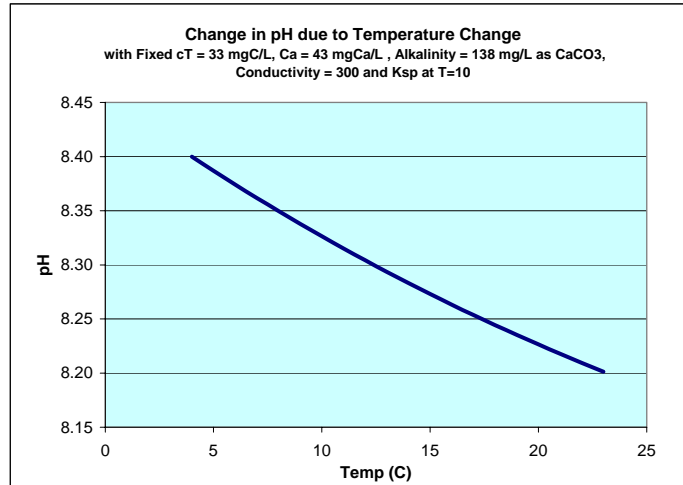


**Figure 5-5 A plot of pH as a function of temperature.**

### **Calcite Precipitation Rate Coefficient: $k_f$**

The temperature dependence of the precipitation rate is expected to follow the Arrhenius equation, which describes the change in the ratio of reaction rates  $r_1$  and  $r_2$  (in moles/m<sup>2</sup>/s) over a temperature range  $T_1$  and  $T_2$ . (Stumm and Morgan 1996)

$$\ln(r_2 / r_1) = E_a / R(T_2 - T_1 / T_1 \cdot T_2) \quad (5-22)$$

where  $E_a$  is the activation energy (kcal/mol), and  $R$  is the Boltzmann gas constant (kcal/mol/K). Putting the activation energy of 48.1 kJ/mol from Inskip and Bloom (1985) into theta form (Chapra 1997) and confirming that the results match the Arrhenius equation, the result is an equation for the rate coefficient as a function of temperature, with  $\theta = 1.072$ .

$$k(T) = k_f \cdot \theta^{(T-20)} \quad (5-23)$$

In order to compare the Arrhenius effect to the impact of temperature on the precipitation rate through the solubility product and carbonate equilibrium, we can again examine the temperature change from 5 to 20. At a temperature of 5°C,  $k(5) = 0.352 \cdot k_f$  and at 20°C,  $k(20) = k_f$ . So the Arrhenius effect of the increase in temperature of 15°C can cause the rate to increase by 84%, as compared to 5-6% in the examples of the temperature effects through the  $K_{sp}$  and  $[\text{CO}_3^{2-}]$  for Torch Lake described above.

### **Primary Production**

Growth of plants through photosynthesis removes  $\text{CO}_2$ , while respiration adds  $\text{CO}_2$ . For periods where net photosynthesis is positive, there is a net  $\text{CO}_2$  removal. This removal of  $\text{CO}_2$  reduces total inorganic carbon ( $c_T$ ) and raises pH. The result is increased  $\text{CO}_3^{2-}$  so oversaturation increases. The amount of phytoplankton growth determines the amount of  $\text{CO}_2$  removed. This growth in turn is determined by the availability of light and nutrients, as well as the temperature. This topic will be described in more detail in Chapter 8.

### **Air/Water Exchange of $\text{CO}_2$**

The exchange of  $\text{CO}_2$  between the air and water is driven by the degree of over or under saturation of the water with respect to the air. The equilibrium between the air and water

is defined by Henry's constant and is temperature dependent. The transfer coefficient represents the influence of wind and temperature on the air exchange rate which is independent of the state of the equilibrium. The removal of  $\text{CO}_2$  decreases total inorganic carbon in the system, and increases the pH. At a pH of  $\sim 8.3$  the result will be an increase in the species  $\text{CO}_3^{2-}$  due to the increase in pH, even though the total amount of carbon is lower. (Note that at different pH levels the result could be different.) Air water exchange will be discussed in more detail in Chapter 6. Analysis of the relative impacts of these factors will be presented in Chapter 10.

In summary, temperature as the largest direct effect on the calcite precipitation rate through the chemical reaction rate represented by the Arrhenius effect on the rate coefficient,  $k_f$ . The temperature dependence of  $K_1$  and  $K_2$  affects the precipitation rate about the same amount as the temperature dependence of  $K_{sp}$  for conditions found in Torch Lake. The precipitation rate can also be impacted indirectly through changes in total inorganic carbon ( $c_T$ ) due to primary production or the air water exchange of  $\text{CO}_2$ .

## ***Calibration Methods***

Various estimation techniques were used in order to check the model calibration of Torch Lake precipitation against all available data. These approaches are summarized in Table 5-3 and described below. Details of the calculations can be found in Appendix C

**Table 5-3 Summary of Torch Lake precipitation rate calibration methods.**

Method	Description	Equation	Data Used	Value
1	Dissolved calcium delta	$\Delta\text{Ca} * 100/40 / \Delta t$	Dissolved calcium	0.06 - 0.17
2	Alkalinity delta	$\Delta\text{Alk} / \Delta t$	Alkalinity	0.06 - 0.17
3	Conductivity delta	$\Delta\text{Cond} / \Delta t$	Conductivity	0.06 - 0.18
4	Accumulation + Settling	Accum = Precip - Settling	Sediment Trap, CaCO <sub>3</sub>	0.16 - 0.18
5	Accumulation + Settling	Accum = Precip - Settling	Sediment Core, CaCO <sub>3</sub>	0.10 - 0.12

A precipitation rate was first calculated solely based on the magnitude of the decrease in dissolved calcium over the time period of the calcite increase. This approach includes the assumption that all of the dissolved calcium is removed by incorporation into calcite. Considering a time horizon from 60 to 90 days and a range of calcium change from 2 to 4 mg/L, the resulting range in calcite precipitation estimated with this method was 0.06 to 0.17 mg/L/day.

The same approach was used again with alkalinity instead of calcium. A precipitation rate calculated solely based on the magnitude of the decrease in alkalinity over the time period of the calcite increase. This approach includes the assumption that all of the alkalinity is removed by incorporation of CO<sub>3</sub><sup>2-</sup> into calcite. The precipitation estimate from the alkalinity differential was the same as the estimate from the dissolved calcium differential, 06 to 0.17 mg/L/day. In other words, the alkalinity delta and dissolved calcium delta both reflect an equal amount of calcite precipitation, given that the changes in alkalinity and dissolved calcium were both changed primarily by calcite precipitation.

The third approach involved a rate calculated solely from the change in conductivity over the precipitation period. The calculation was done by starting with an initial pH, alkalinity and ion balance. The amount of total carbon was calculated from these as well

as the contribution of each ion to conductivity, using the method described in Standard Methods (1995). The total carbon, alkalinity and calcium ions were decreased by the given amount of calcite precipitation and the resulting pH and ion concentrations were used to calculate a new conductivity value. Considering a time horizon from 60 to 90 days and a range of conductivity change from 10 to 20 micro-ohms/cm, the resulting range in calcite precipitation estimated with this method is 0.06 to 0.18 mg/L/day.

The fourth estimation approach involved a mass balance summation using the sediment trap data as the amount settled and the ending calcite concentration as the amount accumulated. The precipitation rate was then calculated as the sum of settling and accumulation. The precipitation rate estimated in this way is 0.16 to 0.18 mg/L/day.

The final approach involved using a sedimentation rate from the MSU sediment core data. Using the flux rate that Long and Parsons calculated from their sediment core data, the settling rate was lower than the rate from the 2006 sediment trap flux used above. The amount of calcite settled using the 2006 trap was 9.2 to 13.7 mg/L whereas the amount settling using Parsons flux was 5.5 to 8.2 mg/L. The precipitation rate based on Parsons sediment core data (~0.11 mg/L/day) is more in line with the other estimation methods, as well as closer to the value used in the calibrated model. The precipitation rate calculated from the 2006 sediment trap data (~0.17 mg/L/day) is higher than the other estimation methods, possibly due to other mass in the trap that was not calcite (e.g., fine clay and silt particles).

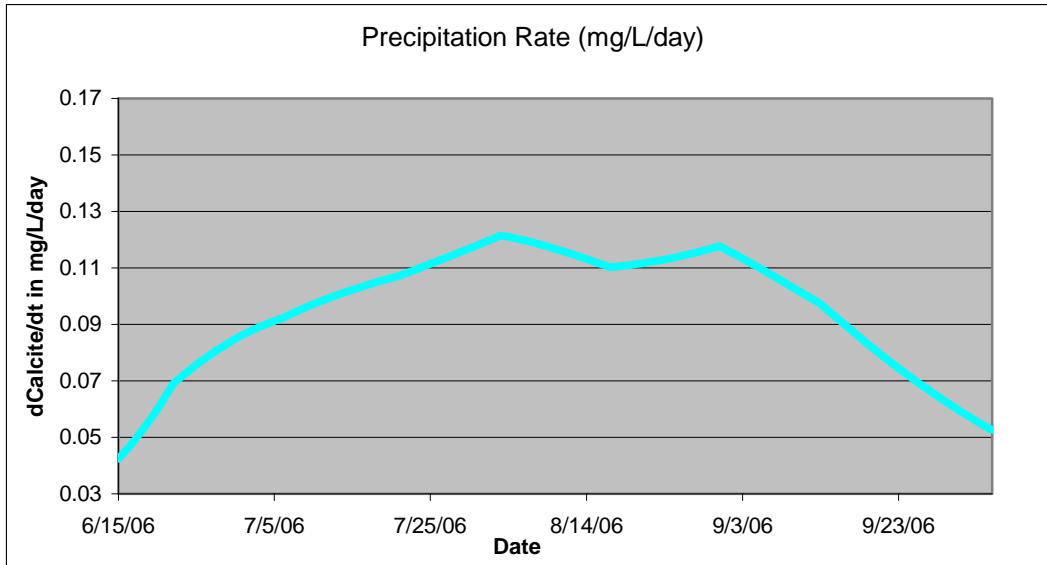


**Figure 5-6 Plot of the model estimate of the Torch Lake precipitation rate over time in mg/L/day  $\text{CaCO}_{3(s)}$ .**

Figure 5-6 shows the modeled precipitation rate over time, with an average value of 0.11 mg/L/day. As shown in Table 5-3, the rate estimations from the data were 0.06 to 0.17 mg/L/day. Ranges of precipitation rates reported for other lakes and normalized to comparable units are 0.2 +/- 0.1 mg/L/day. (Ramisch et al 1999, Holzbecher and Nutzman 2000). The modeled value is thus in the middle of the ranges using the three estimation methods described here, and consistent with rates published for other lakes.

## **Chapter 6 The CO<sub>2</sub> Air-water Exchange Rate**

As the Torch lake calcite model was developed in order to compare the impact of primary production versus temperature change, it became clear that air exchange is a significant process in driving calcite precipitation in Torch Lake. Details of the air exchange model are provided in this chapter, including temperature dependence of the model subcomponents.

The chapter starts with a literature review providing a brief history of air exchange models including air water exchange velocity models and models for chemical enhancement of CO<sub>2</sub> exchange. This is followed by a description of the how the mechanistic models for air exchange velocity and chemical enhancement were selected for this study. Details are then provided of the temperature dependence of these components of the air exchange rate, as well as of the oversaturation level.

The impact of the air-water exchange process will be compared to other factors in Chapter 10.

### ***Literature Review***

The boundary layer models of air-water gas exchange in lakes are based on diffusion of the gas across a thin-film boundary as the rate limiting step. The flux ( $J$ ) is a function of

the transfer velocity ( $v_x$ ) and the concentration differential between the air and water (Schwarzenbach et al 2003, Morel and Herring 1993, O'Connor 1983).

$$J = v_x ([CO_2]_{sat} - [CO_2]) \quad (6-1)$$

In the Whitman thin-film model the air-water transfer velocity ( $v_x$ ) for a liquid-film controlled gas, such as CO<sub>2</sub>, is equal to the ratio of the molecular diffusion coefficient of the gas in water ( $D$ ) to the thickness of the boundary layer ( $z$ ).

$$v_x = D / z \quad (6-2)$$

The boundary layer models include the assumption that the boundary-layer thickness,  $z$ , is independent of the gas being transferred. However the diffusivity of each gas in water is different. Thus the air-water exchange rate for one gas could be scaled to another by the ratio of their diffusion coefficients.

Experimental and field studies suggested that air-water exchange velocities were correlated to the wind speed over the water body. Many empirical models were developed relating the thickness of the boundary layer to the speed of the wind, typically standardized to 10m above the water surface. (Wanninkhof et al (1987), Schwarzenbach et al. 2003, and references there in.)

In addition to wind speed, more detail has been added to some mechanistic models of air-water exchange. In order to consider the impact of viscosity as well as wind speed on the boundary layer thickness, models were developed that separated the viscosity effect

which allowed for more accurate representation of the temperature dependence of the exchange rate. The dependence of the kinematic viscosity ( $\nu$ ) and the diffusivity ( $D$ ) on temperature were added to models most commonly as their ratio in the Schmidt Number,  $Sc = \nu / D$ . Models which use the Schmidt Number for gas or temperature conversions typically use a power relation of  $-1/2$  or  $-2/3$ . (O'Connor 1983, Wanninkhof 1991, Cole and Caraco 1998, Schwarzenbach et al. 2003)

O'Connor, Schwarzenbach and others developed models that define different regimes based on levels of wind speed due to the concept that the mechanisms governing the air-water exchange process change between conditions in a 'smooth surface' regime and a 'rough surface' regime. These regimes are based on wind speed and the resulting interactions between laminar and turbulent layers at the air-water interface. O'Connor proposed that a smooth surface regime applied to wind speeds below 6 m/s, whereas others such as Schwarzenbach proposed a cut off of 4.3 m/s. Additional research has focused on the low wind conditions (< 4 - 6 m/s) which are common for sheltered, inland lakes (Crusius and Wanninkhof 2003, Cole and Caraco 1998.).

For slowly reacting gases like oxygen, the exchange process is transport limited by the rate of diffusion through the film. For carbon dioxide gas exchange there is increasing evidence that carbonate equilibrium reactions are taking place in the boundary layer at rates that are comparable to or faster than the molecular diffusion step. Such reactions tend to enhance CO<sub>2</sub> transfer by adding curvature that increases the gradients within the film.

Emerson (1975) conducted experiments and introduced models that covered a range of chemical enhancement scenarios. In the first scenario, diffusion is significantly faster than the reaction rates and therefore the reactions do not need to be considered. In the second scenario the diffusion rates and reaction rates are comparable so both processes need to be taken into account. In the third scenario, the residence time of CO<sub>2</sub> in the boundary layer is long enough to reach equilibrium, so the total inorganic carbon ( $c_T$ ) in the water replaces the CO<sub>2</sub> concentration in the calculation of the saturation differential. Emerson reported enhancement factors ranging from 5 to 10 times what would be expected from diffusion alone.

Smith (1985) proposed that a high pH and thick boundary layer favor chemical enhancement of the CO<sub>2</sub> gas exchange rate and thus a strong chemical enhancement of CO<sub>2</sub> air-water exchange is possible. Wanninkhof and Knox (1996) measured CO<sub>2</sub> exchange rates in 5 lakes with a range of alkalinities (many extremely high) and concluded that chemical enhancement of CO<sub>2</sub> exchange was an important determinant of the CO<sub>2</sub> flux in these lakes, with an enhancement factor of up to 3 times.

Hoover and Berkshire (1969) modeled enhancement as a function of the transfer velocity, water temperature, the thickness of the boundary layer ( $z$ ), and pH. The model is typically implemented by measuring or modeling an exchange velocity,  $v_x$ , taking  $D$  as given for the gas under consideration and calculating  $z$  as  $D/k$ . Thus the Hoover and Berkshire model includes a relationship between  $z$  and the wind assuming  $v_x$  is a function

of wind speed. The model has been applied to many field and laboratory studies and been shown to be consistent with measured values (Wanninkhof and Knox 1996, Boutin et al. 1999, Kuss and Schneider 2004, Bade and Cole 2006). Wanninkhof and Knox (1996) conclude that the Hoover-Berkshire model offered a simple formulation that provided equally accurate results to alternate, more complex models.

Recent experiments continue to confirm the likelihood of the carbonate equilibrium reactions occurring in the boundary layer and thus influencing the flux rate of CO<sub>2</sub> air-water exchange. Boutin et al. (1999) evaluated the possibility of an enhancement effect on air-sea CO<sub>2</sub> flux and confirmed that models show a possible increase of 20% in CO<sub>2</sub> flux in equatorial regions where higher temperatures and calmer waters are favorable to enhancement. Kuss and Schneider (2004) conducted tank experiments to quantify the chemical enhancement of CO<sub>2</sub> flux by comparing conditions favorable (high pH) to unfavorable to enhancement (low pH). They fit their results to an empirical exponential equation, which showed a stronger relation to pH than the Hoover-Berkshire model, with enhancement factors ranging from 1.1 to 1.6 for their experimental conditions. Bade and Cole (2006) conducted whole-lake field experiments and estimated enhancement by comparing measurements of a reactive gas (CO<sub>2</sub>) and a non-reactive gas (CH<sub>4</sub>). They reported enhancement factors ranging from 3.5 to 7.5.

In summary, various mechanistic models for air-water exchange have evolved from the thin-film model. For CO<sub>2</sub>, the addition of models to predict of chemical enhancement

provides a means for improved accuracy for estimating the overall air water exchange rate.

### **Model Structure**

As discussed in the literature review section, there is general consensus on the overall structure of the air-water exchange rate of CO<sub>2</sub>, shown in equation (6-3). The air exchange rate of CO<sub>2</sub> is driven by the degree of disequilibrium between the CO<sub>2</sub> in the air and the CO<sub>2</sub> in the water, represented by  $[CO_2]_s - [CO_2]$ . The overall air-exchange rate is a product of the amount of this disequilibrium, the air-water exchange velocity, and a chemical enhancement factor.

$$AirExchange = f \cdot k_x ([CO_2]_s - [CO_2]) \quad (6-3)$$

where $f$	Chemical enhancement factor
$k_x$	Air-water exchange rate ( <i>/ day</i> )
$[CO_2]_s$	Saturation concentration of carbon dioxide ( <i>mol/L</i> )
$[CO_2]$	Concentration of carbon dioxide ( <i>mol/L</i> )

As shown in Figure 6-1, similar to the calcite precipitation process, the air-water exchange rate is affected both directly (instantly) and indirectly by temperature. The indirect impacts on air exchange include the same biological processes affecting calcite precipitation since they are both part of the carbon cycle and affect  $c_T$ , though driven by

different inorganic carbon species ( $\text{CO}_2$  versus  $\text{CO}_3^{2-}$ ). Calcite precipitation thus also becomes an indirect driver of air exchange.

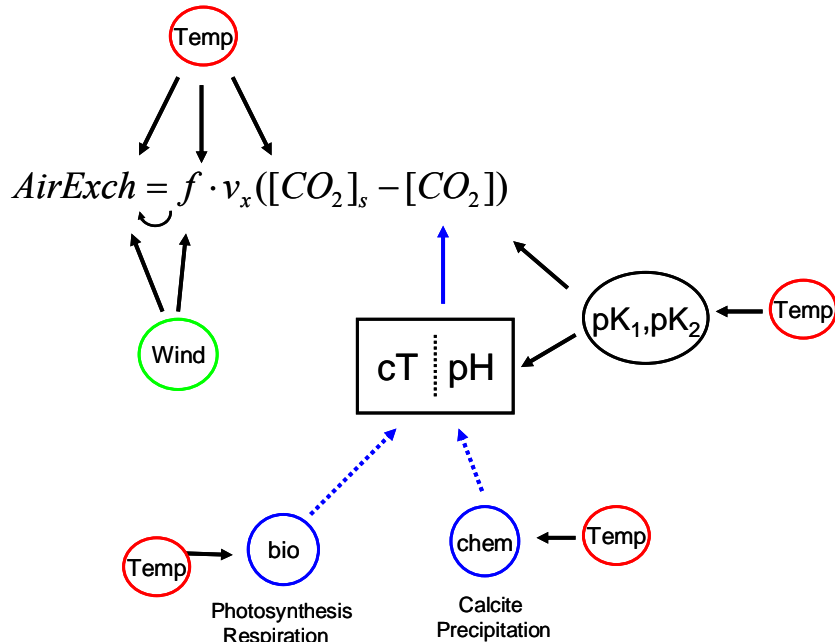


Figure 6-1 Primary factors impacting the air-water exchange rate.

## Gas Transfer Velocity, $v_x$

Three models for gas transfer velocity were evaluated for possible use in the Torch Lake model based on their simplicity and performance. Schwarzenbach et al (2003) propose a three-regime model, of which the smooth surface regime applies to Torch Lake since the wind speed ( $U_w$ ) is always below 4.3 m/s during the time horizon of the model (mid June to mid October). Due to the difficulty in characterizing the relation between wind speed and exchange velocity at low wind speeds they propose a constant gas exchange velocity

of 0.56 m/day, adjusted for temperature (or alternate gas, but in this case we are dealing with CO<sub>2</sub> which happens to be used as the standard) with the Schmidt Number raised to the -0.67 power (Schwarzenbach et al. 2003).

$$v_x = 0.56 \cdot \left( \frac{Sc(T)}{600} \right)^{-0.67} \text{ m/day} \quad (6-4)$$

For comparison note that others have published constant low wind models such as Crusius and Wanninkhof 2003 with 0.24 m/day for  $U_w < 3.7$  m/s and Cole and Caraco 1998 with a constant 0.64 m/day over the summer period.

The second model considered here was developed by Cole and Caraco 1998. They proposed a relationship between the mean wind velocity and mean  $v_x$  based on data for lakes for which whole-system estimates were available. However they assert that it is difficult to estimate the air-water exchange velocity for low wind conditions and hence they concluded that the air exchange velocity is independent of wind speed over the summer. Like Schwarzenbach et al. (2003), temperature conversion is incorporated via the Schmidt number raised to the -0.67 power (Cole and Caraco 1998),

$$v_{x,20} = 0.497 + 0.052 \cdot U_{10}^{1.7} \text{ m/day} \quad (6-5)$$

$$v_x = v_{x,20} \cdot \left( \frac{Sc(T)}{600} \right)^{-0.67} \quad (6-6)$$

The third model is the often-referenced Wanninkhof 1991/1992 model. (Cole and Caraco 1998, Gelda et al. 1996 ). This model was developed by Wanninkhof from a whole-lake tracer gas study which included five lakes of varying sizes. The Schmidt Number power used by Wanninkhof is -0.5.<sup>1</sup> (Wanninkhof 1992, Wanninkhof 1991)

$$v_{x,20} = 0.108 \cdot U_{10}^{1.64} \text{ m/day} \quad (6-7)$$

$$v_x = v_{x,20} \cdot \left( \frac{Sc(T)}{600} \right)^{-0.5} \quad (6-8)$$

Figure 6-2 shows the exchange velocities estimates from these three models for wind speeds from 0 to 6 m/s. Note that the Wanninkhof equation has the air exchange rate at an unrealistic value of 0 when there is no wind, whereas the Cole and Caraco is close to the constant Schwarzenbach model in the case of no wind.

---

<sup>1</sup> Value in article was 0.5 but the missing negative sign was included here for consistency with other articles, and Schmidt Number data.

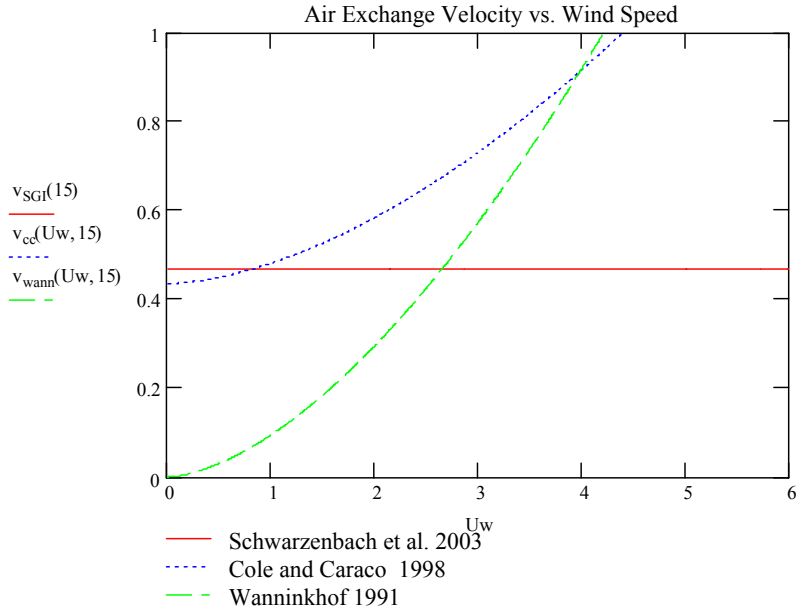


**Figure 6-2 Comparison of models for air exchange velocities of CO<sub>2</sub> at 20C as a function of wind speed.**

All of the models evaluated here use the Schmidt Number to convert between different gases and temperatures. The Schmidt Number is a ratio of the kinematic viscosity (momentum diffusivity) to mass diffusivity. For the Torch Lake model it is the ratio of the kinematic viscosity of water to the mass diffusivity of a gas in water. Both the viscosity of water and the diffusivity of the gas are a function of temperature, thus the Schmidt number is a function of temperature.

$$Sc(T) = \frac{\nu_w(T)}{D_{CO_2-w}(T)} \quad (6-9)$$

The Schmidt number for CO<sub>2</sub> at 20°C is 600, which is typically the standard reported for models of freshwater systems. Gas transfer velocities are reported as CO<sub>2</sub> at 20°C and

converted to other gases or temperatures through the following equation. Various values for the power term,  $a_{Sc}$ , have been reported ranging from -0.5 to -0.67.

$$v_x = v_{x,20} \cdot \left( \frac{Sc(T)}{600} \right)^{a_{Sc}} \quad (6-10)$$

Equations for the viscosity of water and diffusivity of CO<sub>2</sub> in water were developed here using a second-degree polynomial regression from the data provided by Schwarzenbach et al. ( 2003). These equations are:

Water kinematic viscosity (cm<sup>2</sup>/s):

$$v_w(T) = 0.17860 - 5.92325 \cdot 10^{-4} T + 1.25454 \cdot 10^{-5} T^2 - 1.26696 \cdot 10^{-7} T^3 \quad (6-11)$$

Molecular diffusivity of carbon dioxide (cm<sup>2</sup>/s):

$$D_{CO_2}(T) = 9.334271 \cdot 10^{-6} + 2.86518 \cdot 10^{-7} T + 4.31051 \cdot 10^{-9} T^2 \quad (6-12)$$

Schmidt number for carbon dioxide (dimensionless):

$$Sc(T) = 1915.04 - 124.238T + 4.51318T^2 - 9.95852 \cdot 10^{-2} T^3 + 9.93826 \cdot 10^{-4} T^4 \quad (6-13)$$

Figure 6-3 below shows the resulting Schmidt number versus temperature based on these equations.

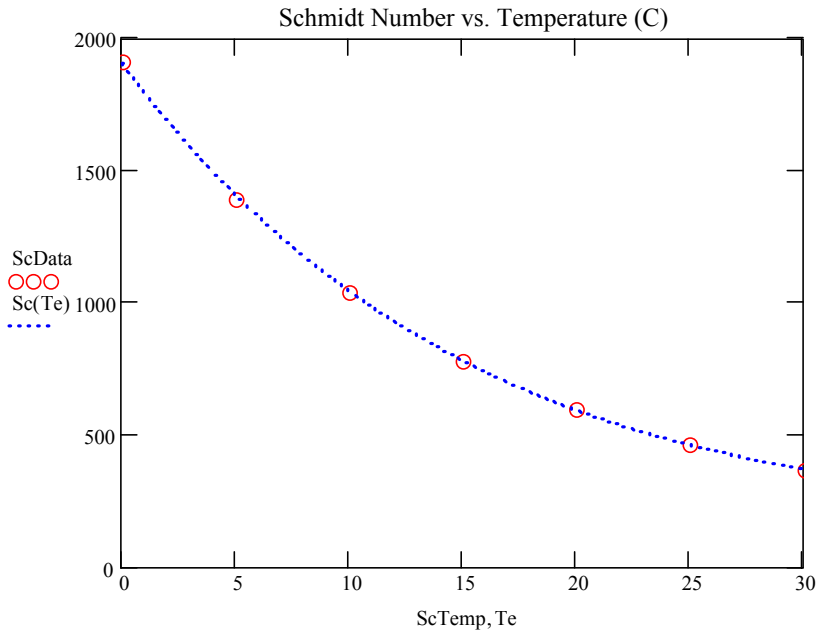


**Figure 6-3 Schmidt number for CO<sub>2</sub> in freshwater as a function of temperature. The red circles are data points from Schwarzenbach et al (2003).**

Figure 6-4 shows the model estimates for Torch Lake air-water exchange velocities over time using the modeled water temperature (interpolated from biweekly hydrolab measurements which were volume weight averaged) and a seasonal average wind speed of 2 m/s for the Cole and Caraco (1998) and the Wanninkhof (1991) models. (The Schwarzenbach model is independent of wind.) The values range from approximately 0.3 to 0.6 m/d, with the constant model from Schwarzenbach et al. (2003) in the middle of the range. Given that the constant model is the simplest and bounded by estimates produced with other sound models, the Schwarzenbach air-water exchange velocity equation was used in the Torch Lake model for this study.

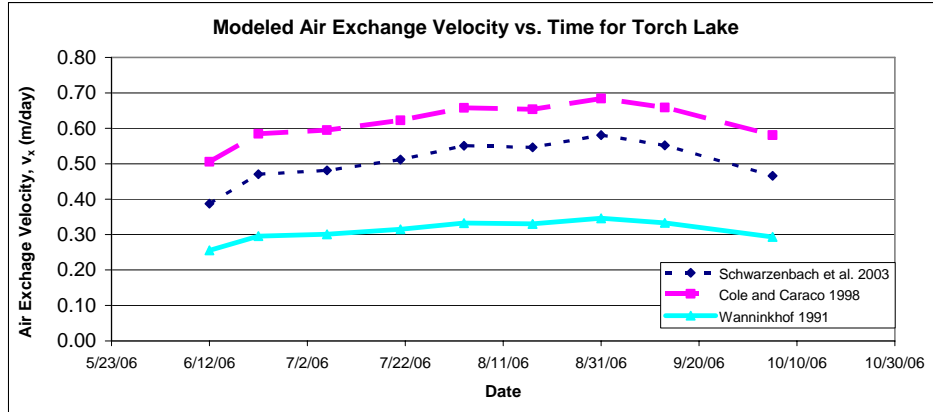
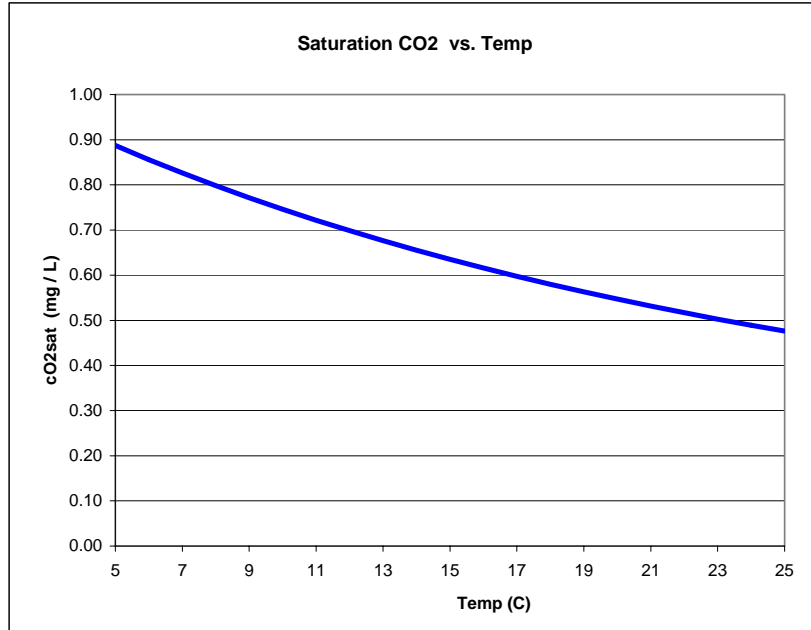


Figure 6-4 Model estimate of air exchange velocity over time using seasonal average wind speed of 2 m/s for Cole and Caraco 1998 and Wanninkhof 1991 models.

### Degree of Oversaturation, $([CO_2]_s - [CO_2])$

The degree of oversaturation is defined as the difference between the amount of  $CO_2$  gas that would occur in the water at equilibrium with the air,  $[CO_2]_s$ , and the amount that is actually in the water,  $[CO_2]$ . The level of  $CO_2$  in equilibrium with air is determined by the atmospheric concentration (typically reported as the partial pressure ( $pCO_2$ )) and Henry's constant ( $K_H$ ) for  $CO_2$ , with  $[CO_2]_s = pCO_2 \cdot K_H(T)$ . Because Henry's constant is temperature dependent,  $CO_2$  saturation is a function of temperature, as shown in Figure 6-5. The value at sea level varies from 0.9 mg/L at  $4^\circ C$  to 0.55 at  $25^\circ C$ .



**Figure 6-5 Saturation CO<sub>2</sub> as a function of temperature.**

At lower temperatures, the saturation level of CO<sub>2</sub> in the water is higher than at higher temperatures. Thus, as the water temperature increases over the summer and the saturation CO<sub>2</sub> level decreases, either more CO<sub>2</sub> leaves the water or less enters, depending on whether a lake is super- or under-saturated. For Torch Lake, which is oversaturated with respect to CO<sub>2</sub> throughout the summer and likely all year, the degree of super-saturation increases over the summer, which then increases the air-exchange rate of CO<sub>2</sub> leaving the lake. Note, however, that as shown in Figure 6-6, the amount of CO<sub>2</sub> in the lake actually increases through August since the pH is decreasing over this period. Thus total inorganic carbon in the lake is decreasing (CO<sub>2</sub> loss to the air as well as CO<sub>3</sub><sup>2-</sup> incorporation into calcite), but of the carbon that remains, a larger percentage of the carbon is in the form of CO<sub>2</sub> due to the decrease in pH. Note that the ‘saturation CO<sub>2</sub>’ level is independent of the lake’s actual c<sub>T</sub>, pH or alkalinity levels.

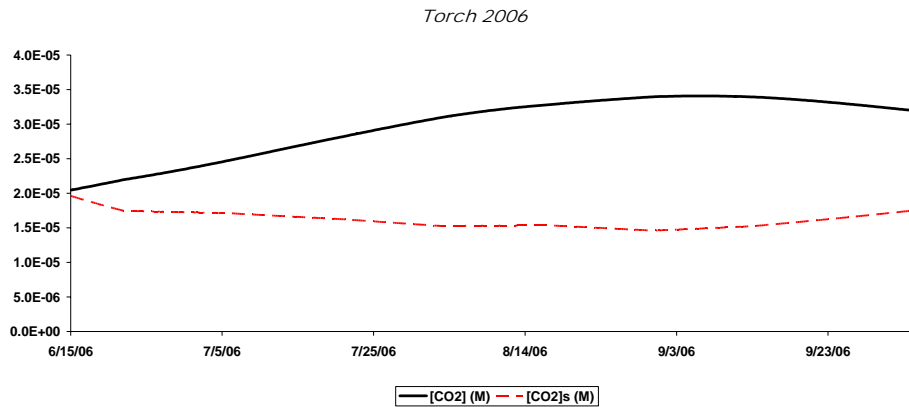


**Figure 6-6 Saturation CO<sub>2</sub> ([CO<sub>2</sub>]<sub>s</sub>) and [CO<sub>2</sub>] in moles/L modeled as a function of time in Torch Lake.**

The level of total inorganic carbon ( $c_T$ ) saturation is related to, but differs from, the carbon dioxide saturation level in that it is dependent on the pH of the water body. The  $c_T$  saturation level is the amount of total inorganic carbon that would result if the CO<sub>2</sub> was at saturation value at the given pH and alkalinity. Given the structure of carbonate equilibrium,  $c_T$  saturation values are very sensitive to pH and increases rapidly for pH values above 8.5, as shown in Figure 6-7.

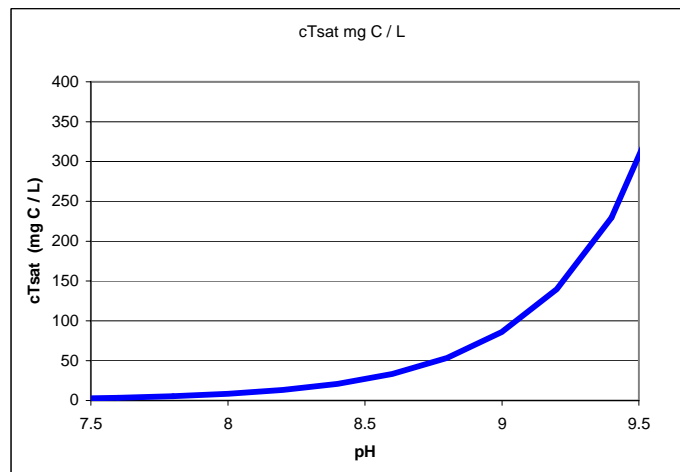


**Figure 6-7 Saturation  $c_T$  as a function of pH with temperature = 20C and conductivity = 300  $\mu\text{m/s}$**

Figure 6-8 shows the range for Torch Lake of total inorganic carbon in relation to the saturation carbon concentration. Note that the pH in Torch Lake would need to reach close to 8.6 for the range of total inorganic carbon in the lake in order to be in equilibrium with  $c_T$  saturation. The pH of the lake does not reach this level and is therefore always oversaturated with respect to total inorganic carbon.

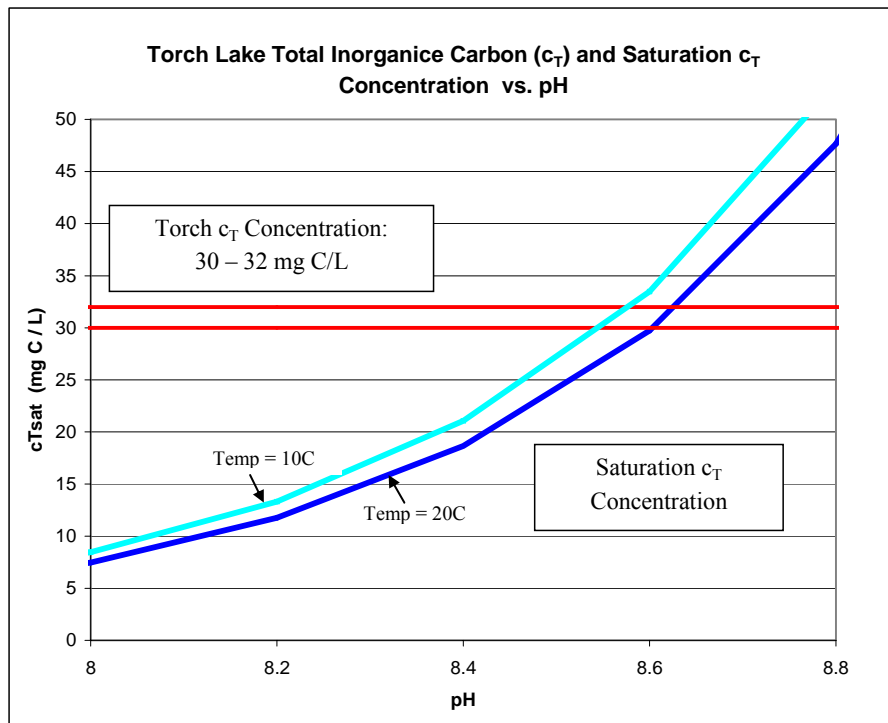


**Figure 6-8 Range of Torch Lake Total Inorganic Carbon ( $c_T$ ) and Saturation  $c_T$  as a function of pH for temperature = 10C and temperature = 20C. (Conductivity = 300  $\mu$ S/cm).**

## **Enhancement Factor, f**

As previously mentioned there is much evidence in the literature of the chemical enhancement of CO<sub>2</sub> air-water exchange. Emerson's three scenarios for the mechanisms involved in air-water exchange provide a useful structure to evaluate the possible models. In the first scenario the diffusion rate is much faster than the chemical reaction rate and therefore no enhancement needs to be considered. Such would be the case for dissolved oxygen. In the second scenario, both diffusion and reactions rates are the same order or magnitude and therefore both should be considered simultaneously. The Hoover and Berkshire model has been developed for this case and results of previous studies suggest that the conditions in Torch Lake fall into this category. In the third scenario the reaction rate is much faster than the diffusion rate and therefore the amount of diffusion can be ignored and the reaction can be assumed to go to equilibrium immediately. This scenario provides the maximum amount of chemical enhancement possible and can be used as an upper bound. The Hoover and Berkshire (1969) model and equilibrium model as applied to Torch Lake are presented below.

Figure 6-9 shows the enhancement factor calculated using the Hoover and Berkshire (1969) model for typical summer conditions in Torch Lake. The enhancement factor is a function of wind speed, air temperature, water temperature and pH, and is independent of  $c_T$ . We can see in Figure 6-9 that the level of chemical enhancement increases steeply for  $\text{pH} > 8.5$ .

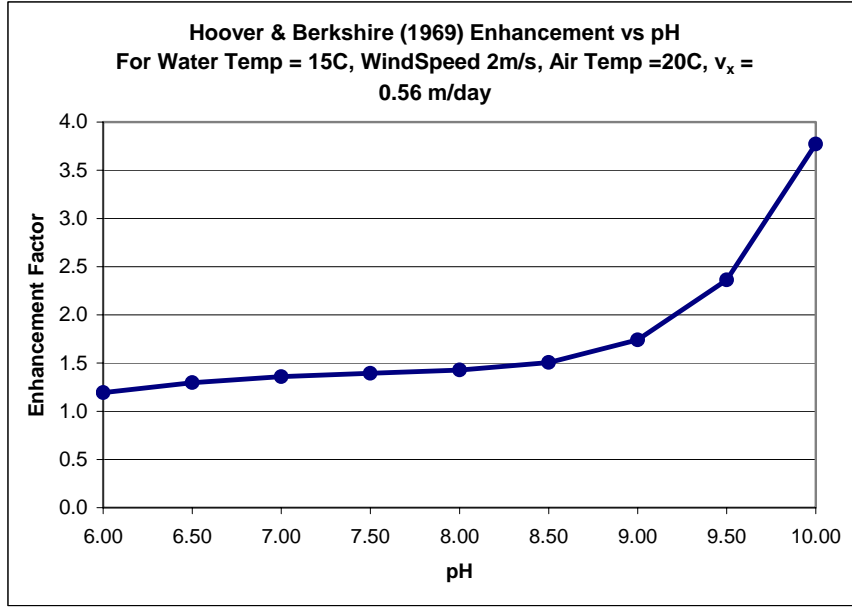


Figure 6-9 Hoover and Berkshire (1969) enhancement as a function of pH

For the ‘equilibrium enhancement’ model described by Morel and Hering (1993), the rate to reach chemical equilibrium is so fast that it can be considered instantaneous. The enhancement factor is independent of wind speed and air temperature, but is sensitive to both the  $c_T$  and pH of the water body.

$$f_{equil} = \frac{\Delta c_T}{\Delta CO_2} \tag{6-14}$$

Using the equilibrium enhancement factor in the  $CO_2$  flux equation is equivalent to using no enhancement ( $f=1$ ) and the total inorganic carbon delta instead of the  $CO_2$  delta, or

$$f_{equil} \cdot k_x \cdot \Delta CO_2 = k_x \cdot \Delta c_T \tag{6-15}$$

Or

$$f_{equil} \cdot k_x \cdot ([CO_2]_s - [CO_2]) = k_x \cdot (c_{T_s} - c_T) \tag{6-16}$$

Figure 6-10 shows equilibrium enhancement versus pH for different levels of  $c_T$ . Note that for the low level of  $c_T$  (1 mg C /L) the alkalinity ranges from 1 – 10 mg/L as  $\text{CaCO}_3$ , and for the high  $c_T$  scenario (40 mg C /L) the alkalinity ranges from 50 – 200 mg/L as  $\text{CaCO}_3$ . For pH values above 8.5 the higher  $c_T$  waters, such as Torch Lake, have a much higher equilibrium enhancement factor than low  $c_T$  waters.

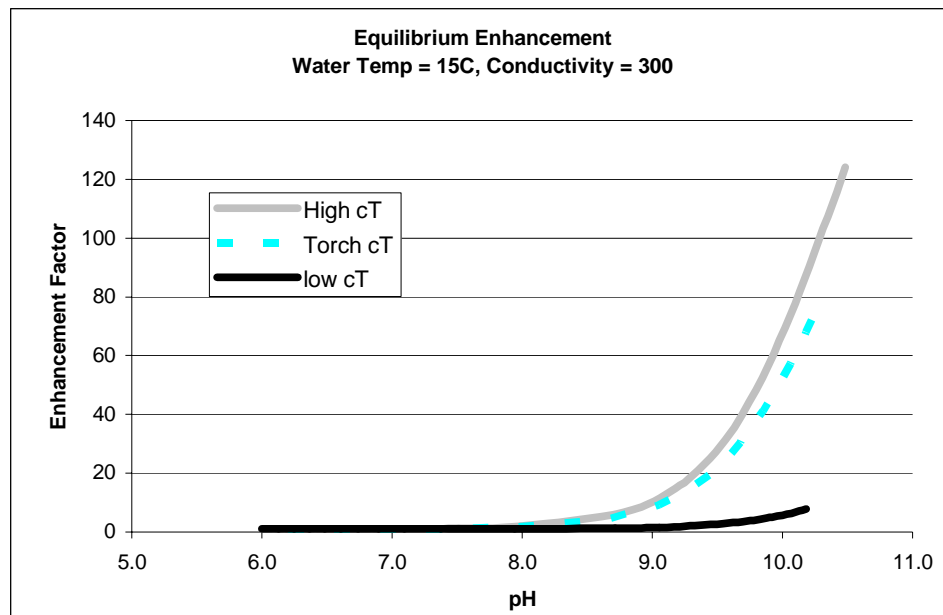


Figure 6-10 Equilibrium enhancement for low (1 mg C /L), Torch Lake  $c_T$  Level (30-32 mgC/L) and high (40 mg C /L)  $c_T$  levels.

The equilibrium enhancement model (Figure 6-10) can be viewed as an upper bound on chemical enhancement of air-water exchange and is clearly much higher than the Hoover & Berkshire prediction for Torch Lake (Figure 6-9).

Evaluating the sensitivity of the Hoover and Berkshire (1969) enhancement model to temperature is complicated by the fact the enhancement factor is a function of the air exchange velocity, and both the enhancement factor and the air exchange velocity are functions of temperature. With  $v_x$  held constant (i.e. not changing with temperature), the

Hoover and Berkshire (H & B) enhancement factor increases with temperature (Figure 6-11), however if the  $v_x$  value input to the H & B calculation is allowed to increase with temperature the resulting enhancement factor decreases (Figure 6-12). This is due to the inverse relationship between the H & B enhancement factor and the air exchange velocity,  $v_x$  shown in Figure 6-13.

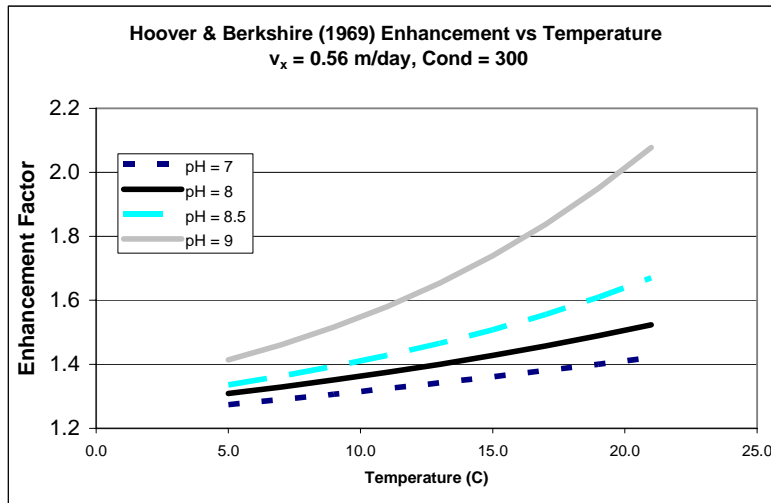


Figure 6-11 H&B enhancement versus temperature, with  $v_x$  held at,  $v_{x-20} = 0.56$ .

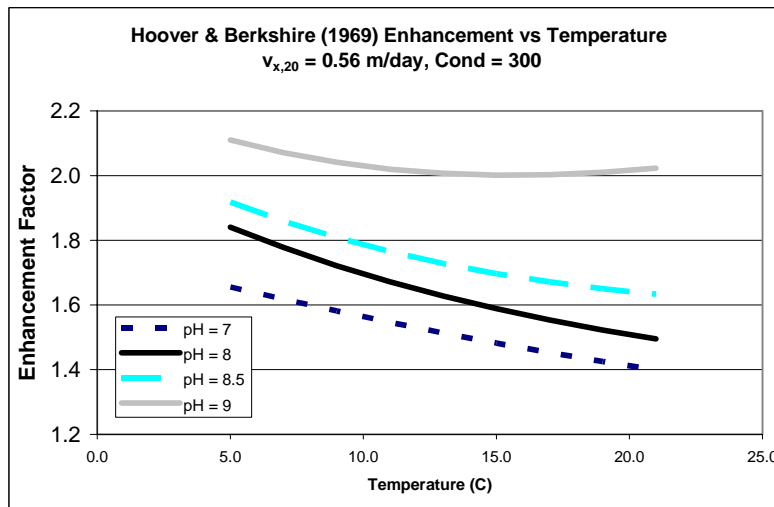
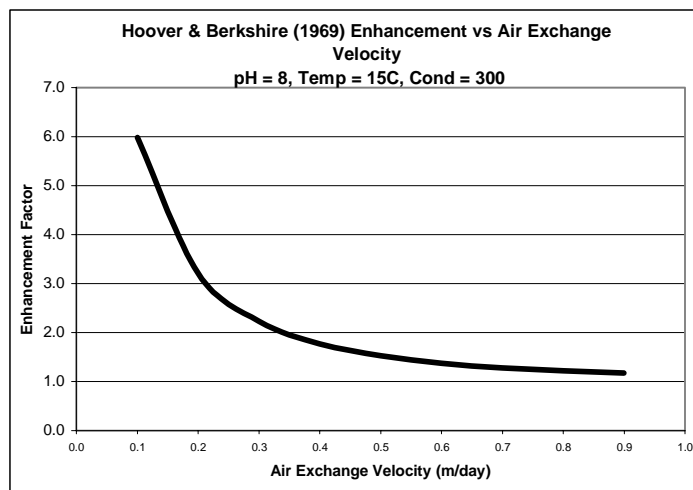


Figure 6-12 H&B enhancement versus temperature, with input  $v_x$  also varying with temp using equation (6-4).



**Figure 6-13 The Hoover and Berkshire (1969) Enhancement Factor as a function of air exchange velocity, with all other inputs held constant as noted.**

Further analysis, implemented with the full model, of the impact of temperature on the air exchange rate as well as the air exchange rate on the amount of precipitation, will be presented in Chapter 9.

## Chapter 7 The Calcite Settling Velocity

The settling of calcite is a key process in the model of a lake's calcite cycle and prediction of the calcite concentration over time. The settling rate can also directly affect the rate of calcite precipitation by reducing particulate surface area for crystal growth as particles settle out of the epilimnion.

The structure of the model is straight forward and without temperature dependence. The product of the settling velocity and concentration provide the flux rate which multiplied by the area determines the mass per time of calcite settled.

$$\text{CalciteSettling} = v_s \cdot A \cdot c_{CaCO_3} \quad (7-1)$$

where

$v_s$	Settling velocity of calcite ( $m / day$ )
$c_{CaCO_3}$	Concentration of calcite ( $CaCO_{3(s)}$ )
$A$	Lake area ( $m^2$ )

### **Calibration Methods**

Four methods were used to check the consistency of the settling velocity parameter value with the various types of available data. The details of these calculations can be found in Appendix C

For the first approach an average downward flux rate ( $J$ ) of calcite over the summer period was calculated from the mass measured in the sediment trap. Using an average calcite concentration ( $c$ ) of 1 mg/L, the settling velocity ( $v = J/c$ ) was 1.6 m/day.

For the second approach a constant load model was used with a precipitation rate (mol/L/day) estimated from the change in dissolved calcium over the summer period. The ending calcite concentration was then used as the steady state concentration, and the velocity was calculated to be 1.1 m/day.

The third approach was to again use the constant load model but with a time-variable calcite concentration. The precipitation rate (mol/L/day) was again estimated from the change in dissolved calcium. Given the precipitation rate, the settling velocity was calculated that would result in the flux rate given by the sediment trap (1.6 m/day). The settling velocity calculated in this way is 1.5 m/day.

For the fourth approach, Stokes' law was used with the particle distribution data to calculate settling velocities for each particle size and a weight-averaged settling velocity was calculated by summing the fluxes for each particle size. Only the particle types assumed to be calcite were included ('ca-rich' and the 'ca-agg' particles). The settling velocities calculated in this way ranged from 2.2 to 4.8 m/day. These velocities should be considered an upper bound since the shape factor used in the calculations is a sphere ( $\alpha = 1$ ), when clearly the particles are angular. (See Figure 3-7). In addition, Stokes law

assumed laminar flow conditions. The actual transport regime in the Torch Lake epilimnion could in fact be turbulent at times during the summer.

The value of the settling velocity parameter used in the model is 1.8 m/day. This value was by selecting a value within the range of estimates described above and matching the model estimate for particulate calcite concentration to the data. This was done after calibrating the amount of calcite precipitation based on the change in dissolved calcium, alkalinity and conductivity.

## **Chapter 8 The Primary Production Rate**

This chapter provides a description of the primary production model used in the Torch Lake model. The structure of the model and how the biological processes affect inorganic carbon is presented. This is followed by a review of published primary production rates for comparable lakes and a description of the model scenarios that were run in order to analyze the possible rates of primary production in Torch Lake. The impact of primary production will be compared to other factors in Chapter 10.

### ***Model Structure***

This section will describe the structure of the primary production model and the points of interaction between the biological processes and the inorganic processes.

A summary of all the processes included in the model are shown here in Table 8-1, an annotated version of a portion of Table 4-2. The three biological processes that impact inorganic carbon are photosynthesis, respiration and the decomposition of organics back to inorganic carbon (represented here by hydrolysis). The settling of calcite affects inorganic phosphorus through coprecipitation – the adsorption of dissolved phosphorus onto calcite which results in the phosphorus settling with the calcite. (See Chapter 9 for more on the model of coprecipitation.)

**Table 8-1 Kinetic interactions and stoichiometry for biological processes.**

Component→ Process↓	$a_p$	$p_o$	$p_i$	$c_T$	$[Ca^{2+}]$	$[CaCO_{3(s)}]$	Process rates, $M/(L^3 T)$
Calcite precipitation				-1	-1	1	$k_r S([Ca][CO_3] - K_{sp})$
CO <sub>2</sub> gas transfer				1			$f k_x ([CO_2]_s - [CO_2])$
Calcite settling			$-K_{dp} F_{dP_i}$			-1	$v_s A [Ca][CO_3]$
Photosynthesis	1		$-r_{pa}$		$-r_{ca}$		$k_g a_p$
Respiration/excretion	-1		$r_{pa}$		$r_{ca}$		$k_{re} a_p$
Hydrolysis		-1	1		$r_{cp}$		$k_{hy} p_o$
Death	-1	$r_{pa}$					$k_{de} a_p$
Phytoplankton settling	-1						$v_s A a_p$
Detrital P settling		-1					$v_s A p_o$

where

- $r_{pa}$  = ratio of phosphorus to chlorophyll ( $\mu\text{gP}/\mu\text{gChla}$ )
- $r_{cp}$  = the ratio of inorganic carbon to phosphorus ( $M/\mu\text{gP}$ )
- $r_{ca}$  = the ratio of inorganic carbon to phytoplankton biomass ( $M/\mu\text{gChla}$ )
- $k_g$  = phytoplankton growth rate (/d)
- $k_{hy}$  = hydrolysis rate (/d)
- $k_{re}$  = phytoplankton respiration/excretion rate (/d)
- $k_{de}$  = phytoplankton death rate (/d)
- $v_a$  = phytoplankton settling velocity (m/d)
- $v_o$  = detrital phosphorus settling velocity (m/d)

The structure of the rate equation for the primary production model is shown in equation (8-1). The units for the growth and respiration are per time. Phytoplankton growth is affected by light, temperature and nutrients, whereas respiration is only affected by temperature. The concentration of plankton is also determined by the death rate and the amount of settling that occurs.

$$NPP = k_g \cdot c_{phyto} - k_r \cdot c_{phyto} \quad (8-1)$$

- where  $k_g$       Phytoplankton growth (photosynthesis) rate (/ day )
- $k_r$       Phytoplankton respiration rate (/ day )
- $a_p$       Concentration of phytoplankton ( $\mu\text{g} / L$ )

Net primary production is presented here as the key biological process since the amount of primary production has been reported for many lakes. The net value is used because it corresponds to the net amount of CO<sub>2</sub> consumed by phytoplankton, since phytoplankton growth (photosynthesis) consumes CO<sub>2</sub> and phytoplankton respiration produces CO<sub>2</sub>. Note that the CO<sub>2</sub> is regenerated in the growth/death cycling of phytoplankton which is represented by ‘hydrolysis’ in Figure 8-1.

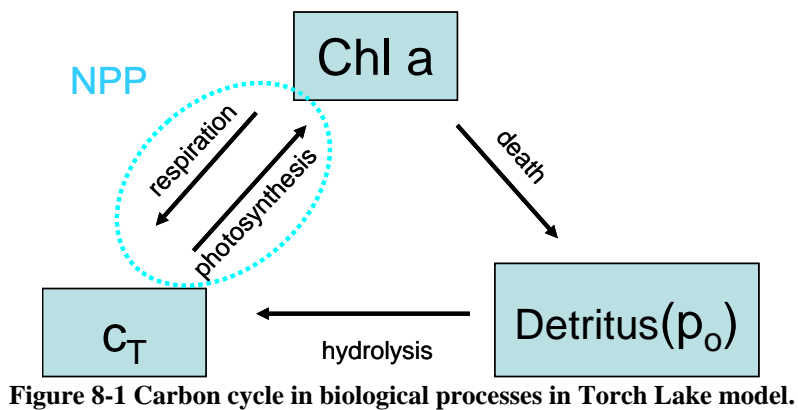


Figure 8-1 Carbon cycle in biological processes in Torch Lake model.

### ***Published Primary Production Rates***

A review of primary production measured in lakes was developed in order to bound the calibration of the Torch Lake Model. Given the measured values of average TP (2.5 µg/L) and average chlorophyll a (0.5 µg/L), Torch Lake is clearly ultraoligotrophic. Dodson (2004) reported a range of 1.3 to 1300 gC/m<sup>2</sup>/yr of net primary production (NPP) for ultraoligotrophic alpine lakes (1.3) to hypereutrophic sewage lagoons (1300). Kalff

(2002) reported a range of 4 to 5700 gC/m<sup>2</sup>/yr but did not confirm these values as net or gross primary production.

Various regression equations (Kalff 2002, Dodson and Chapra 1981, Vollenweider 1974) allow estimates of primary production given a chlorophyll *a* concentration. These equations predict a range for net primary production of 20 – 80 mgC/m<sup>2</sup>/day given Torch Lake's summer chlorophyll *a* level in Torch Lake (0.5 µg/L). Note that two of the three regressions were done only for the Great Lakes but given the proximity and similarity in chemistry, the Great Lakes should be a reasonable estimator for reasonable ranges for Torch Lake primary production. However, the data used for the the Great Lakes regressions likely includes spring blooms so they should be considered an upper limit for bounding estimates of Torch summer primary production levels.

The regeneration rate of dissolved P suggested by the regression equation of Hudson et al (1999), correlating chlorophyll *a* levels to regeneration rate, predicts a regeneration rate that would require 130 mgC/m<sup>2</sup>/day of net primary production in Torch Lake.

In addition to the range of possible net primary production values for Torch from regression equations, we can get a sense of reasonable predictions for Torch Lake by direct comparisons with other lakes with similar TP and chlorophyll *a* levels, though few north temperate lakes have TP and chlorophyll *a* levels as low as Torch Lake. Of the Great Lakes, Lake Superior's trophic state is the closest, with TP of 4.6 µg/L, chlorophyll *a* of 0.7 µg/L and NPP at 137 mg/m<sup>2</sup>/day (Chapra and Dodson 1981). According to

Vollenweider the measurements were “lake-wide averages for the ice-free period”. (Vollenweider 1974). Note that Torch TP averages half that of Lake Superior and has an even lower chlorophyll a, so we should expect that it would have a lower NPP.

From Dodson’s values (Dodson 2004), Torch Lake should fall between Char Lake (NPP = 4.1 gC/m<sup>2</sup>/yr) and Lake 239 (TDP = 10 µg/L, NPP = 21.3 gC/m<sup>2</sup>/yr, or 55-74 mg/m<sup>2</sup>/day when converted to a daily growing season rate.)

These primary production values for oligotrophic lakes from the literature were used to estimate possible ranges of primary production in Torch Lake. This will be discussed in the calibration section, after brief description of the primary production rate used in the Torch Lake model.

### ***Calibration Methods***

Published estimates of primary production were used to predict possible ranges for Torch Lake and select different scenarios to evaluate. All parameters were compared with published ranges. It was most difficult to determine the amount of nutrient recycling occurring in Torch Lake based on the data available, and therefore three different levels of net primary production, driven by three different estimates of nutrient regeneration rates, were evaluated.

## Estimates of Primary Production

It is important to be aware of the risks of comparing data between different lake studies. First, the measurement methods vary and produce different results. Measurements of oxygen and/or carbon are used to estimate primary production rates and various techniques exist for each. For example, the measurement of oxygen through light bottle/dark bottle experiments or DO profile data provided by hydrolab equipment will produce different estimates of NPP. There are also isotopic tracer methods used for both carbon and oxygen and variable interpretations of which method best represents which biological process. This leads to another important consideration which is what does the study intend to represent and is it clear whether the reported rate is net or gross primary production, or carbon fixation?

Incompatibility with another study can also arise from differences in the space and time of the measurement and calculation techniques. Primary production rates are usually reported as either areal or volumetric rates and it is important to know the integration method used to calculate the average rate (throughout the mixed layer, the photic zone, etc) in order to be able to convert and compare rate types. It is also important to consider whether the comparison is intended to be between a fixed volume within each mixed layer or between two columns of water (areal rate) which may vary significantly in photic zone depth and therefore in volume.

Correctly interpreting the time scale of the reported rate is also key to a valid comparison. Does the rate represent only the growing season? If the measurements were

taken only during an ice-free period, how was the rate converted to an annual rate? If the rate reported is per hour, is this a measure at peak light intensity, or is it averaged over a whole day, so the dark period with only respiration is included?

Given all these considerations, it is still useful to attempt to compare rates of primary production between lakes in order to get a sense of the bounds, even with a significant degree of error given all the conversion issues. For lakes in a north-temperate climate where the rate reported was annual as done by Vollenweider (1974) it was assumed that the winter rate was 50% of the growing season rate, and both rates were reported as bounds.

**Table 8-2 Estimates of Primary Production for Torch Lake**

Kalff 2002, regression	6 - 8 mgC/m <sup>2</sup> /day
Chapra/Dobson 1981, GL regression	80 mgC/m <sup>2</sup> /day
Vollenweider 1974, GL regression	55 mgC/m <sup>2</sup> /day
Chapra/Dobson 1981, ½ of Lake Superior Rate	~70 mgC/m <sup>2</sup> /day
Dodson 2004, between Char and Lake 239 Rate	11 - 55 mgC/m <sup>2</sup> /day

Torch Lake primary production may be significantly lower than the estimates based on the Great Lakes because the Great Lakes data include Spring blooms, whereas there is no such bloom in the summer in Torch Lake. There is also much uncertainty in the estimate from the Kalff (2002) regression since the output is “Volumetric Photosynthesis in mgO<sup>2</sup>/m<sup>3</sup>/hr” and thus required conversion to both an areal and a daily rate, and may better represent gross, and not net, primary production. However, despite the uncertainty,

the rate was still included here. It was considered to be a daylight rate and thus converted to a daily rate using a 12 hour photo period.

Chapra and Dobson (1981) as well as Dodson (2004) reported primary production rates in  $\text{gC}/\text{m}^2/\text{yr}$ , but Vollenweider's data (1974) is in yearly, daily and hourly rates. We conclude that Torch Lake's summer primary production could be between 5 – 80  $\text{mgC}/\text{m}^2/\text{day}$ , but is most likely between 5 and 30  $\text{mgC}/\text{m}^2/\text{day}$ , due to the difference in time periods measured.

## **Biological Parameters**

The maximum growth rate parameter was compared to published ranges. Kalff (2002) presents a regression between plankton size and a saturated light, 20°C growth rate. For 1 to 2 micron diameter plankton the maximum growth rate predicted is 1.8 to 2.0 /day. Chapra (1997) gives a range of 1.5 to 3.0 /day. The phytoplankton settling velocity ( $v_a$ ) was set to 0 since picoplankton sinking rates are considered negligible. (Kalff 2002, Weisse 1988)

## **Summary**

Because no measurements were available to quantify the rates of nutrient regeneration, three different model scenarios were evaluated in order to consider the lower and upper

bounds of primary production possible in Torch Lake, and the possible impact of each assumption on our understanding of the whole system. The parameters used for each scenario, along with model output, are shown in Appendix B . The net primary production values are 4, 10 and 26 mgC/m<sup>2</sup>/day. When considering the net impact of biological activity on inorganic carbon it is important to note that ‘NPP – Hydrolysis’ is a closer estimate to the net impact on  $c_T$ . The values of ‘NPP – Hydrolysis’ for the three scenarios range from 2 to 2.5 mgC/m<sup>2</sup>/day.

## **Chapter 9 The Rate of Coprecipitation of Phosphorus**

Primary production, discussed in the previous chapter, can influence the calcite precipitation rate by shifting the carbonate equilibrium. This chapter will now discuss how calcite precipitation can influence the primary production rate. This is possible due to the coprecipitation of phosphorus with calcite which reduces the dissolved inorganic phosphorus available for growth of phytoplankton.

The chapter will start with a literature review of phosphorus coprecipitation models, followed by a description of the model structure for the coprecipitation rate used in this study. An explanation for the calibration process is then provided covering the setting of the partition coefficient based on Torch Lake phosphorus levels. The resulting incorporation ratio of phosphorus to calcium is confirmed to be within the range shown in the sediment data.

### ***Literature Review***

Phosphorus has been shown to coprecipitate with calcite in lake systems with a range of calcite concentrations and phosphorus levels. The coprecipitation, or adsorption of phosphorus to calcite crystals, followed by the settling of these particles can be a significant removal mechanism of inorganic phosphorus and thus a key component of growth cycles in lakes. (Danenlouwerse et al. 1995, Dittrich et al. 1997, Hartley et al. 1997, Kleiner 1988, Vanderploeg et al. 1987)

Various models have been developed to describe the kinetics of phosphorus coprecipitation. Kleiner (1988) measured the change in dissolved calcium and phosphorus in laboratory experiments and found a linear relationship between the crystallization rate of calcium and the coprecipitation rate of phosphorus,

$$R_p = (3.4 \pm 0.2) \frac{\mu\text{gP}}{\text{mgCa}} \cdot R_{Ca} \quad (9-1)$$

where:

$R_{Ca}$	precipitation rate of Ca
$R_p$	coprecipitation rate of P

The experiments were conducted with water from Lake Constance to which calcite seed crystals were added to trigger precipitation. The experimental results were used to estimate that 35% of the total phosphorus removal from Lake Constance was due to coprecipitation with calcite.

House presented a model of phosphorus coprecipitation kinetics based on an adsorption function dependent on pH, total dissolved calcium, total dissolved phosphorus and temperature. The adsorption equation includes equilibrium calculations for phosphate speciation as well as complexation reactions with metals such as calcium. The model "successfully described" coprecipitation kinetics in river waters and was applied by Dittrich et al. (1997) to Lake Dagowsee. However, the model applicability for systems with phosphorus levels under 30  $\mu\text{g/L}$  is not well understood. (House 1990)

Danenlouwerse et al (1995) collected data from phosphorus coprecipitation studies and developed a regression equation in the form of a Freundlich isotherm,

$$Y = 10.9X^{0.5} \quad (9-2)$$

where:

X            dissolved inorganic phosphorus concentration  $\frac{mgP}{L}$

Y            calcite incorporation rate  $\frac{mgP}{gCa}$

As with the House model, the Danenlouwerse regression equation shows the phosphate concentration as the primary predictor of the adsorption rate. This addresses a limitation found with Kleiner's model, Eq. (5-1), which is independent of phosphorus levels. The model has been applied by Dittrich and Koschel (2002) to Lake Luzin in Germany.

Additional studies of phosphorus coprecipitation in lakes supports the adsorption models. (Hartley et al 1997, Dittrich 1997, Holzbecher, and Nutzmann 2000)

Incorporation rates have been reported from 0.7 mgP/gCa (Dittrich and Koschel 2002) to 1 mgP/gCa (Dittrich 1997) and have included applications of both the House and Danenlouwerse coprecipitation models.

## **Model Structure**

As just described in the previous literature review, recent studies have shown the coprecipitation rate to be correlated to the phosphorus level and thus a constant incorporation rate model such as developed by Kleiner is only applicable to certain conditions. House's model attempts to add mechanistic detail but the benefits are unproven, especially for systems with low total phosphorus.

The approach taken by Danenlouwerse et al (1995) of regressing from data points representing previous studies and producing an adsorption isotherm is simpler and supported by more data. Given the very low levels of TP in Torch Lake, a linear model shown in equation (9-3) can be used to represent the relation between the phosphorus concentration (mgP/L) and the incorporation rate (mgP/gCa).

$$Y = K_d X \quad \left( \text{for TP} < 100 \frac{\mu\text{g}}{\text{L}} \right) \quad (9-3)$$

where:

X	dissolved, not adsorbed, inorganic phosphorus	$\frac{\text{mgP}}{\text{L}}$
Y	calcite incorporation rate	$\frac{\text{mgP}}{\text{gCa}}$

The Danenlouwerse regression isotherm for the range of inorganic phosphorus found in Torch Lake was used to determine the slope of the regression line,  $K_d$ . With the equation in this form,  $K_d$  becomes the partition coefficient (Chapra 1997), and the fraction of inorganic phosphorus that is dissolved and the fraction adsorbed can be calculated using the following equations.

The fraction sorbed on calcite is calculated as

$$F_p = \frac{K_d [\text{CaCO}_{3(s)}]}{1 + K_d [\text{CaCO}_{3(s)}]} \quad (9-4)$$

where  $K_d$  = partition coefficient ( $M^{-1}$ ).

Note that the fraction of inorganic phosphorus in dissolved form is then computed as

$$F_d = 1 - F_p = \frac{1}{1 + K_d [\text{CaCO}_{3(s)}]} \quad (9-5)$$

The rate equation for the settling of the absorbed, or coprecipitated, phosphorus becomes the following:

$$Co\ Pr\ ecip = v_s \cdot A \cdot F_p p_i \quad (9-6)$$

where

$v_s$	Settling velocity of calcite ( $m / day$ )
$p_i$	Concentration of inorganic phosphorus ( $\mu g / L$ )
$F_p$	Fraction of inorganic phosphorus adsorbed to particulate $\text{CaCO}_{3(s)}$
$A$	Lake area ( $m^2$ )

The rate of coprecipitation is thus a function of the calcite settling velocity, the inorganic phosphorus concentration and the fraction of  $p_i$  adsorbed to calcite. The fraction

adsorbed ( $F_p$ ) in turn is a function of the calcite concentration as shown in (9-4). The change in the fraction as a function of calcite concentration is shown in Figure 9-1. As expected a higher fraction of phosphorus is adsorbed as the calcite concentration increases.

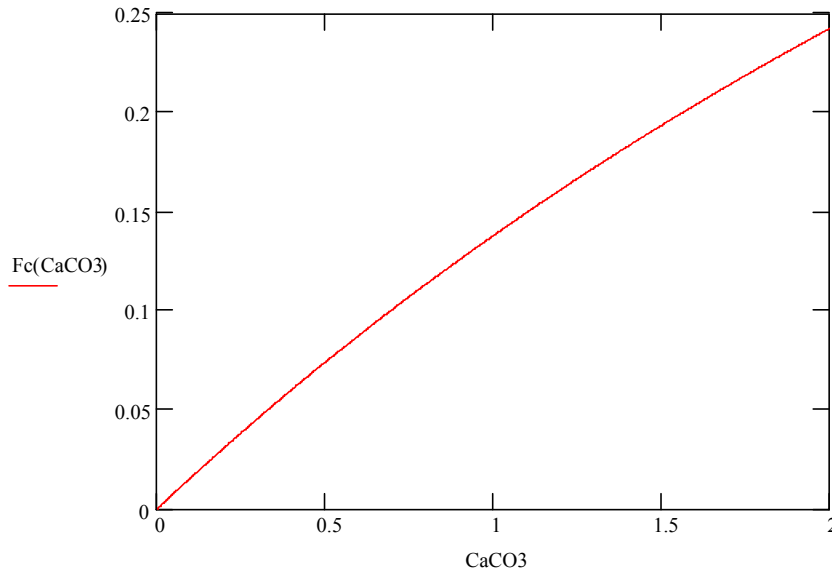


**Figure 9-1 The fraction of phosphorus that is adsorbed to particulate CaCO<sub>3</sub> ( $F_p$ ) as a function of CaCO<sub>3</sub> concentration (mg/L) using the linear model with  $K_d = 400$ .**

It can be shown that the phosphorus coprecipitation rate, or settling rate of phosphorus adsorbed to calcite, is related to the calcite settling rate by the incorporation ratio ( $Y$ ). Defining the dissolved fraction of inorganic phosphorus ( $X$ ) in equation (9-3) using  $F_d$  defined in (9-5),

$$X = F_d \cdot p_i \quad (9-7)$$

and then substituting into equation (9-3) results in the incorporation ratio defined as

$$Y = K_d \cdot F_d \cdot p_i \quad (9-8)$$

Thus this definition of the incorporation ratio in equation (9-8) and the product of the calcite settling rate from equation (7-1) result in the coprecipitation rate. (Equation (9-9) below). This calculation also involves that fact that  $K_d[\text{CaCO}_{3(s)}] \cdot F_d = F_p$  which combines equations (9-4) and (9-5).

$$v_s \cdot A \cdot c_{\text{CaCO}_3} K_d \cdot F_d \cdot p_i = v_s \cdot A \cdot (K_d \cdot c_{\text{CaCO}_3} \cdot F_d) \cdot p_i = v_s \cdot A \cdot F_p \cdot p_i \quad (9-9)$$

This is consistent with the terms shown in Table 4-2 relating the calcite settling process with the state variable for inorganic phosphorus.

### **Calibration Methods**

The model structure and the setting of the partition coefficient were verified using both the sediment core and the sediment trap data for Torch Lake, as well as compared to incorporation rates published for other lakes. The data as it is relevant to coprecipitation is described below and compared to the model results.

### **Sediment Core**

The Michigan State University 2002 sediment cores of Torch Lake contained 354 mg/kg (or 0.035%) phosphorus and 311760 mg/kg (or 31.2 %) calcium. The phosphorus to calcium ratio of the sediments is thus 1.1 mgP/gCa. This value is potentially an

overestimate of the incorporation ratio during coprecipitation due to the possible dissolution of calcium or interactions between iron and phosphorus during sedimentation.

## **Sediment Traps**

Sediment traps set during the TLA/GLEC 2005 water quality study were set at depths from 10m – 74m over different seasons. The content of these traps were analyzed for total phosphorus and the values ranged from 185 mg/kg to 465 mg/kg. The sediment trap set in 2006 for the calcite study at a depth of 40m was analyzed for calcium and the value was 429500 mg/kg. Using these ranges of trap data, though from different years, the incorporation rate ranges from 0.4 to 1.1 mgP/gCa.

## **Published Incorporation Rates for Other Lakes**

Dittrich reported a phosphorus incorporation rate of 0.72 mgP/gCa for Lake Luzin and described the results as being well represented by the Danenlouwerse adsorption model. (Dittrich et al. 2002) For Lake Dagosee calculations from an enclosure experiment produced an incorporation rate of 1 mgP/gCa. (Dittrich et al. 1997)

The oligotrophic systems that were included in the set of studies in the Danenlouwerse regression reported incorporation rates of 0.4 and 0.8 mgP/gCa for lakes with 1 µg/L and 5 µg/L of TP respectively. (Danenlouwerse 1995)

## **Summary**

The incorporation rate using a linear portion of the Danenlouwerse (1995) adsorption isotherms for the low phosphorus levels in Torch Lake ranged between 0.35 to 0.44 mgP/gCa with a  $K_d$  of 400. The average incorporation ratio based on total cumulative phosphorus coprecipitated versus total cumulative precipitated calcium over the whole model time horizon was 0.4 mgP/Ca. This value falls within the range of ratios from the sediment core and sediment trap data of 0.4 to 1.1 mgP/gCa and is consistent with published incorporation ratios for other low phosphorus lakes ranging from 0.4 to 1 mgP/gCa.

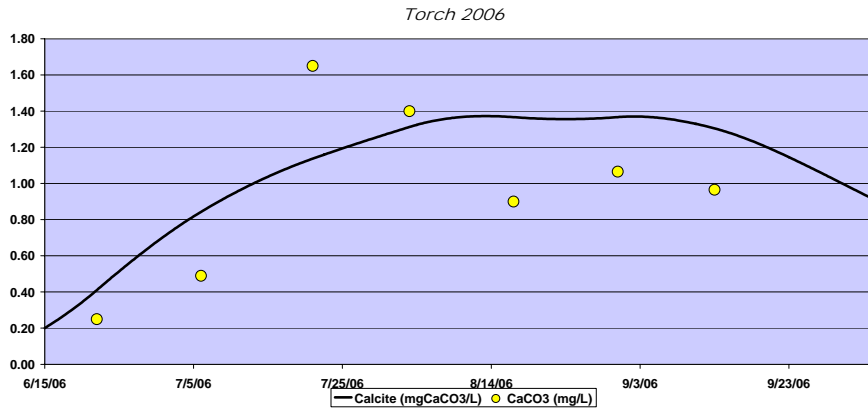
## Chapter 10 Results and Analysis

Developing and calibrating a mass balance model of calcite precipitation creates a tool that can be used to quantify the interactions of physical, chemical and biological processes. This chapter will start with comparisons of model predictions with data for Torch Lake from June to October, 2006. The purpose of this exercise is to demonstrate how well the Torch Lake model is able to estimate values over the time horizon for the major chemical state variables,  $\text{CaCO}_{3(s)}$ ,  $c_T$ , and  $[\text{Ca}^{2+}]$ . Model predictions will then be compared to data for the calculated variables pH, alkalinity, and conductivity as well as for the optical variables. These model results will be followed by an analysis section that assesses the relative importance of the processes driving calcite precipitation in Torch Lake.

### **Results**

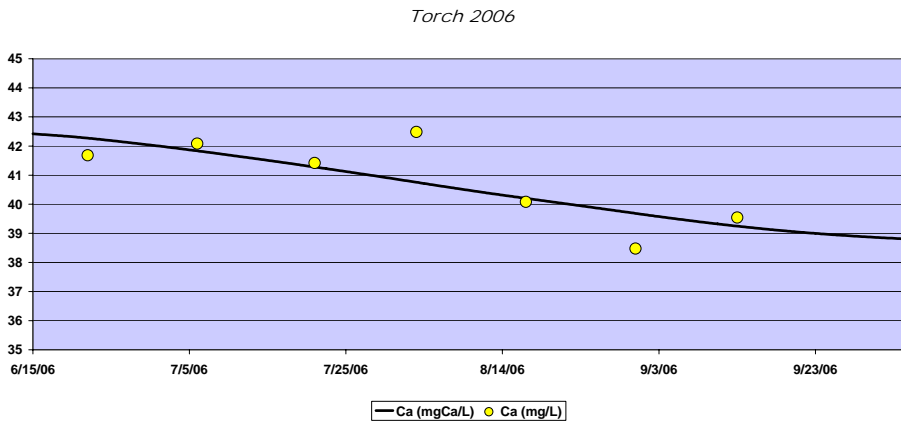
Three scenarios were run with varying levels of Net Primary Production (NPP), as described in Chapter 8. Model output for the state variables, calcite, dissolved calcium and  $c_T$  are shown in Figure 10-1 through Figure 10-3. The concentrations of calcite, dissolved calcium and  $c_T$  were similar for all three scenarios of primary production levels, so the mid level results are shown here for an average  $\text{NPP} = 10 \text{ mgC/m}^2/\text{day}$ . The output for the biological state variables, chlorophyll a, inorganic phosphorus and detrital phosphorus for all three scenarios can be found in Appendix B

Figure 10-1 shows the calcite concentration peaking from mid July through August. The calcite data is from particulate calcium measured by TLA by filtering composite epilimnion samples on board within two hours of sample collection.



**Figure 10-1 Model output (line) and data (circle) for the state variable, particulate calcite, over time.**

The dissolved calcium concentration, shown in Figure 10-2, decreases as calcium moves from the dissolved to the solid phase due to calcite precipitation. Total inorganic carbon ( $c_T$ ), shown in Figure 10-3, also decreases due to the removal of carbon by calcite precipitation as well as loss of CO<sub>2</sub> to the air and to primary production.



**Figure 10-2 Model output (line) and data (circle) for the state variable, dissolved calcium, over time.**

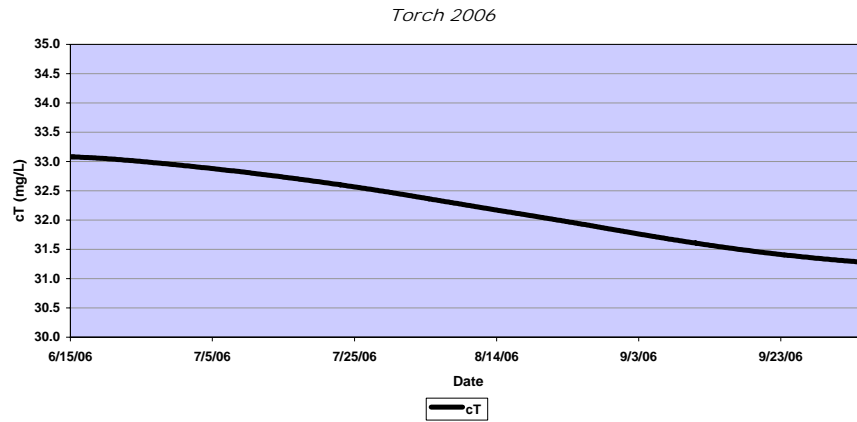


**Figure 10-3 Model output for the state variable, total inorganic carbon ( $c_T$ ), over time.**

Model output for the calculated variables pH, alkalinity and conductivity are shown in Figure 10-4 through Figure 10-6. The change in pH (Figure 10-4) is due to many simultaneous processes acting on inorganic carbon and alkalinity. The loss of  $\text{CO}_2$  to the air and primary production should raise pH but the loss of  $\text{CO}_3^{2-}$  to calcite precipitation dominates through August and leads to the decline in pH. As the calcite precipitation declines at the end of August, air exchange of  $\text{CO}_2$  continues and the pH starts to rise in September.

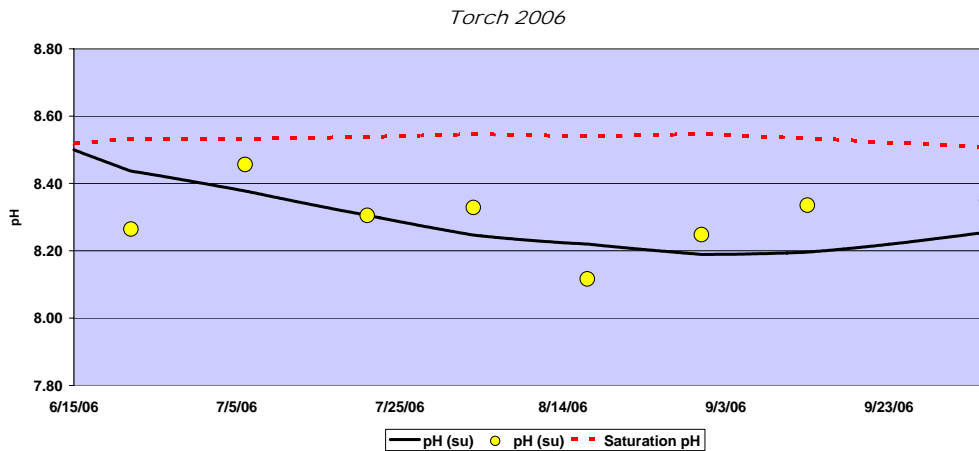


**Figure 10-4 Model output (line) and data (circle) for the calculated variable, pH, over time.**

Alkalinity decreases as calcite precipitates due to the removal of  $\text{CO}_3^{2-}$ . Two lines are shown in Figure 10-5 for alkalinity. One line represents dissolved alkalinity and the other the total alkalinity which includes both dissolved alkalinity and particulate calcite. Calcite is included because the standard measurement technique for alkalinity is a titration which involves adding acid to the sample which potentially dissolves particulate calcite and the  $\text{CO}_3^{2-}$  from the calcite may be included in the measurement as alkalinity.

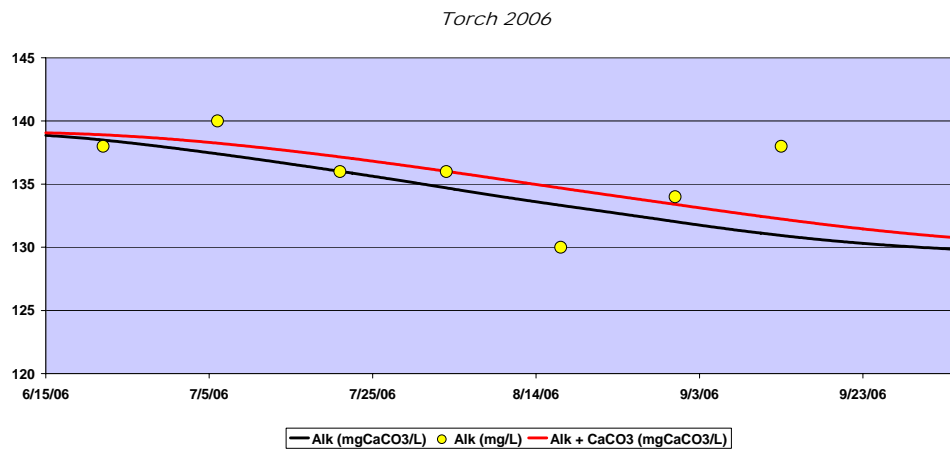


**Figure 10-5 Model output (line) and data (circle) for the calculated variable, alkalinity, over time.**

Conductivity decreases due to the removal of both  $\text{CO}_3^{2-}$  and  $\text{Ca}^{2+}$  since each ion contributes to the specific conductance. The model conductivity is calculated using equations (4-3) and (4-4) as explained in Chapter 4.

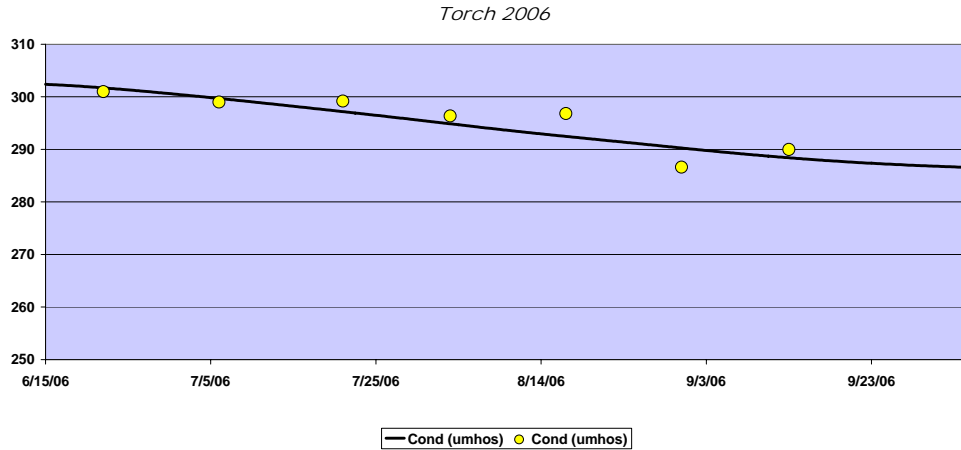


**Figure 10-6 Model output (line) and data (circle) for the calculated variable, conductivity, over time.**

The model output for three calculated optical variables are shown along with data in Figure 10-7 through Figure 10-9. As in equation (4-7), turbidity is modeled as a function of the amount of scattering. For Torch Lake, scattering is primarily from calcite particles, so the turbidity estimate follows the prediction for the calcite concentration in the lake (Figure 10-1). Light extinction, calculated as shown in equation (4-5), is dominated by absorption, but scattering does contribute. The model for Secchi Depth (SD) in equation (4-6) includes both absorption and scattering.

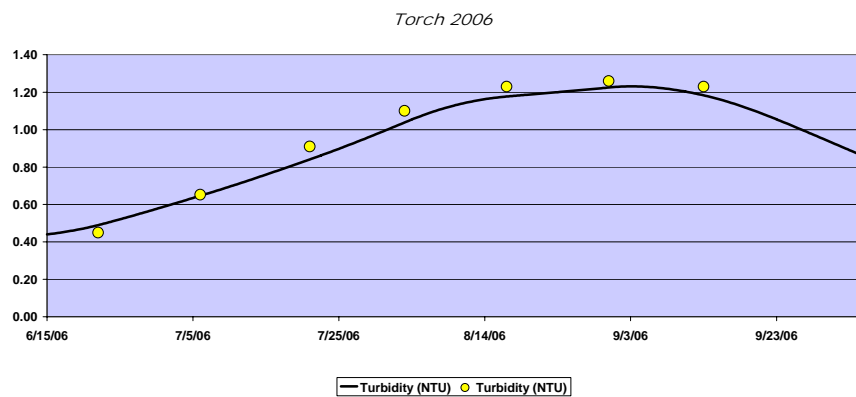


**Figure 10-7 Model output (line) and data (circle) for the calculated variable, Turbidity, over time.**

Torch 2006

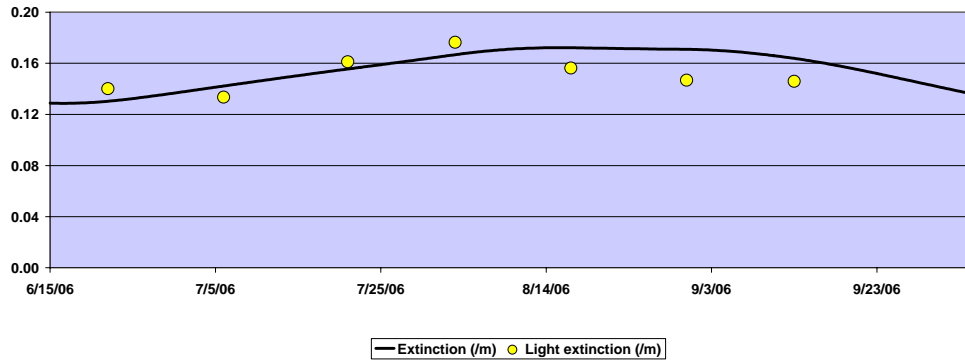


Figure 10-8 Model output (line) and data (circle) for the calculated variable, light extinction, over time.

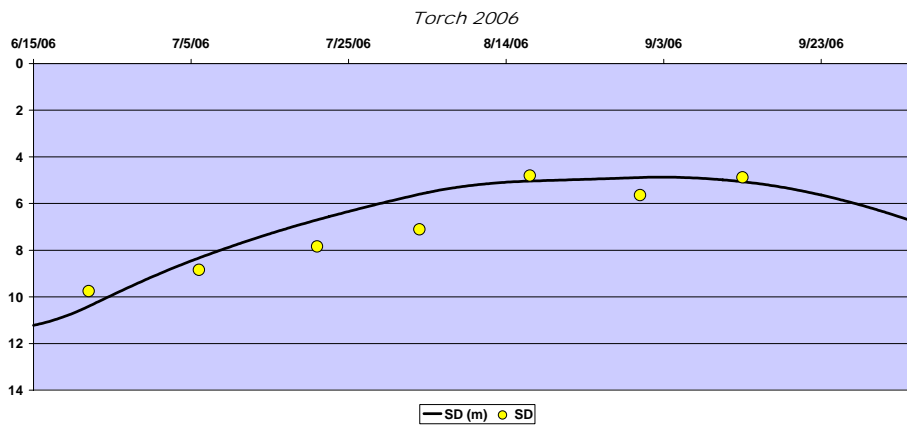


Figure 10-9 Model output (line) and data (circle) for the calculated variable, Secchi Depth, over time.

## Analysis

The model was used to evaluate various hypotheses related to which mechanisms drive calcite precipitation in Torch Lake. Two different analytical approaches are presented here, one using factorial experiments and the other with a sensitivity analysis.

## Factorial Experiment

In order to quantify the impact of the temperature rise compared to other factors driving precipitation, a factorial experimental setup was used. (Berthouex and Brown 1994)

Though this approach is most commonly used for experimental design (i.e., to reduce cost by running fewer data-collection experiments), the benefit of using it here despite minimal cost per experiment (model run) is the insight it provides into the interaction effects of the different factors influencing calcite precipitation.

The three factors evaluated were temperature change, primary productivity and air exchange. To consider the temperature change, a typical temperature rise (from 10°C to 22 °C) over the summer was compared to keeping the temperature constant at 10°C. For both air exchange and primary productivity, comparisons were made between model runs with and without the processes. Table 10-1 shows the results of the analysis.

**Table 10-1 Summary of the Main and Interaction Effects of Predicted Factors on Cumulative Calcite Precipitation in Torch Lake (in mg/L CaCO<sub>3(s)</sub>)**

Factors	Effect	%
Average	6.2	57.4%
Temp	4.7	43.8%
AirExch	2.7	25.1%
PrPr	0.0	-0.2%
Temp-AirExch	1.8	17.1%
Temp-PrPr	0.0	-0.3%
AirExch-PrPr	0.0	-0.1%
Temp-AirExch-PrPr	0.0	-0.1%

The cumulative calcite precipitation amount predicted for the ‘normal’ simulation (temperature normal and both air exchange and primary production processes included) is

10.8 mg/L. The average shown in the table of 6.2 mg/L is the average of all 8 model runs ( $2^3$ ) and is lower since it includes the scenarios when the temperature is fixed at 10 °C and there is no air exchange or primary production. The next three rows show the effect of each individual factor. This number is the difference between two averages – the average of all the runs with the parameter low and the average of all the runs with the parameter high. For example, the results show that the amount of total calcite precipitation with normal temperature changes as compared to a fixed temperature is an increase of 4.7 mg/L.

The interactions measure the amount that the individual effects cannot be simply added together to result in the combined effect. This is calculated as the average difference between the effect of a factor at the low setting of another factor with the effect of the factor at the high setting of the other factor. In other words is the effect of a factor being influenced by the setting of another factor (Berthouex and Brown, 1994)?

This analysis shows that keeping temperature fixed at 10 °C (that is, it does not gradually increase to 22 °C mid summer and then start to decrease again) has more of an impact on the expected total amount of calcite precipitating over the season than not allowing air exchange of CO<sub>2</sub>. As we would expect, there is an interaction effect between temperature and air exchange (1.8 mg CaCO<sub>3(s)</sub>/L) so we should note that, not surprisingly, one of the impacts of fixing the temperature at 10 °C is to decrease the air exchange.

In comparison, the presence or absence of primary production appears to have a negligible effect. Note that this effect is limited to the change in pH driving calcite saturation levels caused by the phytoplankton growth. Other possible roles of picoplankton, such as providing surface area or other special conditions in their microenvironment that facilitate calcite precipitation, are not considered here.

## **Local Sensitivity over Time**

The other analytical approach taken was to investigate the sensitivity of both the saturation index and the precipitation rate to each factor. A percent change approach was considered and rejected since a critical flaw to this method is how to consider a percent change in temperature in comparison to a percent change in primary production or air exchange. This difficulty was resolved by using the model to compare the sensitivity of the saturation index, and the precipitation rate, to the removal of each process (e.g., no temperature change, no primary production) for each time step in the model calculations. The common unit allowing comparisons between all the factors is the time span of the calculation step. Another benefit of this approach is that the sensitivity calculation is referenced to the calibrated model, which avoids unrealistic combinations of model parameters. Figure 10-10 and Figure 10-11 show this sensitivity analysis on the saturation index for two model scenarios – with the low and high values of NPP, 4 and 26 mgC/m<sup>2</sup>/day average net primary production.

### **The Saturation Index**

At each model time step the saturation index was calculated with and without one factor held constant. For example, the temperature was kept fixed at the temperature of the previous time step, and the saturation index was compared to the normal temperature for that time step. For air exchange and primary production, the SI was calculated with and without the change in  $c_T$  due to each process. (Note that the plot of delta SI due to temperature change shows clusters of relatively straight lines because the slope of the interpolation line between two temperature data points is straight.)

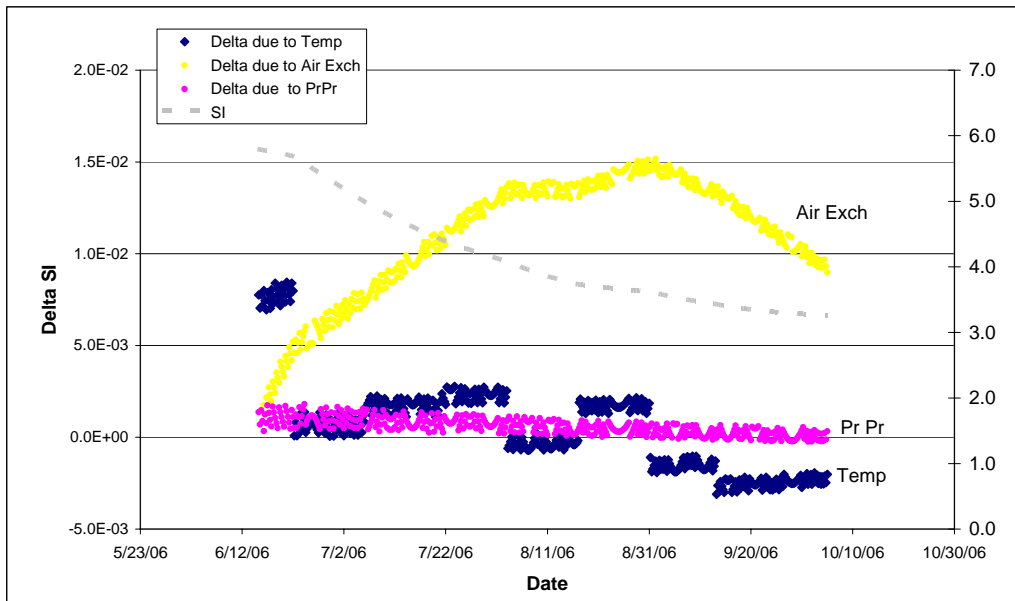


Figure 10-10 Change in the saturation index at each model time step due to air exchange, primary production or the temperature change. NPP = 4 mgC/m<sup>2</sup>/day

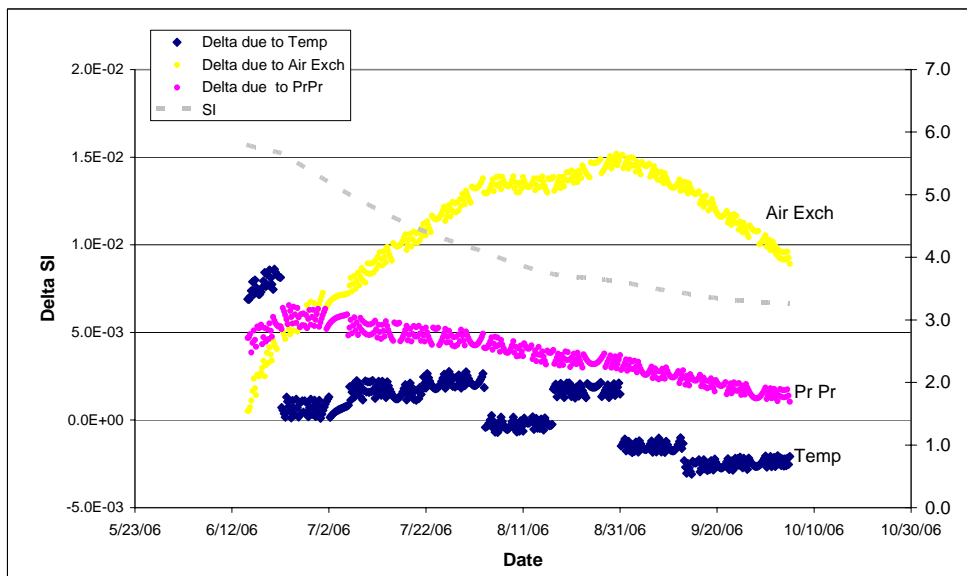
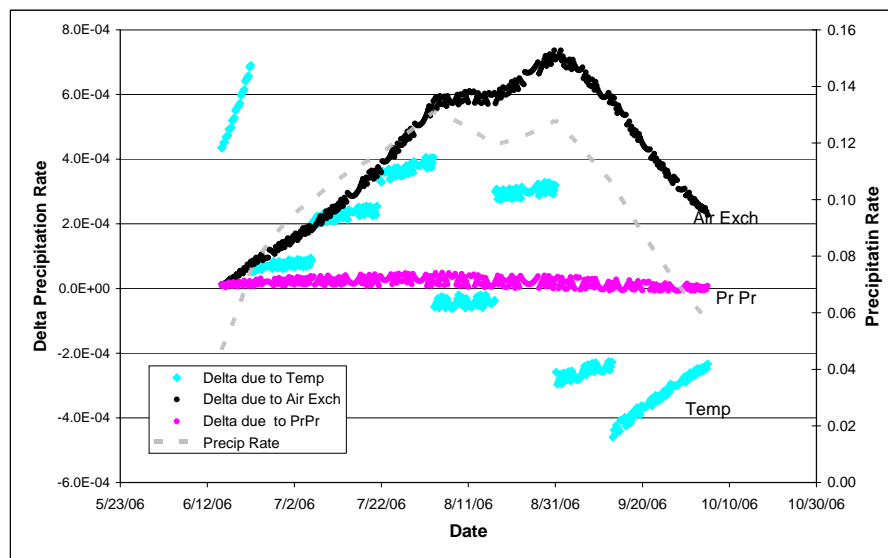


Figure 10-11 Change in the saturation index at each model time step due to air exchange, primary production or the temperature change. NPP = 26 mgC/m<sup>2</sup>/day

The results of this analysis suggest that air exchange is the most significant factor in changing the saturation index. For the scenario with an average NPP = 26 mgC/m<sup>2</sup>/day, temperature and primary production are higher at the start of the model horizon in June. Through October, temperature has a less significant impact on the saturation index than both air exchange and primary production. For the scenario with an average NPP = 4 mgC/m<sup>2</sup>/day, primary production has a minimal effect on the saturation index throughout the time horizon. In fact, as shown in Figure 10-10 the line for the change in the saturation index due to the removal of primary production is close to zero.

### The Precipitation Rate

Figure 10-12 and Figure 10-13 below show the results of the local sensitivity analysis described above applied to the precipitation rate.



**Figure 10-12 Change in the calcite precipitation rate at each model time step due to air exchange, primary production, or the temperature change. NPP = 4 mgC/m<sup>2</sup>/day**

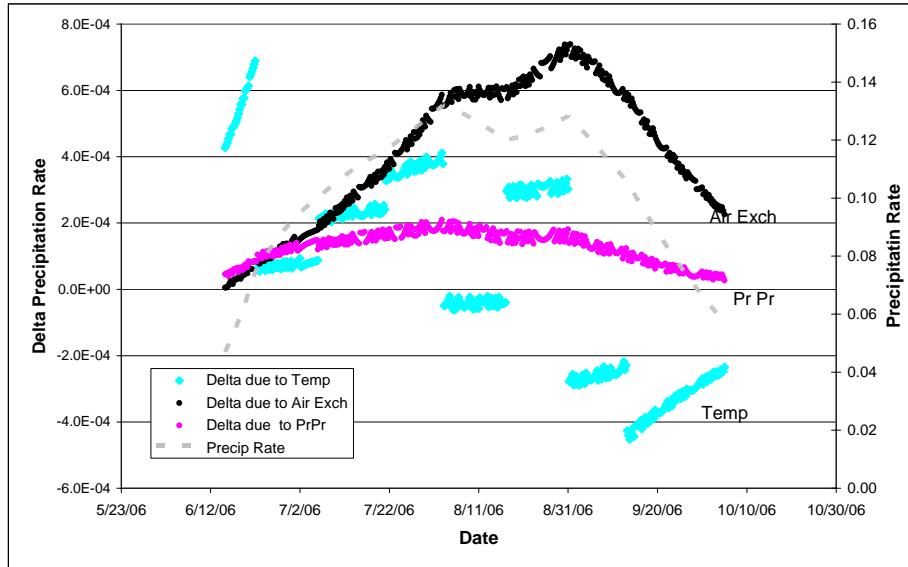


**Figure 10-13 Change in the calcite precipitation rate at each model time step due to air exchange, primary production, or the temperature change. NPP = 26 mgC/m<sup>2</sup>/day**

Air exchange of CO<sub>2</sub> still has the largest effect compared to the other factors, but for the precipitation rate temperature has a much greater effect than primary production, for either scenario. The sensitivity of the precipitation rate to primary production is minimal in the NPP = 4 mgC/m<sup>2</sup>/day scenario and still significantly lower than temperature and air exchange in the NPP = 26 mgC/m<sup>2</sup>/day scenario.

The fact that temperature has a much more significant impact on the precipitation rate as compared to the SI is consistent with the results of the analysis described in Chapter 5 showing the direct temperature effect on the chemical reaction rate as being much larger than the temperature effects on the solubility product ( $K_{sp}$ ) or the carbonate equilibrium constants ( $K_1$  and  $K_2$ ).

## **Conclusions**

Temperature affects the rate of calcite precipitation in many ways. The direct effects include reducing the solubility, represented by the temperature dependence of  $K_{sp}$ , the shift in the carbon system represented by temperature dependence of  $K_1$  and  $K_2$ , as well as the increase in the chemical reaction rate represented by the Arrhenius effect.

Temperature also affects the rate calcite precipitation indirectly through the temperature dependences of primary production rates, the air exchange rate and the timing and length of the stratified period in a lake.

Changes in the solubility ( $K_{sp}$ ) due to temperature are often cited as a driver of calcite precipitation, but the shift in the carbonate system was shown to be of equal significance to the precipitation rate for the conditions found in Torch Lake. The predicted Arrhenius effect of the temperature change on the chemical reaction of calcite precipitation was found to be an order of magnitude greater than either of these changes (from  $K_{sp}$  or  $K_1/K_2$ ) to the saturation level.

For Torch Lake, the model shows the saturation level and the calcite precipitation rate are affected more by air exchange than by primary production. Or in other words, the  $\text{CO}_2$  flux to the air is greater than the  $\text{CO}_2$  use by primary production in the period from June to October in Torch Lake. Note that is might not be the case for more eutrophic systems.

Air exchange needs to be considered when analyzing the drivers of calcite precipitation in oligotrophic lakes. Mass balance models can be useful tools in furthering our understanding of the various processes involved in calcite precipitation in lakes.

## References

- Berthouex, P. M., and Brown, L. C. (1994). "Statistics for environmental engineers." 335. Chapter 27 & 28.
- Beven, K., and Freer, J. (2001). "Equifinality, data assimilation, and uncertainty estimation in mechanistic modelling of complex environmental systems using the GLUE methodology." *Journal of Hydrology*, 249(1-4), 11-29.
- Bretz, N., Branson, D., Hannert, T., Roush, P. and D. Endicott. 2005. Characterization of Groundwater Phosphorus in Torch Lake. Three Lakes Association. Bellaire, MI.
- Brezonik, P.L. 1994. Chemical Kinetics and Process Dynamics in Aquatic Systems. Lewis Publications-CRC Press, Boca Raton, Fla., 754 pp.
- Brown, C. A., Compton, R. G., and Narramore, C. A. (1993). "The Kinetics of Calcite Dissolution Precipitation." *J. Colloid Interface Sci.*, 160(2), 372-379.
- Cariboni, J., Gatelli, D., Liska, R., and Saltelli, A. (2007). "The role of sensitivity analysis in ecological modelling." *Ecol. Model.*, 203(1-2), 167-182.
- Chapra, S.C. 1997. Surface water quality modeling. New York, McGraw-Hill.
- Chapra, S.C. and Canale, R.P, Numerical Methods for Engineers, 5th ed., McGraw-Hill, New York, N.Y., 2006.
- Chapra, S.C. and Dobson, H.F.H. 1981. "Quantification of the Lake Trophic Typologies of Naumann (Surface Quality) and Thienemann (Oxygen) with Special Reference to the Great Lakes," *Internat. Assoc. Great Lakes Res.* 7(2): 182-193.
- Chou, L., Garrels, R. M., and Wollast, R. (1988). "Comparative-Study of the Dissolution Kinetics and Mechanisms of Carbonates in Aqueous-Solutions." *Chem. Geol.*, 70(1-2), 77-77.
- Cole, J. J., and Caraco, N. F. (1998). "Atmospheric exchange of carbon dioxide in a low-wind oligotrophic lake measured by the addition of SF<sub>6</sub>." *Limnol. Oceanogr.*, 43(4), 647-656.
- Cole, J. J., Caraco, N. F., Kling, G. W., and Kratz, T. K. (1994). "Carbon-Dioxide Supersaturation in the Surface Waters of Lakes." *Science*, 265(5178), 1568-1570.

- Compton, R. G., and Pritchard, K. L. (1990). "The Dissolution of Calcite at pH-Greater-Than-7 - Kinetics and Mechanism." *Philosophical Transactions of the Royal Society of London Series A-Mathematical Physical and Engineering Sciences*, 330(1609), 47-70.
- Crusius, J., and Wanninkhof, R. (2003). "Gas transfer velocities measured at low wind speed over a lake." *Limnol.Oceanogr.*, 48(3), 1010-1017.
- Danenlouwerse, H. J., Lijklema, L., And Coenraats, M. (1995). "Coprecipitation of Phosphate with Calcium-Carbonate in Lake Veluwe." *Water Res.*, 29(7), 1781-1785.
- Depinto, J. V., Scheffe, R. D., Booty, W. G., and Young, T. C. (1989). "Predicting Reacidification of Calcite Treated Acid Lakes." *Can.J.Fish.Aquat.Sci.*, 46(2), 323-332.
- Dituro, D. M. (1995). "Evaluation of Methods for Computing the Thermodynamic Properties of Aqueous Chemical-Species." *Abstracts of Papers of the American Chemical Society*, 210 56-ENVR.
- Dittrich, M., Dittrich, T., Sieber, I., and Koschel, R. (1997). "A balance analysis of phosphorus elimination by artificial calcite precipitation in a stratified hardwater lake." *Water Res.*, 31(2), 237-248.
- Dittrich, M., and Koschel, R. (2002). "Interactions between calcite precipitation (natural and artificial) and phosphorus cycle in the hardwater lake." *Hydrobiologia*, 469(1-3), 49-57.
- Dittrich, M. and Obst, M. 2004. Are picoplankton responsible for calcite precipitation in lakes? *Ambio*, 33(8), 559-564.
- Dittrich, M., Kurz, P., and Wehrli, B. 2004. The role of autotrophic picocyanobacteria in calcite precipitation in an oligotrophic lake. *Geomicrobiol.J.*, 21(1), 45-53.
- Dodson, S.I. 2004 *Introduction to Limnology*. New York, McGraw-Hill.
- Emerson, S. (1975). "Chemically Enhanced CO<sub>2</sub> Gas-Exchange in a Eutrophic Lake - General Model." *Limnol.Oceanogr.*, 20(5), 743-753.
- Endicott, D., Branson, D., Bretz, N., and Hannert, T, March 17, 2006, "Development of a predictive nutrient-based water quality model for Torch Lake", Three Lakes Association, Bellaire, Michigan 49615, MDEQ Grant PO# 761P40021 (<http://3lakes.com/downloads/torchmodel06.pdf>)

- Fahey, Timothy J. and Alan K. Knapp, Eds. 2007. Principles and Standards for Measuring Primary Production. Oxford University Press.
- Hartley, A. M., House, W. A., Callow, M. E., and Leadbeater, B. S. C. (1997). "Coprecipitation of phosphate with calcite in the presence of photosynthesizing green algae." *Water Res.*, 31(9), 2261-2268.
- Hartley, A. M., House, W. A., Callow, M. E., and Leadbeater, B. S. C. (1995). "The Role of a Green-Alga in the Precipitation of Calcite and the Coprecipitation of Phosphate in Fresh-Water." *Int.Rev.Gesamt.Hydrobiol.*, 80(3), 385-401.
- Hodell, D. A., Schelske, C. L., Fahnenstiel, G. L., and Robbins, L. L. (1998). "Biologically induced calcite and its isotopic composition in Lake Ontario." *Limnol.Oceanogr.*, 43(2), 187-199.
- Holzbecher, E., and Nutzmann, G. (2000). "Influence of the subsurface watershed on eutrophication - Lake Stechlin case study." *Ecol.Eng.*, 16(1), 31-38.
- Homa, E. S., and Tufts University. Dept. of Environmental and Water Resources Engineering. (2005). "Modeling the effects of calcite precipitation and dissolution on the chemistry of natural waters." Masters thesis.
- Hornberger, G. M., and Spear, R. C. (1981). "An Approach to the Preliminary-Analysis of Environmental Systems." *J.Environ.Manage.*, 12(1), 7-18.
- House, W. A. (1990). "The Prediction of Phosphate Coprecipitation with Calcite in Fresh-Waters." *Water Res.*, 24(8), 1017-1023.
- House, W. A. (1987). "Inhibition of Calcite Crystal-Growth by Inorganic-Phosphate." *J.Colloid Interface Sci.*, 119(2), 505-511.
- House, W. A., And Donaldson, L. (1986). "Adsorption and Coprecipitation of Phosphate on Calcite." *J.Colloid Interface Sci.*, 112(2), 309-324.
- Hudson, J. J., and Taylor, W. D. (1996). "Measuring regeneration of dissolved phosphorous in planktonic communities." *Limnol.Oceanogr.*, 41(7), 1560-1565.
- Hudson, J. J., Taylor, W. D., and Schindler, D. W. (2000). "Phosphate concentrations in lakes." *Nature*, 406(6791), 54-56.
- Hudson, J. J., Taylor, W. D., and Schindler, D. W. (1999). "Planktonic nutrient regeneration and cycling efficiency in temperate lakes." *Nature*, 400(6745), 659-661.

- Inskeep, W. P., and Bloom, P. R. (1985). "An Evaluation of Rate-Equations for Calcite Precipitation Kinetics at Pco<sub>2</sub> Less than 0.01 Atm and pH Greater than 8." *Geochim.Cosmochim.Acta*, 49(10), 2165-2180.
- Johnson, K. S. (1982). "Carbon-Dioxide Hydration and Dehydration Kinetics in Sea-Water." *Limnol.Oceanogr.*, 27(5), 849-855.
- Jonsson, A., Aberg, J., Lindroth, A., and Jansson, M. (2008). "Gas transfer rate and CO<sub>2</sub> flux between an unproductive lake and the atmosphere in northern Sweden." *Journal of Geophysical Research-Biogeosciences*, 113(G4), G04006.
- Kalff, J. (2002) *Limnology*. Prentice-Hall, Englewood Cliffs, NJ
- Kleiner, J. (1988). "Coprecipitation of Phosphate with Calcite in Lake Water - a Laboratory Experiment Modeling Phosphorus Removal with Calcite in Lake Constance." *Water Res.*, 22(10), 1259-1265.
- Koschel, R., J. Benndorf, G. Proft and F. Recknagel. 1987. Model-assisted evaluation of alternative hypotheses to explain in the self-protection mechanism of lakes due to calcite precipitation. *Ecol. Model.* 39: 59-65.
- Lenhart, T., Eckhardt, K., Fohrer, N., and Frede, H. G. (2002). "Comparison of two different approaches of sensitivity analysis." *Phys.Chem.Earth*, 27(9-10), 645-654.
- Lin, Y. P., and Singer, P. C. (2005). "Effects of seed material and solution composition on calcite precipitation." *Geochim.Cosmochim.Acta*, 69(18), 4495-4504.
- Morel, F., and Hering, J. G., 1993. Principles and applications of aquatic chemistry. New York, Wiley-Interscience.
- Nancolla.Gh, and Reddy, M. M. (1971). "Crystallization of Calcium Carbonate .2. Calcite Growth Mechanism." *J.Colloid Interface Sci.*, 37(4), 824-&.
- Nilsson, O., and Sternbeck, J. (1999). "A mechanistic model for calcite crystal growth using surface speciation." *Geochim.Cosmochim.Acta*, 63(2), 217-225.
- Obst, M., Dittrich, M., and Kuehn, H. (2006). "Calcium adsorption and changes of the surface microtopography of cyanobacteria studied by AFM, CFM, and TEM with respect to biogenic calcite nucleation." *Geochemistry Geophysics Geosystems*, 7 Q06011.
- O'Connor, D. J. (1998). "Chemical reactions and gas transfer in natural waters." *Journal of Environmental Engineering-Asce*, 124(2), 85-93.
- O'Connor, D.J. (1983). "Wind Effects on Gas-Liquid Transfer Coefficients." *Journal of Environmental Engineering*, 109(3):731-752.

- Peng, F., and Effler, S. W. (2005). "Inorganic tripton in the Finger Lakes of New York: importance to optical characteristics." *Hydrobiologia*, 543 259-277.
- Plant, L. J., and House, W. A. (2002). "Precipitation of calcite in the presence of inorganic phosphate." *Colloids and Surfaces A-Physicochemical and Engineering Aspects*, 203(1-3), 143-153.
- Plummer, L. N., Wigley, T. M. L., and Parkhurst, D. L. (1978). "Kinetics of Calcite Dissolution in CO<sub>2</sub>-Water Systems at 5-Degrees-C to 60-Degrees-C and 0.0 to 1.0 Atm CO<sub>2</sub>." *Am.J.Sci.*, 278(2), 179-216.
- Plummer, L.N. and Busenberg, E. 1982. The solubilities of calcite, aragonite and vaterite in CO<sub>2</sub>-H<sub>2</sub>O solutions between 0 and 90 oC, and an evaluation of the aqueous model for the system CaCO<sub>3</sub>-CO<sub>2</sub>-H<sub>2</sub>O. *Geochim. Cosmochim. Acta* 46:1011-1040.
- Portielje, R., and Lijklema, L. (1995). "Carbon-Dioxide Fluxes Across the Air-Water-Interface and its Impact on Carbon Availability in Aquatic Systems." *Limnol.Oceanogr.*, 40(4), 690-699.
- Proft, G., and Stutter, E. (1993). "Calcite Precipitation in Hard Water Lakes in Calculation and Experiment." *Int.Rev.Gesamt.Hydrobiol.*, 78(2), 177-199.
- Reichert, P., and Omlin, M. (1997). "On the usefulness of overparameterized ecological models." *Ecol.Model.*, 95(2-3), 289-299.
- Saltelli, A., Ratto, M., Tarantola, S., Campolongo, F., European Commission, and Joint Res Ctr Ispra. (2006). "Sensitivity analysis practices: Strategies for model-based inference." *Reliab.Eng.Syst.Saf.*, 91(10-11), 1109-1125.
- Saltelli, A., Tarantola, S., and Campolongo, F. (2000). "Sensitivity analysis as an ingredient of modeling." *Statistical Science*, 15(4), 377-395.
- Scavia, D. (1979). "Examination of Phosphorus Cycling and Control of Phytoplankton Dynamics in Lake-Ontario with an Ecological Model." *Journal of the Fisheries Research Board of Canada*, 36(11), 1336-1346.
- Schwarzenbach, R. P., Gschwend, P. M., and Imboden, D. M. (2003). "Environmental organic chemistry." xiii, 1313.
- Smith, S. V. (1985). "Physical, Chemical and Biological Characteristics of CO<sub>2</sub> Gas Flux Across the Air Water Interface." *Plant Cell and Environment*, 8(6), 387-398.

- Snoeyink, V.L. and Jenkins D. 1980. *Water Chemistry.*, New York, John Wiley & Sons, Inc.
- Stumm, W. and Morgan, J.J. 1996. *Aquatic Chemistry*, 3rd Ed., New York, Wiley-Interscience, 1022 pp
- Teng, H. H., Dove, P. M., and De Yoreo, J. J. (2000). "Kinetics of calcite growth: Surface processes and relationships to macroscopic rate laws." *Geochim.Cosmochim.Acta*, 64(13), 2255-2266.
- Thompson, J. B., and Ferris, F. G. (1990). "Cyanobacterial Precipitation of Gypsum, Calcite, and Magnesite from Natural Alkaline Lake Water." *Geology*, 18(10), 995-998.
- Thompson, J. B., SchultzeLam, S., Beveridge, T. J., and DesMarais, D. J. 1997. Whiting events: Biogenic origin due to the photosynthetic activity of cyanobacterial picoplankton. *Limnol. Oceanogr.*, 42(1), 133-141.
- Vanderploeg, H. A., Eadie, B. J., Liebig, J. R., and Tarapchak, S. J. (1987). "Contribution of Calcite to the Particle-Size Spectrum of Lake-Michigan Seston and its Interactions with the Plankton." *Can.J.Fish.Aquat.Sci.*, 44(11), 1898-1914.
- Vollenweider, R, Munawar, M., and Stadelma.P. (1974). "Comparative Review of Phytoplankton and Primary Production in Laurentian Great Lakes." *Journal of the Fisheries Research Board of Canada*, 31(5), 739-762.
- Wanninkhof, R., and Knox, M. (1996). "Chemical enhancement of CO<sub>2</sub> exchange in natural waters." *Limnol.Oceanogr.*, 41(4), 689-697.
- Weisse, T. (1988). "Dynamics of Autotrophic Picoplankton in Lake Constance." *J.Plankton Res.*, 10(6), 1179-1188
- Wollast, R. (1990) "Rate and Mechanism of Dissolution of Carbonates in the System CaCO<sub>3</sub> – MgCO<sub>3</sub>." *Aquatic Chemical Kinetics: Reaction Rates of Processes in Natural Waters* edited by W. Stumm, Wiley, New York, NY, 431-446
- Yates, K. K., and Robbins, L. L. (1998). "Production of carbonate sediments by a unicellular green alga." *Am.Mineral.*, 83(11-12), 1503-1509.
- Yohn, Sharon S., Parsons, Matthew J., Long, David, T., Giesy, John P., Scholle, Lydia, and Patino, Lina C., *Inland Lakes Sediment Trends: Sediment Analysis Results for Six Michigan Lakes, Yearly report: 2002-2003*, Houghton Lake, Hubbard Lake, Imp Lake, Round Lake (North Manistique), Torch Lake, Witch Lake, Aqueous & Environmental Geochemical Labs, Dept. Geological Sciences, Michigan State University, E. Lansing, MI (<http://www.deq.state.mi.us/documents/deq-wb-sw-as-sedimenttrend0203finalreport.pdf>)

Zheng, Y., and Keller, A. A. (2006). "Understanding parameter sensitivity and its management implications in watershed-scale water quality modeling." *Water Resour. Res.*, 42(5), W05402.

# APPENDICES

<b>Appendix A 2006 Notation</b> .....	2
<b>Appendix B Model Settings and Parameters</b> .....	3
<b>Appendix C Calibration Calculations</b> .....	8
Calcite Precipitation Rate Estimation Methods .....	8
Calcite Settling Velocity Estimation Methods.....	12
<b>Appendix D pH2K Model Documentation</b> .....	18

## Appendix A 2006 Notation

Variable	Symbol	Units*
$a_p$	Phytoplankton	$\mu\text{gChla/L}$
$A$	lake surface area	$\text{m}^2$
$Alk$	alkalinity	$\text{eq/L}$
$[\text{Ca}^{2+}]$	total dissolved calcium concentration	$\text{M}$
$\text{CaCO}_{3(s)}$	calcite	$\text{M}$
$\text{CO}_2$	carbon dioxide	$\text{M}$
$[\text{CO}_2]_s$	saturation concentration of carbon dioxide	$\text{M}$
$\text{CO}_3^{2-}$	carbonate ion	
Cond	specific conductance	$\mu\text{S}\cdot\text{cm}^{-1}$
$c_T$	total inorganic carbon	$\text{M}$
$F_d$	fraction of inorganic phosphorus dissolved	
$F_p$	fraction of inorganic phosphorus associated with calcite	
$\text{HCO}_3^-$	bicarbonate ion	
IAP	ion activity product	
$k_d$	phytoplankton death rate	$/\text{d}$
$K_{dp}$	partition coefficient of inorganic phosphorus on calcite	$\text{M}^{-1}$
$k_e$	extinction coefficient	$/\text{m}$
$k_f$	area-specific precipitation rate	$\text{L}/(\text{M}\cdot\text{m}^2\cdot\text{d})$
$k_g$	gross phytoplankton growth rate	$/\text{d}$
$K_H$	Henry's constant	$\text{M}/\text{atm}$
$k_{hy}$	hydrolysis rate	$/\text{d}_s$
$k_r$	phytoplankton respiration/excretion rate	$/\text{d}$
$K_{sp}$	calcite solubility product	$\text{M}^2$
$k_{sp}$	dissolved inorganic phosphorus half-saturation constant	$\mu\text{gP/L}$
$p_{\text{CO}_2}$	partial pressure of carbon dioxide in atmosphere	$\text{atm}$
pH	pH	
$p_i$	Inorganic phosphorus	$\mu\text{gP/L}$
$p_o$	Detrital phosphorus	$\mu\text{gP/L}$
$r_{ca}$	ratio of inorganic carbon to phytoplankton biomass	$\text{M}/\mu\text{gChla}$
$r_{cp}$	ratio of inorganic carbon to phosphorus	$\text{M}/\mu\text{gP}$
$r_{pa}$	ratio of phosphorus to chlorophyll	$\mu\text{gP}/\mu\text{gChla}$
$S$	particulate surface area	$\text{m}^2$
$T_a$	absolute temperature	$\text{K}$
$V$	epilimnion volume	$\text{m}^3$
$v_a$	phytoplankton settling velocity	$\text{m}/\text{d}$
$v_s$	calcite settling velocity	$\text{m}/\text{d}$
$v_o$	detrital phosphorus settling velocity	$\text{m}/\text{d}$

## Appendix B Model Settings and Parameters

Initial time	6/15/06	d
Final time	10/5/06	d
Calculation step	.0625	d
Print step	1.0000	d
Time of run	0.1065	minutes

Parameter	mass/vol	
Chlorophyll	0.40	ugA/L
SRP	2.00	ugP/L
Porg	0.10	ugP/L
pH	8.50	
CaCO3	0.20	mgCaCO3/L
Ca	42.50	mgCa/L
Mg	10.00	mg/L
Na	7.00	mg/L
K	0.70	mg/L
Cl	7.00	mg/L
SO4	14.00	mg/L
Calcium alkalinity	106.0432	mgCaCO3/L
Non-calcium Alkalinity	32.8165	mgCaCO3/L
Total Alkalinity	138.8598	mgCaCO3/L

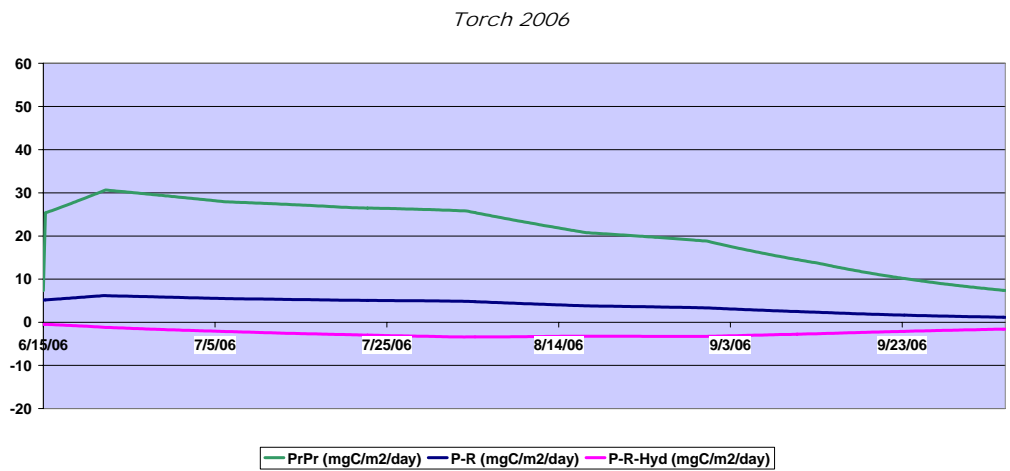
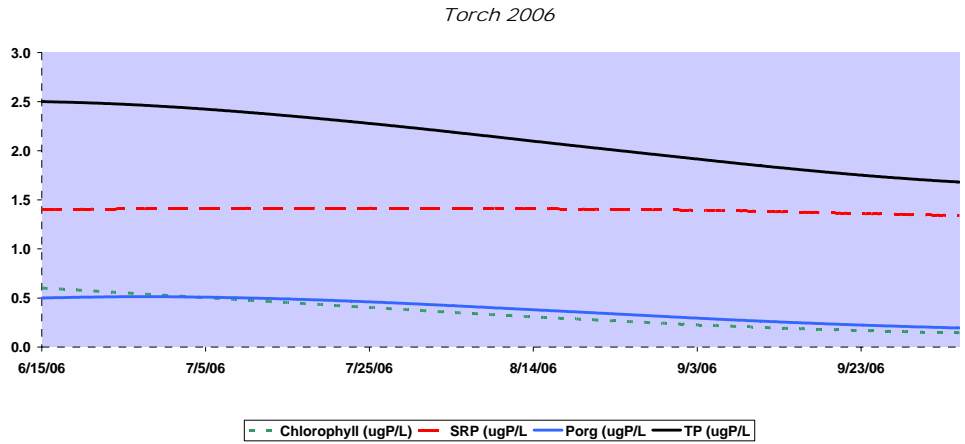
Parameter	Value	Units
Depth	10	m
pCO2	0.0003837	atm
Uw	1.5	m/s
KP	55000	L2/mol/m2/day
vCaCO3	1.800	m/d
vs-phytoplankton	0.000	m/d
Non-calcite ISS	0.500	mgD/L
Color absorption coefficient	0.050	/m

Thermocline diffusion	0.055	cm2/s
Thermocline thickness	10.000	m
Thermocline area	46702400	m2
Epilimnion volume	1118187019	m3
Surface area	68227000	m2
vo-organic P	0.000	m/d

Parameter	Value	Unit
Forward scattering fraction	0.94	/m
Water absorption coefficient	0.012	/m
Chlorophyll absorption constant	0.03	m <sup>2</sup> /mgA
Inorganic suspended solids absorption constant	0	m <sup>2</sup> /gD
Detritus absorption constant	0.016	m <sup>2</sup> /mgP
Calcite absorption constant	0	m <sup>2</sup> /gCaCO <sub>3</sub>
Water scattering coefficient	0.0015	/m
Chlorophyll scattering constant	0.1	m <sup>2</sup> /mgA
Inorganic suspended solids scattering constant	0.6	m <sup>2</sup> /gD
Detritus scattering constant	0.024	m <sup>2</sup> /mgP
Calcite scattering constant	0.8	m <sup>2</sup> /gCaCO <sub>3</sub>

### Three Primary Production Scenarios

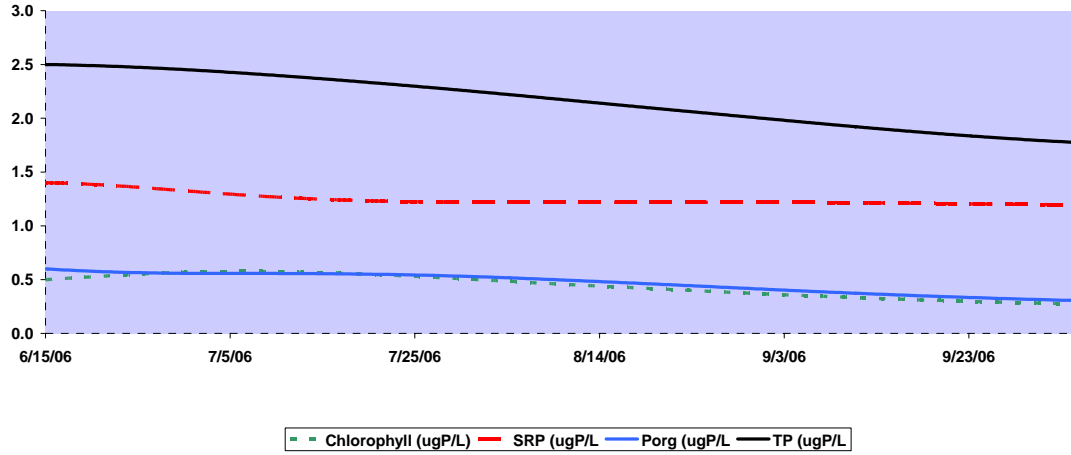
LOW, NPP = 4 mgC/m<sup>2</sup>/day



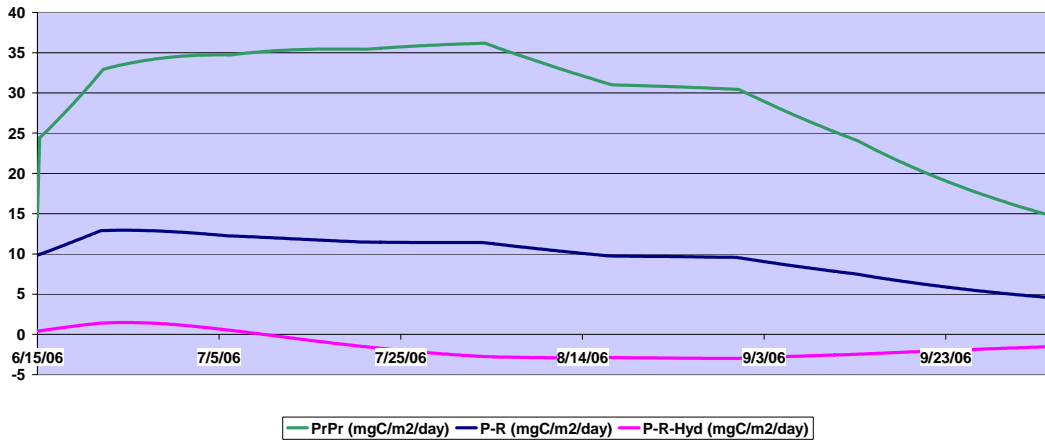
<b>kde</b>	<b>0.050</b>	<b>/d</b>
<b>kg</b>	<b>1.000</b>	<b>/d</b>
<b>khyd</b>	<b>0.050</b>	<b>/d</b>
<b>ksrp</b>	<b>6.000</b>	<b>ugP/L</b>
<b>kr</b>	<b>0.150</b>	<b>/d</b>

MID NPP = 10 mgC/m2/day

Torch 2006



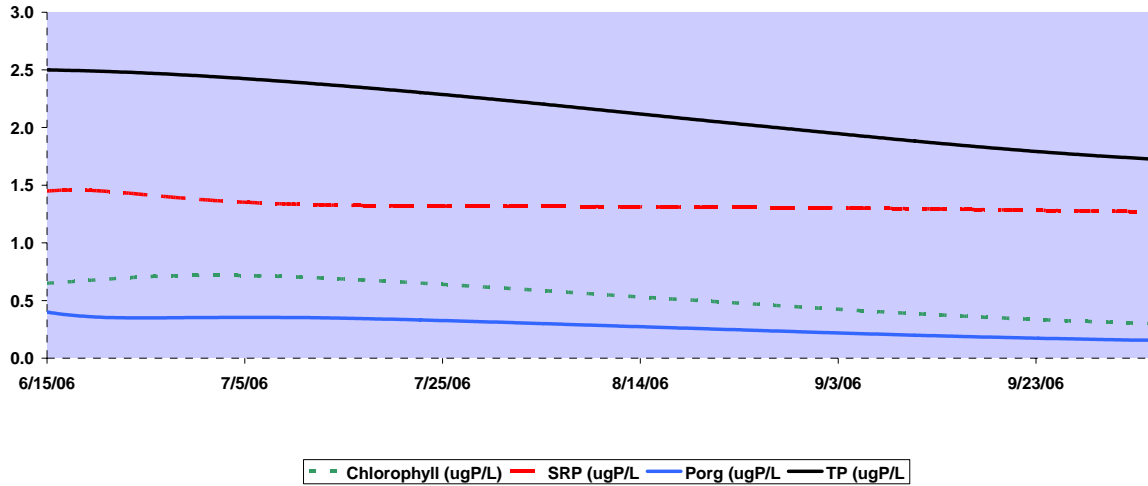
Torch 2006



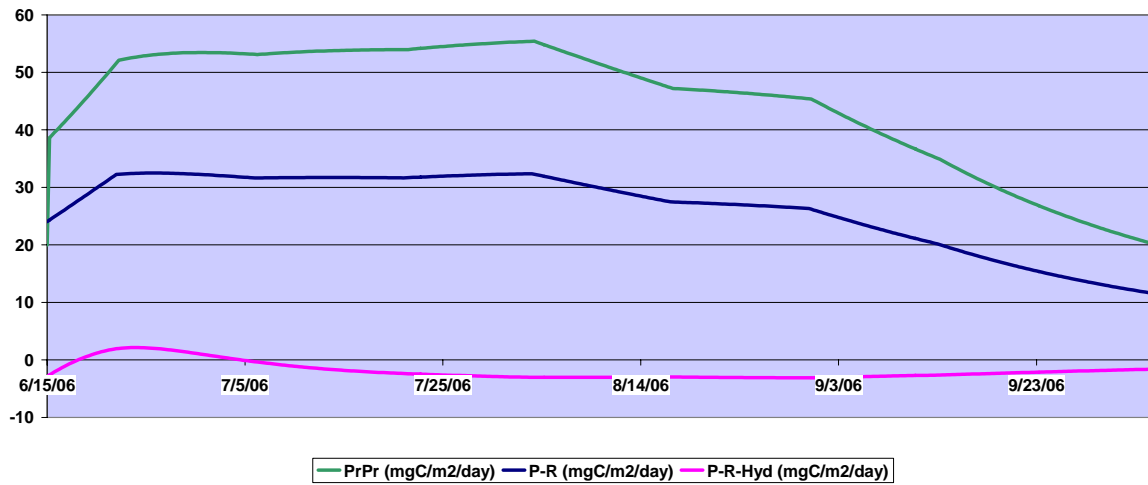
<b>kde</b>	<b>0.070</b>	<b>/d</b>
<b>kg</b>	<b>1.000</b>	<b>/d</b>
<b>khyd</b>	<b>0.070</b>	<b>/d</b>
<b>ksrp</b>	<b>5.000</b>	<b>ugP/L</b>
<b>kr</b>	<b>0.130</b>	<b>/d</b>

HIGH NPP = 27 mgC/m2/day

Torch 2006



Torch 2006



kde	0.150	/d
kg	1.000	/d
khyd	0.300	/d
ksrp	4.000	ugP/L
kr	0.100	/d

## Appendix C Calibration Calculations

### Calcite Precipitation Rate Estimation Methods

#### 1. Dissolved Calcium Delta

$\Delta t := 90\text{day}$  Time of calcite increase. This is not the same as the whole time of the summer model horizon.

$\Delta\text{Ca} := 2 \frac{\text{mg}}{\text{L}}$  Range from 2- 4 mg/L

$\Delta\text{Precip} := \Delta\text{Ca} \cdot \frac{100}{40}$   $\Delta\text{Precip} = 5 \frac{\text{mg}}{\text{L}}$

$S_{\text{CaCO}_3} := \frac{\Delta\text{Precip}}{\Delta t}$   $S_{\text{CaCO}_3} = 0.056 \frac{\frac{\text{mg}}{\text{L}}}{\text{day}}$

A precipitation rate was calculated solely based on the magnitude of the decrease in dissolved calcium over the time period of the calcite increase. This approach includes the assumption that all of the dissolved calcium is removed by incorporation into calcite.

Considering the a time horizon from 60 to 90 days and a range of calcium change from 2 to 4 mg/L, the resulting range in calcite precipitation estimated with this method is 0.06 to 0.17 mg/L/day.

#### 2. Alkalinity Delta

Precipitation Rate from Alkalinity Differential

$\Delta t := 90\text{day}$  Time of calcite increase. This is not the same as the whole time of the summer model horizon.

$\Delta\text{Alk} := 5 \frac{\text{mg}}{\text{L}}$  Range from 5 -10 mg/L as CaCO<sub>3</sub>

$\Delta\text{Precip} := \Delta\text{Alk}$   $\Delta\text{Precip} = 5 \frac{\text{mg}}{\text{L}}$

$S_{\text{CaCO}_3} := \frac{\Delta\text{Precip}}{\Delta t}$   $S_{\text{CaCO}_3} = 0.056 \frac{\frac{\text{mg}}{\text{L}}}{\text{day}}$

The same approach was used again but with a alkalinity instead of calcium. A precipitation rate was calculated solely based on the magnitude of the decrease in alkalinity over the time period of the calcite increase. This approach includes the assumption that all of the alkalinity is removed by incorporation of  $[CO_3^{2-}]$  into calcite.

The precipitation estimate from the alkalinity differential matches the estimate from the dissolved calcium differential. Or in other words, the alkalinity delta and dissolved calcium delta both reflect an equal amount of calcite precipitation, given that the changes in alkalinity and dissolved calcium were both changed primarily by calcite precipitation.

### 3. Conductivity Delta

Before				Change				After	
pH	8.4			5.5 mg/L		CaCO3		pH	7.93
cT	2.77E-03			5.5E-05 mole/L		CaCO3		cT	2.72E-03
alk	2.78E-03			2.20 mg/L		Ca		alk	2.67E-03
				5.50 Alk in mg/L as CaCO3					
BEFORE									
	mg/L	MW	mole/L	mM/L	abs(z)	lamda	z*lam*mM	z^2*mM	
Ca	42.5	40.078	1.06E-03	1.06	2	59.5	126.19	4.242	5.5E-05
Mg	10	24.305	4.11E-04	0.41	2	53.1	43.69	1.646	
Na	7	22.990	3.04E-04	0.30	1	50.1	15.25	0.304	
K	0.7	39.098	1.79E-05	0.02	1	73.5	1.32	0.018	
H			3.98E-09	0.00	1	350	0.00	0.000	
CO3			3.05E-05	0.03	2	72	4.40	0.122	
HCO3			2.72E-03	2.72	1	44.5	120.87	2.716	5.5E-05
SO4	14	96.064	1.46E-04	0.15	2	80	23.32	0.583	
Cl	7	35.4527	1.97E-04	0.20	1	76.4	15.08	0.197	
NO3	0.3	62	4.84E-06	0.00	1	71.4	0.35	0.005	
OH			2.51E-06	0.00	1	198.6	0.50	0.003	
							<b>350.97</b>	<b>9.84</b>	
									<b>339.45</b>
									<b>9.49</b>
Ionic Strength								0.004745	
Monovalent ion activity coefficient, y								0.93	
Conductivity							BEFORE	303.6	micro-ohm/cm
							AFTER	293.6	
							Delta	10.0	

The amount of calcite precipitation that would explain Conductivity changing by 10-20 micro-ohms/cm is 5.5 - 11 mg/L, which is consistent with the rates predicted using the other methods. The calculation was done by starting with an initial pH, alkalinity and ion balance. The amount of total carbon was calculated from these as well as the contribution of each ion to conductivity, using the method described in Standard Methods (1995). The total carbon, alkalinity and calcium ions were decreased by the given amount of calcite precipitation and the resulting pH and ion concentrations were used to calculate a new conductivity value. Different amounts of calcite precipitation were entered until the conductivity delta of 10 (or 20 ) micro-ohms/cm was found. (The measurements of conductivity show the change over the season to be within this range.)

Considering the a time horizon from 60 to 90 days and a range of conductivity change from 10 to 20 micro-ohms/cm, the resulting range in calcite precipitation estimated with this method is 0.06 to 0.18 mg/L/day.

Note that the only change to total carbon in this calculation is due to calcite precipitation, whereas in the lake (and as shown in the pH2K model) there is also plankton growth and respiration as well as air-water exchange that is affecting the total carbon in the lake over this period. The ending pH calculated in this way thus should not be expected to exactly match the pH in the lake. (The calculation above shows an ending pH of 7.9, whereas the in lake data for the epilimnion does not go below 8.1 .)

See Standard Methods, 19th edition 1995. Page 2.43-45.

#### 4. Ending Calcite Concentration and Sediment Trap Data

Accumulation = Precipitation (IN) - Settling (OUT)

Settling

$$J := 1.6 \frac{\text{gm}}{\text{m}^2 \cdot \text{day}} \quad \text{Flux calculated with sediment trap data}$$

$$A = 7.4 \times 10^7 \text{m}^2 \quad \text{Total Surface Area}$$

$$V_{\text{ep}} = 7.8 \times 10^8 \text{m}^3 \quad \text{Volume of Epilimnion}$$

$$\frac{J \cdot A}{V_{\text{ep}}} = 0.153 \frac{\text{mg}}{\text{L} \cdot \text{day}} \quad \text{Calcite Settling Rate}$$

Accumulation

$$\frac{1 \frac{\text{mg}}{\text{L}}}{90\text{day}} = 0.011 \frac{\text{mg}}{\text{L} \cdot \text{day}} \quad \text{to} \quad \frac{1.5 \frac{\text{mg}}{\text{L}}}{60\text{day}} = 0.025 \frac{\text{mg}}{\text{L} \cdot \text{day}}$$

Accumulation + Settling = Precipitation

$$\frac{1 \frac{\text{mg}}{\text{L}}}{90\text{day}} + \frac{J \cdot A}{V_{\text{ep}}} = 0.164 \frac{\text{mg}}{\text{L} \cdot \text{day}}$$

$$\frac{1.5 \frac{\text{mg}}{\text{L}}}{60\text{day}} + \frac{J \cdot A}{V_{\text{ep}}} = 0.178 \frac{\text{mg}}{\text{L} \cdot \text{day}}$$

This estimation approach involves a simple mass balance summation using the sediment trap data and ending calcite concentration to represent settling and accumulation. Rearranging the mass balance equation of Accumulation = Precipitation (IN) - Settling (OUT) in order to calculate the precipitation rate as the sum of accumulation and settling. The precipitation rate estimated in this way is 0.16 to 0.18 mg/L/day.

#### 5. Ending Calcite Concentration and Sediment Core Data

Using the flux rate from Long and Parsons calculated from their sediment core data, the settling rate is lower than the rate from the 2006 sediment trap flux used above. The amount of calcite settled using the 2006 trap was 9.2 to 13.7 mg/L whereas the amount settling using Parson's flux was 5.5 to 8.2 mg/L. The precipitation rate based on Parson's sediment core data (~0.11 mg/L/day) is more in line with the other estimation methods, as well as closer to the value used in the calibrated model. The precipitation rate calculated from the 2006 sediment trap data (~0.17 mg/L/day) is higher than the other estimation methods which could be due to other mass in the trap that was not calcite.

## Calcite Settling Velocity Estimation Methods

### 1. Sediment trap data and average calcite concentration

The sedimentation traps were located within a hundred yards of the north deep basin, about a mile southwest of the Camp Hays Went Ha point where all the calcite samples were collected this past summer. The traps were placed 135 ft below the surface for 100 days. Diameter of the opening of the traps was 10 cm

$$r := \frac{10\text{cm}}{2} \quad A := \pi \cdot r^2 \quad A = 7.854 \times 10^{-3} \text{m}^2$$

$$t_{\text{trap}} := 102\text{day}$$

$$M := 1.277\text{gm}$$

$$J := \frac{M}{A \cdot t_{\text{trap}}} \quad J = 1.6 \frac{\text{gm}}{\text{m}^2 \cdot \text{day}} \quad \text{Total dry weight}$$

### Settling velocity

Use average calcite concentration = 1 mg/L

$$c := 1 \frac{\text{mg}}{\text{L}}$$

Velocity = Flux / Concentration  $v := \frac{J}{c}$

$$v = 1.6 \frac{\text{m}}{\text{day}}$$

Higher average calcite concentration

$$\frac{J}{1.5 \frac{\text{mg}}{\text{L}}} = 1.1 \frac{\text{m}}{\text{day}}$$

Lower average calcite concentration

$$\frac{J}{0.5 \frac{\text{mg}}{\text{L}}} = 3.2 \frac{\text{m}}{\text{day}}$$

Assumes dry weight = 100% calcite, so it is an upper bound. If any of the mass came from other sources the settling velocity would be lower. But most of the precipitation could have taken place in a time less than the total 102 days, and a reduced time would increase the calculated settling velocity.

## 2. Dissolved calcium delta and ending calcite concentration

$$H := 10\text{m}$$

Depth of epilimnion

$$\Delta t := 60\text{day}$$

Time of calcite increase. This is not the same as the whole time of the summer model horizon.

$$\Delta Ca := 4 \frac{\text{mg}}{\text{L}}$$

Range from 3 - 5 mg/L

$$\Delta \text{Precip} := \Delta Ca \cdot \frac{100}{40}$$

$$\Delta \text{Precip} = 10 \frac{\text{mg}}{\text{L}}$$

$$S_{\text{CaCO}_3} := \frac{\Delta \text{Precip}}{\Delta t}$$

$$S_{\text{CaCO}_3} = 0.167 \frac{\frac{\text{mg}}{\text{L}}}{\text{day}}$$

$$\text{CaCO}_3 := 1.5 \frac{\text{mg}}{\text{L}}$$

Ending calcite concentration after period of increase

$$v := \frac{H \cdot S_{\text{CaCO}_3}}{\text{CaCO}_3}$$

$$v = 1.1 \frac{\text{m}}{\text{day}}$$

$$v = \frac{H \cdot S_{\text{CaCO}_3}}{\bar{c}}$$

Derived from constant load model from Chapra 1997 p.68, equation 4.11

Delta Ca = 3 to 8 mg/L as Ca, Delta CaCO<sub>3</sub> = 1.0 to 2.0 mg/L, and time 60 – 90 days  
 $\Rightarrow v = 0.3$  to  $3.2$  m/day

### 3. Sediment trap data and calcium delta

$$H = 10 \text{ m} \quad S = 0.18 \frac{\text{mg}}{\text{L} \cdot \text{day}}$$

Precip rate (from calcium differential data)

$$t = 60 \text{ days} \quad J_{\text{settle}} := 1.6 \frac{\text{gm}}{\text{m}^2 \cdot \text{day}}$$

Flux rate from sediment trap data

$$\text{Init } v := 1.0$$

$$\text{Given } J_{\text{settle}} = S \cdot H \cdot \left[ 1 - \frac{H}{v \cdot t} \cdot \left( 1 - e^{-\frac{v}{H} \cdot t} \right) \right]$$

$$v_{\text{settle}} := \text{Find}(v) \quad v_{\text{settle}} = 1.5$$

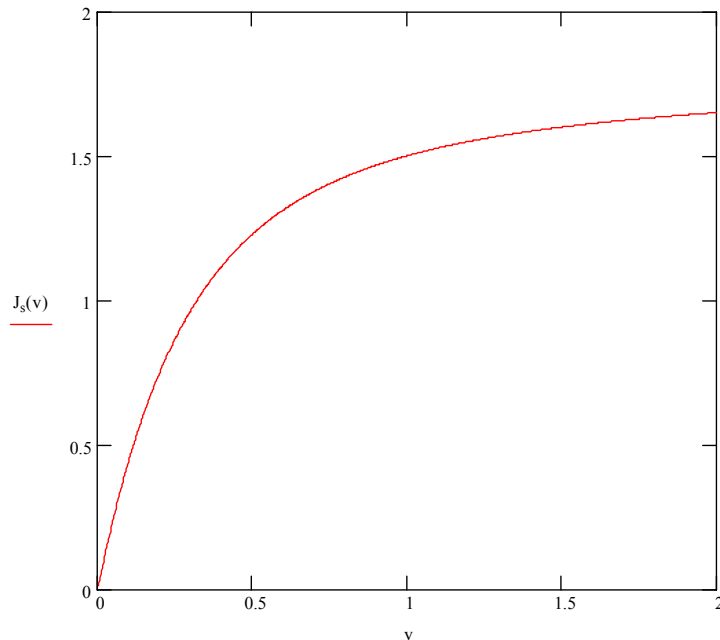
For the given flux rate and precip rate, find the settling velocity.

Check calcite concentration

$$c(t) := \frac{S \cdot H}{v_{\text{settle}}} \cdot \left( 1 - e^{-\frac{v_{\text{settle}}}{H} \cdot t} \right)$$

$$c(60) = 1.2$$

$$J_s(v) := S \cdot H \cdot \left[ 1 - \frac{H}{v \cdot t} \cdot \left( 1 - e^{-\frac{v}{H} \cdot t} \right) \right]$$



#### 4. Stokes Law

$\alpha := 1$  Form factor - effect of particle shape on settling velocity. For a sphere = 1

Stokes Law

$$v(d, T) := \alpha \cdot \frac{g}{18} \cdot \left( \frac{\rho_p - \rho_w}{\mu(T)} \right) \cdot d^2$$

From Chapra 1997 p300 eq 17.1

#### viscosity of water

The viscosity of water is  $8.90 \times 10^{-4}$  Pa·s or  $8.90 \times 10^{-3}$  dyn·s/cm<sup>2</sup> or 0.890 cP at about 25 °C.

As a function of temperature  $T$  (K):  $\mu(\text{Pa}\cdot\text{s}) = A \times 10^{B/(T-C)}$   
where  $A = 2.414 \times 10^{-5}$  Pa·s ;  $B = 247.8$  K ; and  $C = 140$  K.

Dynamic Viscosity as a function of T in K

$$\mu(T) := 2.414 \cdot 10^{-5} \text{Pa}\cdot\text{s} \cdot 10^{\frac{247.8}{(T+273.15-140)}}$$

$$\mu(10) = 0.013 \frac{\text{gm}}{\text{cm}\cdot\text{s}}$$

$$\mu(5) = 0.015 \frac{\text{gm}}{\text{cm}\cdot\text{s}}$$

1. All Calcite

$$\rho_{\text{calcite}} = 2.711 \frac{\text{gm}}{\text{cm}^3}$$

$$\frac{\rho_{\text{calcite}} - \rho_w}{\mu(10)} \cdot \frac{\text{g}}{18} \cdot \mu\text{m}^2 = 0.0620 \frac{\text{m}}{\text{day}}$$

$$v_{\text{cal}}(d) := 0.062 \cdot d^2$$

2. All plankton

$$\rho_{\text{biomass}} := 1.09 \frac{\text{gm}}{\text{cm}^3}$$

Chapra's Revised biomass surface area estimates.doc  
-> Reynolds 1984

$$\frac{\rho_{\text{biomass}} - \rho_w}{\mu(10)} \cdot \frac{\text{g}}{18} \cdot \mu\text{m}^2 = 3.2600 \times 10^{-3} \frac{\text{m}}{\text{day}}$$

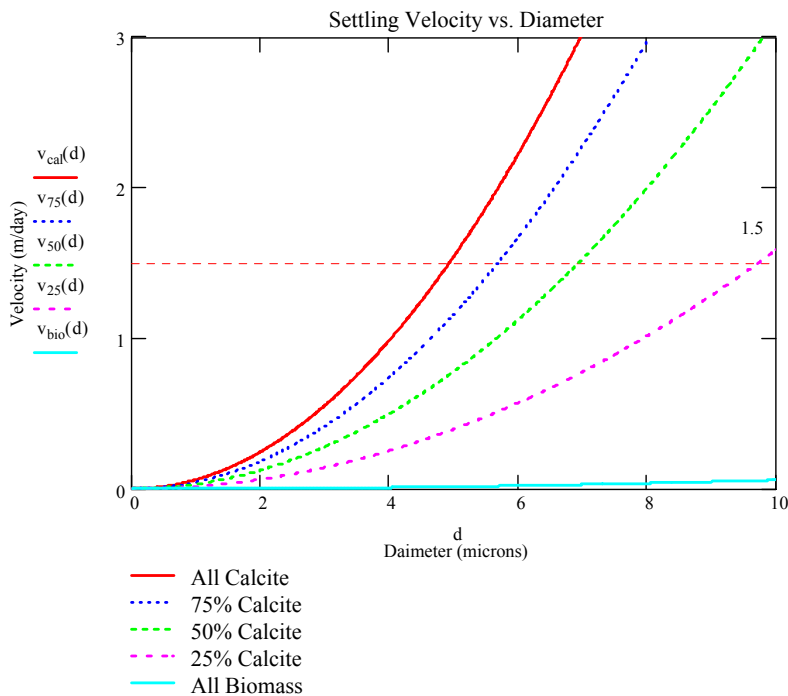
$$v_{\text{bio}}(d) := 3.2600 \times 10^{-3} \cdot d^2$$

3. 50% biomass, 50% calcite

$$\rho_{\text{mix}} := \frac{\rho_{\text{calcite}} + \rho_{\text{biomass}}}{2}$$

$$\frac{\rho_{\text{mix}} - \rho_w}{\mu(10)} \cdot \frac{\text{g}}{18} \cdot \mu\text{m}^2 = 0.0326 \frac{\text{m}}{\text{day}}$$

$$v_{\text{mix}}(d) := 0.0326 \cdot d^2$$



The relationship between the diameter and the Stokes settling velocity is shown in the plot above. Each line represents a different particle density. For these densities the velocities should be considered an upper limit since the form factor is assumed to be a sphere ( $\alpha = 1$ ).

Median Size ( <i>d</i> )	Particle (Ca-rich & Ca-agg) Volume in each bin (mm <sup>3</sup> /L)	Calcite Conc in each bin (mg/L) - assumes 100% CaCO <sub>3</sub>				
		<i>r</i> (micron)	<i>v</i> ( <i>r</i> ) in m/day	<i>v</i> ( <i>r</i> ) * <i>c</i>		
0.19	1.50E-07	0.10	2.24E-03	4.06E-07	9.09E-10	
0.22	5.19E-07	0.11	3.00E-03	1.41E-06	4.22E-09	
0.26	3.31E-06	0.13	4.19E-03	8.97E-06	3.75E-08	
0.31	3.90E-06	0.16	5.95E-03	1.06E-05	6.29E-08	
0.36	6.75E-06	0.18	8.03E-03	1.83E-05	1.47E-07	
0.43	1.02E-05	0.22	1.15E-02	2.77E-05	3.17E-07	
0.5	5.16E-05	0.25	1.55E-02	1.40E-04	2.17E-06	
0.59	0.0001139	0.30	2.16E-02	3.09E-04	6.66E-06	
0.7	0.0001651	0.35	3.04E-02	4.48E-04	1.36E-05	
0.83	0.0005585	0.42	4.27E-02	1.51E-03	6.46E-05	
0.98	0.000974	0.49	5.95E-02	2.64E-03	1.57E-04	
1.15	0.001266	0.58	8.19E-02	3.43E-03	2.81E-04	
1.36	0.002022	0.68	1.15E-01	5.48E-03	6.28E-04	
1.6	0.003199	0.80	1.59E-01	8.67E-03	1.38E-03	
1.89	0.003763	0.95	2.21E-01	1.02E-02	2.26E-03	
2.23	0.005361	1.12	3.08E-01	1.45E-02	4.48E-03	
2.63	0.006433	1.32	4.29E-01	1.74E-02	7.47E-03	
3.11	0.01057	1.56	5.99E-01	2.87E-02	1.72E-02	
3.67	0.005628	1.84	8.34E-01	1.53E-02	1.27E-02	
4.33	0.007623	2.17	1.16E+00	2.07E-02	2.40E-02	
5.11	0.01326	2.56	1.62E+00	3.59E-02	5.82E-02	
6.03	0.01634	3.02	2.25E+00	4.43E-02	9.98E-02	
7.11	0.0298	3.56	3.13E+00	8.08E-02	2.53E-01	
8.39	0.04001	4.20	4.36E+00	1.08E-01	4.73E-01	
9.91	0.06133	4.96	6.08E+00	1.66E-01	1.01E+00	
11.69	0.03301	5.85	8.47E+00	8.95E-02	7.58E-01	
13.8	0.02014	6.90	1.18E+01	5.46E-02	6.44E-01	
16.28	0	8.14	1.64E+01			
				<b>0.71</b>	<b>3.37</b>	<b>4.75</b>

Settling velocity for each bin size is calculated using Stokes. Flux is calculated for each bin given this Stoke settling velocity and the calcite concentration in the bin. The flux summed across bins and then divided by the total concentration of calcite (also a sum across bins) to give the settling velocity. For the sampling date 8/17 this weight-averaged settling velocity is 4.75 m/day.

The velocities calculated in this way range from 2.2 to 4.8 m/day on the four sampling dates: 7/7, 7/21, 8/3 and 8/17.

## **Appendix D pH2K Model Documentation**